CIVIL ENGINEERING STUDIES
Illinois Center for Transportation Series No. 21-017
UILU-ENG-2021-2017
ISSN: 0197-9191

Aggregate Subgrade Improvements Using Quarry By-products: A Field Investigation

Prepared By
Issam I. A. Qamhia, PhD
Erol Tutumluer, PhD
Han Wang
University of Illinois at Urbana-Champaign

Research Report No. FHWA-ICT-21-012

A report of the findings of

ICT PROJECT R27-SP43
Aggregate Subgrade Improvements Using Quarry By-products: A Field Investigation

https://doi.org/10.36501/0197-9191/21-017

Illinois Center for Transportation

June 2021

TECHNICAL REPORT DOCUMENTATION PAGE

1. Report No.	2. Government Accession No.	3. Recipient's Catalog No.
FHWA-ICT-21-012	N/A	N/A

4. Title	5. Report Date
Aggregate Subgrade Improvements Using Quarry By-products: A Field Investigation	June 2021
	6. Performing Organization Code N/A

7. Authors	8. Performing Organization Report No.
Issam I. A. Qamhia, https://orcid.org/0000-0002-2020-8437 Erol Tutumluer, https://orcid.org/0000-0003-3945-167X Han Wang, https://orcid.org/0000-0001-8300-0791	ICT-21-017 UILU-2021-2017

9. Performing Organization Name and Address	10. Work Unit No.
Illinois Center for Transportation Department of Civil and Environmental Engineering University of Illinois at Urbana-Champaign 205 North Mathews Avenue, MC-250 Urbana, IL 61801	N/A **11. Contract or Grant No.** R27-SP43

12. Sponsoring Agency Name and Address	13. Type of Report and Period Covered
Illinois Department of Transportation (SPR) Bureau of Research 126 East Ash Street Springfield, IL 62704	Final Report 5/16/20–6/30/21 **14. Sponsoring Agency Code**

15. Supplementary Notes

Conducted in cooperation with the U.S. Department of Transportation, Federal Highway Administration.
https://doi.org/10.36501/0197-9191/21-017

16. Abstract

This report presents a case study for constructing aggregate subgrade improvement (ASI) layers using quarry by-product aggregates (QBA), a quarry mix of large primary crushed rocks (PCR) and sand-sized quarry fines. The construction took place at Larry Power Road in Bourbonnais Township in Kankakee County, Illinois, where the Illinois Department of Transportation placed two QBA mixes. The first mix (QBA_M1) consisted of 45% quarry by-products and 55% railroad ballast–sized 3×1 PCR. The second mix (QBA_M2) consisted of 31% and 69% quarry by-products and PCR, respectively. Two conventional ASI sections were also constructed conforming to Illinois Department of Transportation's CS02 gradation. All sections consisted of a 9 in. (229 mm) QBA/PCR layer topped with a 3 in. (76 mm) dense-graded capping layer. Laboratory studies preceded the construction to recommend optimum quarry by-product content in the QBA materials and construction practice. The Illinois Center for Transportation research team monitored the quality and uniformity of the construction using nondestructive testing techniques such as dynamic cone penetrometer, lightweight deflectometer, and falling weight deflectometer. The segregation potential was monitored by visual inspection and imaging-based techniques. Short-term field evaluation of the constructed QBA layers, particularly QBA_M2 with a 31% quarry by-product content, showed no evidence of abnormal segregation and did not jeopardize the structural integrity of the QBA ASI layers, which had slightly lower but comparable strength and stiffness profiles to the conventional ASI sections. The use of QBA materials in ASI was field validated as a sustainable construction practice to provide stable pavement foundation layers.

17. Key Words	18. Distribution Statement
Aggregate Subgrade Improvement, Quarry By-product Aggregates, Field Evaluation, Case Study, Sustainable Construction, Nondestructive Testing, Back-calculation, Aggregate Blends	No restrictions. This document is available through the National Technical Information Service, Springfield, VA 22161.

19. Security Classif. (of this report)	20. Security Classif. (of this page)	21. No. of Pages	22. Price
Unclassified	Unclassified	56 + appendices	N/A

ACKNOWLEDGMENT, DISCLAIMER, MANUFACTURERS' NAMES

This publication is based on the results of **ICT-R27-SP43: Aggregate Subgrade Improvements Using Quarry By-products: A Field Investigation**. ICT-R27-SP43 was conducted in cooperation with the Illinois Center for Transportation; the Illinois Department of Transportation; and the U.S. Department of Transportation, Federal Highway Administration.

Members of the Technical Review Panel (TRP) were the following:

- Michael Short, TRP Chair, Illinois Department of Transportation
- Andrew Stolba, Illinois Department of Transportation
- Chad Nelson, Illinois Department of Transportation
- Dennis Bachman, Federal Highway Administration
- Heather Shoup, Illinois Department of Transportation
- James Trepanier, Illinois Department of Transportation
- Jeremy Brown, Illinois Department of Transportation
- Megan Swanson, Illinois Department of Transportation
- Michael Copp, Illinois Department of Transportation

The authors would like to extend their appreciation to the TRP Chair and TRP members for their time and significant contributions to this research project, particularly for their help with material procurement, documentation of field activities, and facilitating data collection activities in the field. Special thanks are extended to the TRP Chair (Michael Short) for finding and coordinating this project to demonstrate the construction and performance of this initiative. Sincere acknowledgments are also extended to IDOT engineers and staff who helped with the collection of field data, particularly dynamic cone penetration data. Many thanks to John Senger, IDOT, for his help with facilitating and coordinating the collection of falling weight deflectometer data.

The authors express their great appreciation to Applied Pavement Technology (APTech) for collecting and organizing the falling weight deflectometer data, particularly Arturo Espinoza Luque for checking and organizing the field data.

The help of the Illinois Center for Transportation research engineers Greg Renshaw and Uthman Mohamed Ali with research activities at the Advanced Transportation Research and Engineering Laboratory is also greatly appreciated. Thanks are also extended to Marc Killion from the machine shop at the University of Illinois for his help with equipment preparation and repair.

The authors would like to express their sincere gratitude to all University of Illinois and ICT students from Prof. Tutumluer's research group who helped with sample preparation and field work: Zhongyi Liu, Mingu Kang, and Kelin Ding. Many thanks to Haohang Huang and Jiayi Luo for their efforts in the segmentation and analyses of the collected field images.

Finally, thanks are extended to McCall Macomber for her help with editing this report and to Kristi Anderson and Audrey Donoho for their contribution to ICT project management.

EXECUTIVE SUMMARY

This report summarized a case study for constructing aggregate subgrade improvement (ASI) layers using quarry by-product aggregates (QBA), a quarry mix of primary crushed rocks (PCR) and sand-sized quarry fines. The construction took place at Larry Power Road in Bourbonnais Township in Kankakee County, Illinois, where the research team evaluated placement of two QBA mixes. The first mix (QBA_M1) consisted of 55% railroad ballast–sized 3×1 PCR and 45% quarry by-products (QB). The second mix (QBA_M2) consisted of 69% and 31% PCR and QB, respectively. Two conventional ASI control sections conforming to Illinois Department of Transportation (IDOT) CS02 gradation with 6 in. (152 mm) top size aggregate were also constructed for comparison purposes. For the conventional ASI sections, one section (RCA_1) was constructed with recycled CS02 concrete aggregates and topped with a reclaimed asphalt pavement capping layer, while the second (PCR_1) was constructed with virgin CS02 aggregates and topped with a virgin crushed stone capping material. All sections consisted of 9 in. (229 mm) of QBA/RCA/PCR topped with a 3 in. (76 mm) dense-graded capping layer. The field project provided the opportunity to investigate proper construction methods and study the effects of property variation in the field, such as QB and large aggregate composition, on constructability and performance.

A special provision titled “Aggregate Subgrade Improvement 12 in. Special” was prepared by IDOT and added to the notice to bidders to specify the details and requirements of a QBA material. Specifically, the special provision stated the following:

> [QBA] shall consist of a mixture of surplus quarry stone sand and primary crushed stone. The surplus quarry stone sand and primary crushed stone shall be combined in the presence of the Engineer with 25% to 50% by weight surplus quarry stone sand to create the quarry by-product aggregate ... The surplus quarry stone sand shall be defined as surplus materials from the aggregate production process and shall be 100% passing the 3/8 in. (9.5 mm) sieve ... The gradation of the combined material shall be 100% passing the 6 in. (150 mm) sieve and 8% to 12% passing the No. 200 sieve ... The quarry by-product aggregate shall not be permitted to segregate during mixing, stockpiling, transporting, or placing. In the event segregation is not prevented … then all mixing shall be performed at the job site at the point of placement.

Prior to the field construction, materials were shipped to the Advanced Transportation Research and Engineering Laboratory (ATREL) for characterization. Materials used in the construction of QBA sections were studied and characterized in the laboratory. Conducted laboratory tests included grain size distribution, specific gravity and absorption of the large PCR, packing box studies, and illustration tests of the effect of QB content on the packing of the mixture and the rock-to-rock contacts. From the packing box studies and laboratory illustrations, a QBA mix of 75% PCR and 25% QB (3:1 mix) was deemed as the optimized mix to fill the voids without losing contact between the PCR, i.e. rock-to-rock contact. Higher QB contents led to separating the larger rocks acting as the primary structure, which decreased the number of contact points between them, reducing the shear strength and load-carrying capacity.

Construction of subgrade improvements with QBA at Larry Power Road took place on July 27, 2020. The material was plant mixed using loaders at the quarry and brought to the construction site using trucks. Truck loads were dumped near the construction location and spread using a bulldozer. Visual inspection of the truck loads and videos/images collected for the stockpiles and the spread material did not show evidence of severe material segregation. The segregation levels were similar to those commonly observed in normal operation for dense-graded aggregate materials. Field sampling of the materials showed that the QBA_M1 mix had 45.5% QB-sized materials passing No. 4 sieve (4.75 mm) and 54.5% 3×1 PCR aggregates, while the QBA_M2 mix had, on average, 30.9% QB-sized materials and 69.1% large-sized 3×1 PCR. The segregation potential and mixing ratios were also closely monitored by imaging-based techniques taking advantage of an AI–based segmentation algorithm developed to determine the uniformity of the mixes, identify the sizes and shapes of PCR in the captured images, and estimate a pixel-wise area of QB and PCR from the image analyses.

Field characterization and pavement test data were collected from the site's road sections during and after construction of the different pavement layers as well as in the early stages of the traffic-use phase. The constructability, longevity, and overall field performance trends of aggregate subgrade improvements with QB subjected to real traffic loads and environmental conditions were investigated. Specific details related to the subgrade improvements with QBA were documented to establish adequate standard practice for pavement construction and rehabilitation.

The quality and uniformity of the construction was closely monitored using nondestructive techniques such as dynamic cone penetrometer (DCP), lightweight deflectometer (LWD), and falling weight deflectometer (FWD). DCP data were collected on top of the capping layers for the ASI layers and from the underlying prepared subgrade. Although the DCP data showed some variability in construction quality in all ASI layers, the general observation was that the constructed QBA layers were comparable in strength with the conventional aggregate subgrade layers routinely constructed for subgrade improvement. In fact, the QBA_M1 section with the higher QB content had the highest strength profile measured by DCP. In contrast, LWD on top of the capping layers showed that the stiffness of the QBA layers was slightly compromised compared to conventional ASI sections; the QBA_1 section had the lowest back-calculated composite surface modulus with LWD. Similarly, FWD data on top of the capping layers and on top of the hot-mix asphalt (HMA) showed similar trends. Overall, using QBA layers did not jeopardize the structural functioning of the ASI layers, which had slightly lower but comparable mechanical behavior characteristics (strength and stiffness profiles) to the conventional ASI sections. The use of QBA materials was recommended as a sustainable and durable construction practice to provide stable layers and potentially reduce long-term deformation, particularly when QBA mixes had a maximum of 25%–30% QB content.

Generally, the presence of 31% QB in the QBA_M2 mix, which is higher than the maximum percentage of 25% recommended by the packing box study, slightly reduced the structural integrity of the ASI layer with QBA. The increase in the QB content to 45% in QBA_M1 caused a further reduction in the stiffness and layer moduli, as more QB was available to separate the large rock contact points and possibly compromised the shear strength of the mix. When individual FWD drop locations as well as the ranges (min., max.) of moduli were taken into consideration, the back-calculated ASI layer moduli for the QBA_M2 mix with the lower QB content of 31% was within the

same range as RCA_1 and PCR_1 mixes, and even higher at some drop locations. In conclusion, the QBA_M2 mix was adequate as an ASI layer. For the QBA_M1 with higher QB content of 45%, the ASI layer moduli were consistently lower in several locations. Given that a thick HMA layer was constructed in general, all the sections were anticipated to show good performance because the ASI layer was buried deep in the pavement and received relatively low stress states from moving traffic.

The ASI designs with QBA can be deemed sustainable and adequate in this project and are expected to show good performance. In cases where the ASI layers receive higher stress states, i.e., in flexible pavement sections with lower HMA thicknesses, the use of QBA layers as a sustainable design that consumes large volumes of QB is also recommended, but the QB content shall not exceed 25% in order to maintain contact between the large aggregates. If these QBA layers are well designed to minimize loss of contacts between the large particles, the QBA layers can also benefit from higher stability and lower layer deformation as the QB fines pack inside the voids and increase the structural capacity of the designed ASI layers with QBA.

TABLE OF CONTENTS

CHAPTER 1: INTRODUCTION 1

BACKGROUND AND MOTIVATION 1

OBJECTIVE AND SCOPE 5

REPORT ORGANIZATION 5

CHAPTER 2: PROJECT DESCRIPTION 7

SITE LOCATION AND DESCRIPTION 7

RESEARCH SCOPE 8

QUARRY BY-PRODUCT AGGREGATE SPECIAL PROVISION 8

DESCRIPTION OF FIELD TEST SECTIONS 10

CHAPTER 3: MATERIAL EVALUATION—LAB 12

GRAIN SIZE DISTRIBUTION 12

Grain Size Distribution of 3×1 PCR Aggregates 12

Grain Size Distribution of Quarry By-product Material 13

Grain Size Distribution of Quarry By-product Aggregate Mixes 13

SPECIFIC GRAVITY AND ABSORPTION OF PCR AGGREGATES 14

PACKING BOX STUDIES 15

PAN ILLUSTRATION FOR QUARRY BY-PRODUCT CONTENT 17

CHAPTER 4: FIELD CONSTRUCTION AND EVALUATION 19

CONSTRUCTION 19

FIELD SAMPLING OF QUARRY BY-PRODUCT AGGREGATE MATERIALS 20

FIELD EVALUATION—DYNAMIC CONE PENETROMETER 21

FIELD EVALUATION—LIGHTWEIGHT DEFLECTOMETER 27

FIELD EVALUATION—FALLING WEIGHT DEFLECTOMETER 31

Falling Weight Deflectometer Tests on Top of Capping Layers 32

Falling Weight Deflectometer on Top of Hot-mix Asphalt—After Construction 34

Falling Weight Deflectometer on Top of HMA—200 Days after Opening to Traffic 41

FIELD EVALUATION—IMAGE ANALYSIS 47

PRELIMINARY PERFORMANCE EVALUATION—ROUGHNESS MEASUREMENT AND VISUAL SURVEYS 49

CHAPTER 5: SUMMARY AND CONCLUSIONS 51

SUMMARY AND CONCLUSIONS 51

RECOMMENDATIONS FOR FUTURE WORK 53

REFERENCES 55

APPENDIX A: AGGREGATE SUBGRADE IMPROVEMENT 12" SPECIAL 57

APPENDIX B: PHOTOS OF FIELD ACTIVITIES 59

APPENDIX C: DYNAMIC CONE PENETRATION DATA ON TOP OF PREPARED NATURAL SUBGRADE (WEST SIDE OF BRIDGE) 64

APPENDIX D: DYNAMIC CONE PENETRATION DATA ON TOP OF PREPARED NATURAL SUBGRADE (EAST SIDE OF BRIDGE) 69

APPENDIX E: DYNAMIC CONE PENETRATION DATA ON TOP OF CAPPING MATERIALS (WEST SIDE OF BRIDGE) 75

APPENDIX F: DYNAMIC CONE PENETRATION DATA ON TOP OF CAPPING MATERIALS (EAST SIDE OF BRIDGE) 78

APPENDIX G: LIGHTWEIGHT DEFLECTOMETER DATA ON TOP OF PREPARED NATURAL SUBGRADE 81

APPENDIX H: LIGHTWEIGHT DEFLECTOMETER DATA ON TOP OF THE QUARRY BY-PRODUCT AGGREGATE MIXTURES 82

APPENDIX I: LIGHTWEIGHT DEFLECTOMETER DATA ON TOP OF THE CAPPING MATERIALS 83

APPENDIX J: FALLING WEIGHT DEFLECTOMETER DATA ON TOP OF CAPPING MATERIAL (WEST SIDE OF BRIDGE) 86

APPENDIX K: FALLING WEIGHT DEFLECTOMETER ON TOP OF CAPPING MATERIAL (EAST SIDE OF BRIDGE) 89

APPENDIX L: FALLING WEIGHT DEFLECTOMETER DATA ON TOP OF HMA—AFTER CONSTRUCTION (WEST SIDE OF BRIDGE) 91

APPENDIX M: FALLING WEIGHT DEFLECTOMETER DATA ON TOP OF HMA—AFTER CONSTRUCTION (EAST SIDE OF BRIDGE) 95

APPENDIX N: FALLING WEIGHT DEFLECTOMETER DATA ON TOP OF HMA—AFTER OPENING TO TRAFFIC (WEST SIDE OF BRIDGE) 99

APPENDIX O: FALLING WEIGHT DEFLECTOMETER DATA ON TOP OF HMA—AFTER OPENING TO TRAFFIC (EAST SIDE OF BRIDGE) 103

LIST OF FIGURES

Figure 1. Photo. UIUC packing box used to test aggregate subgrade improvements with QB. 2
Figure 2. Photo. Construction of QBA test sections for ICT project R27-168 (Qamhia et al. 2018). 3
Figure 3. Graph. Rutting progression in the aggregate subgrade improvement layers with and without QB (test sections from ICT projects R27-168 and R27-124). 4
Figure 4. Illustration. Diagram. Larry Power Road project site over I-57 in Kankakee County, IL. 7
Figure 5. Illustration. Proposed Section 1 of Larry Power Road with 12 in. ASI (special)— Stations 2360+00 to 2366+05. 8
Figure 6. Illustration. Test section locations relative to the bridge over I-57. 10
Figure 7. Graph. Grain size distribution of 3×1 PCR aggregates. 12
Figure 8. Graph. Grain size distribution of QB material (washed and dry gradations). 13
Figure 9. Graph. Proposed grain size distributions of different QBA mixes. 14
Figure 10. Equation. Calculating relative density (specific gravity) 14
Figure 11. Equation. Calculating percent absorption. 14
Figure 12. Equation. Calculating volume of solids 15
Figure 13. Equation. Calculating porosity (%). 15
Figure 14. Equation. Calculating void ratio (%). 16
Figure 15. Photos. Packing box studies for 3×1 rocks and the 3:1 QBA mix. 16
Figure 16. Illustration. Packing of QBA mixes with different mixing ratios. 17
Figure 17. Photo. Placement and spreading of QBA_M1 material in the field. 19
Figure 18. Photo. Comparison of QBA_M1 and QBA_M2 after placement and before compaction. 20
Figure 19. Graph. Grain size distributions of field samples collected from QBA_M1 mix. 21
Figure 20. Graph. Grain size distributions of field samples collected from QBA_M2 mix. 21
Figure 21. Equation. Calculating IBV (%) from DCP penetration rate in inches per blow. 22
Figure 22. Graph. Sample DCP depth profiles for the prepared natural subgrade under all sections. 22
Figure 23. Plot. Achieved IBV(%) in the prepared natural subgrade (west side of bridge). 23
Figure 24. Plot. Achieved IBV(%) in the prepared natural subgrade (east side of bridge). 24
Figure 25. Diagram. Summary of average DCP (IBV) results for prepared natural subgrade. 24
Figure 26. Graph. Sample DCP depth profiles on top of ASI capping layers 25
Figure 27. Plot. Achieved average IBV(%) in the ASI layers (west side of bridge). 26

Figure 28. Plot. Achieved average IBV(%) in the ASI layers (east side of bridge). 26

Figure 29. Diagram. Summary of average DCP (IBV) results for the different ASI layers..... 27

Figure 30. Plot. Subgrade moduli in MN/m^2 measured with LWD for sections west of the bridge. (1 ksi = 6.89 MN/m^2) 28

Figure 31. Plot. Composite surface moduli in MN/m^2 on top of QBA mixes, measured with LWD. (1 ksi = 6.89 MN/m^2) 28

Figure 32. Plot. Composite surface moduli in MN/m^2 on top of capping layer for QBA sections on the west side of the bridge. (1 ksi = 6.89 MN/m^2). 30

Figure 33. Plot. Composite surface moduli in MN/m^2 on top of capping layer for conventional ASI sections on the east side of the bridge. (1 ksi = 6.89 MN/m^2). 30

Figure 34. Diagram. Summary of LWD composite surface moduli on top of capping layers (1 ksi = 6.89 MN/m^2). 31

Figure 35. Plot. FWD surface deflections (mils) of center geophone (D_0) on top of capping layer, normalized to a 12 kip (53 kN) load level. 33

Figure 36. Diagram. Summary of FWD surface deflections (mils) of center geophone (D_0) on top of capping layer, normalized to a 12 kip (40 kN) load level. 33

Figure 37. Chart. Recorded average FWD deflections for sensors D_0–D_3. 34

Figure 38. Equation. Calculating surface curvature index from FWD deflections. 35

Figure 39. Equation. Calculating base damage index from FWD deflections. 36

Figure 40. Equation. Calculating base curvature index from FWD deflections. 36

Figure 41. Chart. FWD deflection basin parameters (average values): SCI, BDI, and BCI. 36

Figure 42. Equation. Calculating F1 shape factor from FWD deflections. 37

Figure 43. Equation. Calculating F2 shape factor from FWD deflections. 37

Figure 44. Chart. FWD deflection basin parameters (average values): shape factors F1 and F2. 37

Figure 45. Equation. Calculating AREA parameter from FWD deflections. 38

Figure 46. Equation. Calculating AUPP from FWD deflections. 38

Figure 47. Chart. FWD deflection basin parameters (average values): AREA parameter. 38

Figure 48. Chart. FWD deflection basin parameters (average values): Area under pavement profile.. 39

Figure 49. Chart. Recorded average FWD deflections for sensors D_0–D_3 (after traffic). 42

Figure 50. Chart. FWD deflection basin parameters after traffic (average values): SCI, BDI, and BCI... 43

Figure 51. Chart. FWD deflection basin parameters (average values before and after traffic): shape factors F1 and F2. 44

Figure 52. Chart. FWD deflection basin parameters (average values before and after traffic): AREA parameter. 45
Figure 53. Chart. FWD deflection basin parameters after traffic (average values): Area under pavement profile. 45
Figure 54. Photo. Raw and segmented images of QBA_M1 section before compaction. 48
Figure 55. Photo. Raw and segmented images of QBA_M2 section before compaction. 49
Figure 56. Photo. Scooping primary crushed rocks for blending at the quarry. 59
Figure 57. Photo. Weighing by-product sand in loader bucket to prepare quarry by-product aggregates. 59
Figure 58. Photo. Blended stockpile for the QBA_M1 material. 60
Figure 59. Photo. Dumping quarry by-product aggregate materials at the job site. 60
Figure 60. Photo. Spreading quarry by-product aggregate materials using a bulldozer. 61
Figure 61. Photo. Final finished surface of the QBA_M1 material after compaction. 61
Figure 62. Photo. Conducting lightweight deflectometer testing on top of QBA_M1 layer. 62
Figure 63. Photo. Conducting falling weight deflectometer testing on top of the capping layer of the PCR_1 test section. 62
Figure 64. Photo. Final road surface—east side of bridge (April 6, 2021). 63
Figure 65. Photo. Final road surface—west side of bridge (April 6, 2021). 63
Figure 66. Plot. Achieved IBV(%) in the prepared natural subgrade (west side of bridge). 64
Figure 67. Graphs. DCP profiles for the prepared subgrade at different measuring points (west side of bridge). 68
Figure 68. Plot. Achieved IBV(%) in the prepared natural subgrade (west side of bridge). 69
Figure 69. Graphs. DCP profiles of prepared subgrade at different measuring points (east side of bridge). 74
Figure 70. Plot. Achieved average IBV (%) in the ASI layers (west side of bridge). 75
Figure 71. Graphs. IBV profiles from DCP tests on top of the capping layers (west side of bridge). 77
Figure 72. Plot. Achieved average IBV (%) in the ASI layers (east side of bridge). 78
Figure 73. Graphs. IBV profiles from DCP test on top of capping layers (east side of bridge). 80
Figure 74. Plot. FWD average surface deflections (mils) of center geophone (D_0) on top of capping layer, normalized to a 12-kip (53-kN) load level. 86
Figure 75. Graphs. FWD data on top of the capping layers at different measuring points in the QBA sections. 88

Figure 76. Plot. FWD average surface deflections (mils) of center geophone (D_0) on top of capping layer, normalized to a 12-kip (53-kN) load level. 89

Figure 77. Graphs. FWD data on top of the capping layers at different measuring points in the conventional ASI sections. 90

Figure 78. Plot. FWD test locations on top of HMA (west side of bridge). 91

Figure 79. Graphs. FWD data on top of the HMA layer at different measuring points in the QBA sections (after construction). 94

Figure 80. Plot. FWD test locations on top of HMA (east side of bridge). 95

Figure 81. Graphs. FWD data on top of the HMA layer at different measuring points in the conventional ASI sections (after construction). 98

Figure 82. Plot. FWD test locations on top of HMA (west side of bridge). 99

Figure 83. Graphs. FWD data on top of the HMA layer at different measuring points in the QBA sections (after opening to traffic). 102

Figure 84. Plot. FWD test locations on top of HMA (east side of bridge). 103

Figure 85. Graphs. FWD data on top of the HMA layer at different measuring points in the conventional ASI sections (after opening to traffic). 106

LIST OF TABLES

Table 1. Selected IDOT Gradation Bands 11
Table 2. Description of Field Test Sections 11
Table 3. Summary of Packing Box Test Matrix 16
Table 4. Average DCP and LWD Results on Top of Capping Layers 31
Table 5. Some Commonly Used Back-calculation Programs 39
Table 6. PCASE Back-calculation Results (after Construction)— Layer Moduli (Average and Range of Values) 41
Table 7. ELMOD 6 Back-calculation Results (after Construction)— Layer Moduli (Average and Range of Values) 41
Table 8. PCASE Back-calculation Results (after Traffic)—Layer Moduli (Average and Range of Values) 47
Table 9. ELMOD 6 Back-calculation Results (after Traffic)—Layer Moduli (Average and Range of Values) 47
Table 10. International Roughness Index results for the Westbound Conventional Sections 50
Table 11. International Roughness Index Results for the Eastbound QBA Sections 50
Table 12. Summary of LWD Data on Top of Prepared Subgrade—West Side of Bridge 81
Table 13. Summary of LWD Data on Top of QBA Mixes—West Side of Bridge 82
Table 14. Summary of LWD Data on Top of Capping Material—QBA_M1 Section 83
Table 15. Summary of LWD Data on Top of Capping Material—QBA_M2 Section 84
Table 16. Summary of LWD Data on Top of Capping Material—RCA_1 Section 84
Table 17. Summary of LWD Data on Top of Capping Material—PCR_1 Section 85

CHAPTER 1: INTRODUCTION

BACKGROUND AND MOTIVATION

Quarry by-products (QB) are industrial by-products of aggregate quarry processes such as blasting, crushing, and screening. They are typically less than 1/4 in. (6 mm) in size and consist of coarse, medium, and fine sand particles as well as a small clay/silt fraction. Quarry by-products are found abundantly at quarries located in the state of Illinois. The excessive QB produced each year exceeds 950,000 tons, according to a questionnaire responded to by some of the 20 largest quarries in Illinois in the Illinois Center for Transportation (ICT) project R27-125 (Tutumluer et al. 2015). The annual production of QB in Illinois thus far exceeds this estimate if the production by smaller producers is also considered.

Research work conducted at ICT has evaluated the characteristics of QB materials collected from different quarries across the state of Illinois and studied potential uses of QB in pavement applications. As part of R27-125, Tutumluer et al. (2015) conducted a laboratory study to characterize the engineering properties of QB materials produced in the primary, secondary, and tertiary aggregate production stages from four different quarries operating in Illinois (Tutumluer et al. 2015; Hou et al. 2019). They performed property tests for determining aggregate gradation, particle shape characteristics, and mineralogical analyses of the QB samples as well as observed differences in shape and gradation properties of QB materials produced in each crushing stage. Because the unconfined compressive strength for QB materials was low (less than 11 psi or 76 kPa), Portland cement and Class C fly ash chemical admixture stabilizers were used to improve the strength properties of QB materials. For the chemically stabilized QB samples, a 2% cement or 10% Class C fly ash increased the unconfined compressive strength by up to 30 times when compared to unstabilized QB samples.

More recently, Qamhia et al. (2018) conducted the ICT project R27-168 to investigate the field performance trends of QB materials in sustainable pavement applications. The project evaluated new sustainable applications of QB or QB mixed with marginal, virgin, or recycled aggregate materials in unbound and chemically stabilized pavement layers tested under realistic wheel loads and environmental conditions. Sixteen full-scale test sections were constructed to evaluate the performance trends of QB materials used in pavement base, subbase, and aggregate subgrade applications through accelerated pavement testing (APT). The unbound (unstabilized) applications investigated the use of QB to fill the voids between large aggregate subgrade materials commonly used for rockfill applications on top of very soft subgrade soils (Immediate bearing value, IBV ≤ 1%), as well as using dense-graded aggregate subgrade layers with higher fines content (up to 15% passing No. 200 sieve) for soft subgrade remediation. The bound applications investigated the use of QB or recycled coarse aggregates mixed with QB and stabilized with 3% cement or 10% fly ash in pavement base and subbase courses constructed over prepared subgrade with an IBV of 6%. The test sections were evaluated for performance trends using APT. Field materials characterization testing and forensic analysis techniques applied included falling weight deflectometer (FWD) tests conducted before and after trafficking, hot-mix asphalt coring, dynamic cone penetrometer (DCP) profiling of subsurface layers, and pavement cross trenching to determine as-constructed pavement layer

thicknesses and permanent deformation contribution of each pavement layer to the measured surface rutting.

Four of the test sections in R27-168, i.e., two construction platforms and two flexible pavement sections, studied aggregate subgrade improvements with large primary crushed rocks (PCR) and QB filling the voids (Qamhia et al. 2018). Prior to the field study, a laboratory investigation was conducted to ascertain the optimized blend of the PCR and QB in a single lift and in two lifts. A customized compaction steel box (called the UIUC packing box) was built to investigate the packing efficiency of the two materials. The box, shown in Figure 1, is 24 in. by 24 in. and 21 in. in height (1 in. = 25.4 mm). One side of the box has plexiglass to observe the aggregate packing inside the box and obtain a high-resolution image of the cross-section to further study the percolation of QB through the PCR. Large-sized PCR were first placed in the box and then QB was added from the surface to percolate into the large voids with a vibratory action.

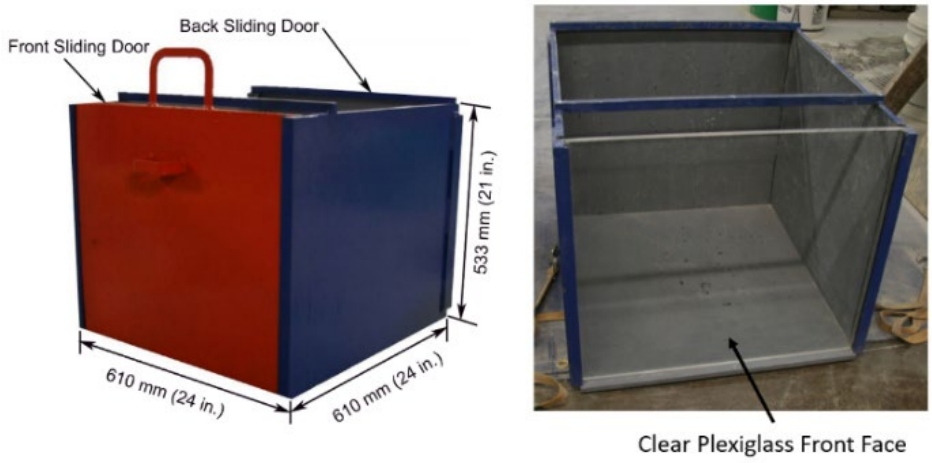

(A) UIUC packing box

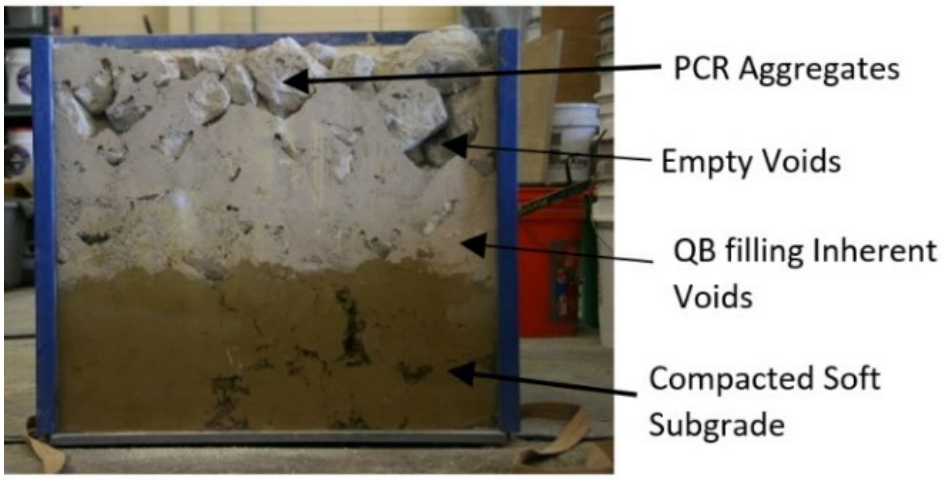

(B) Packing PCR and QB on top of weak (IBV = 1%) subgrade

Figure 1. Photo. UIUC packing box used to test aggregate subgrade improvements with QB.

Qamhia et al. (2018) investigated four variables in the UIUC packing box in R27-168. The first is the number of constructed lifts, which considered both a single 21 in. lift and two 10.5 in. lifts (1 in. = 25.4 mm). The second is the quantity of the QB, which was varied between 20% and 40% by the weight of the PCR. The third is the moisture content of the QB, which was varied from 0% to 2.5%, and the fourth is the support condition, which was changed from a rigid steel bottom to a very soft IBV = 1% subgrade soil. Laboratory experiments did not show a significant difference in densities and percolation trends between the single- and two-lift experiments when dry QB was added. However, as the moisture content was increased, it was more difficult to percolate a similar percentage by weight of the QB into PCR. Typically, 30% was found to be the optimum quantity in the case of dry QB, and 25% was the optimum for QB with a 2.5% moisture content (Qamhia et al. 2017a, 2018).

Four full-scale test sections were constructed as part of R27-168 with PCR and QB (two paved and two unpaved), following the recommendations and conclusions of the UIUC packing box study on the quantities of QB. Two sections were constructed as one 21 in. lift, while the other two were constructed in two 10.5 in. lifts. The PCR were placed first and then QB were manually spread on the surface in increments. When the surface was completely covered with QB, the QBs were then shaken into the voids using a vibratory roller, and the process was repeated until no further QB could be vibrated into the voids. Approximately, 16.7% QB by weight of PCR was vibrated in the single-lift construction (equivalent to 85.7% PCR and 14.3% QB) while 25% QB by weight of PCR could be packed in the two-lift construction (80% PCR and 20% QB). Figure 2 presents part of the construction activities.

(A) Compaction of QBA layers with a vibratory roller (B) Top view of compacted QBA layer

Figure 2. Photo. Construction of QBA test sections for ICT project R27-168 (Qamhia et al. 2018).

The constructed test sections of R27-168 were monitored for performance through APT (Qamhia et al. 2018). Performance monitoring was conducted by periodic surface profile measurements at a certain number of passes, along with other nondestructive testing methods such as FWD, DCP, and lightweight deflectometer (LWD). Figure 3 shows the progression of average surface rut accumulations for both the single- and two-lift construction platform sections with increasing number of passes. Both sections showed improved performance when compared to the sections constructed with similar PCR from a previous full-scale test research study (R27-124) with no QB used in the aggregate subgrade (Kazmee and Tutumluer 2015). In general, positive results were obtained from the R27-168 flexible pavement test sections, which had less than 0.3 in. of rutting after 90,000 APT wheel passes for both the single- and two-lift construction alternatives of the 21 in. thick aggregate subgrade layer (Qamhia et al. 2017b, 2017c). These promising results of R27-168 were the basis to

recommend common use of QB in IDOT's standard practice, and accordingly, specifications for aggregate subgrade and QB construction were drafted to be applied in field demonstration projects, such as this project (R27-SP43).

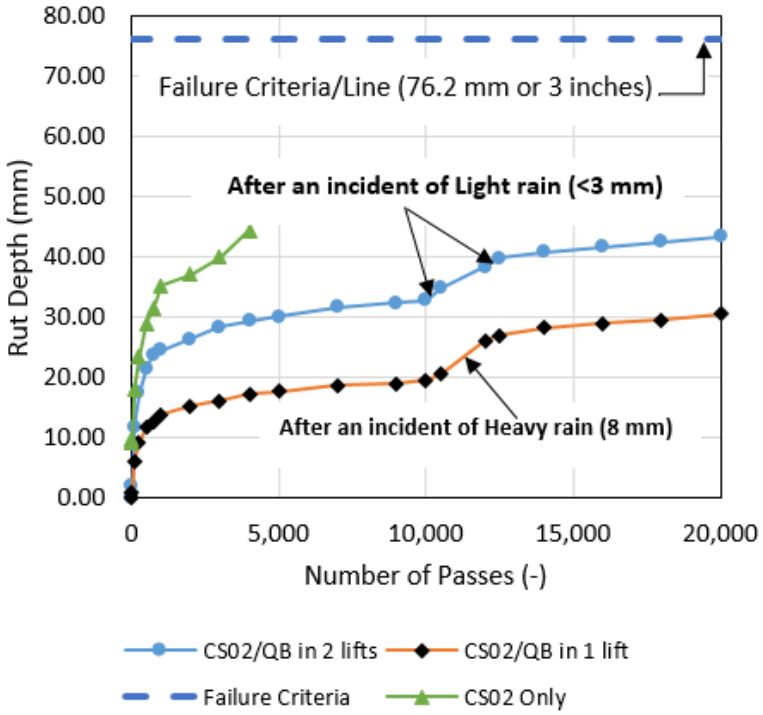

Figure 3. Graph. Rutting progression in the aggregate subgrade improvement layers with and without QB (test sections from ICT projects R27-168 and R27-124).

The findings from R27-168 on the use of QB in sustainable pavement applications have indicated that when QB are mixed with PCR or soil improvement, density and stability of the aggregate subgrade layer is improved and settlement potential decreases (Qamhia et al. 2018). Such a promising QB application advocates more sustainable pavement construction practices by reducing excess QB accumulating on a yearly basis in large quarries in Illinois. Therefore, in order for the proposed QB application in R27-168 to be deemed readily implementable, this project was undertaken to construct subgrade improvements with quarry by-product aggregates (QBA), defined as mixes of PCR with a maximum 6 in. (152 mm) top size aggregate intermixed with QB materials to fill the voids. The PCR and QB are to be blended at the quarry to achieve better mixing and verification of intended material weights and blending ratios. Specifically, test sections were constructed as part of the removal and replacement of structure number (SN) 046-0087 on Larry Power Road over I-57 in Bourbonnais Township in Kankakee County, Illinois.

The construction effort provides the opportunity to investigate proper construction methods and study the varied property effects such as QB content on constructability and performance. Pavement performance data to be collected from the project site field sections during the construction and traffic-use phases provide an implementation project case study for this QB technology. Accordingly, the purpose of this project was to investigate the constructability, longevity, and overall field

performance of aggregate subgrade improvements with QB subjected to real traffic loads and environmental conditions, as well as to incorporate the successful subgrade improvements with QBA into IDOT's standard practices for pavement construction and rehabilitation.

OBJECTIVE AND SCOPE

The objective of this project was to investigate proper methods to characterize QB and construct stable and well-performing aggregate subgrade improvement sections using mixes of PCR and QB, termed herein as QBA. The construction and performance monitoring was achieved by constructing a road with QBA as part of a field project planned for the removal and replacement of a two-span bridge (SN 046-0087) with continuous, composite, wide-flange steel beams supporting a reinforced concrete deck on Larry Power Road over I-57 in Kankakee County, Illinois. Proper construction methods as well as quality assurance and quality control measures were investigated during the construction. Quarry samples were collected and characterized in the laboratory using the UIUC packing box. Pavement performance data was collected and analyzed throughout the project to study and to understand the performance of aggregate subgrade layers with QBA technology subjected to vehicular traffic and environmental conditions.

To achieve the overall objective of this one-year project, the following tasks were conducted:

- Task 1—Observe, monitor, and document construction of subgrade improvements with QBA at Larry Power Road in Bourbonnais Township and evaluate effectiveness through testing listed in subsequent tasks.
- Task 2—Evaluate QBA in the laboratory using UIUC packing box and other characterization techniques.
- Task 3—Collect field performance data—DCP, LWD, FWD, field images, crack/pavement condition surveys, etc.
- Task 4—Compile, analyze, and interpret results.

REPORT ORGANIZATION

This report consists of five chapters, including this introductory chapter.

Chapter 2, titled "Project Description," provides details on the project location, scope, construction plans, the special provision used to construct ASI layers with QBA, and the description of the constructed field test sections, including materials and specified gradations.

Chapter 3, titled "Material Evaluation—Lab," provides details on the conducted laboratory tests to characterize the QB, large-sized aggregates, and QBA materials. Laboratory tests include grain size distribution, specific gravity and absorption, packing study of QB and larger rocks using UIUC packing box, and pan illustration of the effects of QB content in the QBA blends.

Chapter 4, titled “Field Construction and Evaluation,” provides details for the field construction of test sections, field sampling of QBA materials for laboratory testing, field evaluation of the constructed test sections using DCP, LWD, and FWD, as well as field evaluation of QBA mixes using image segmentation and analysis techniques. The analysis and interpretation of field collected data is also provided in this chapter along with the back-calculated layer stiffness properties of all constructed layers using surface deflection data from FWD tests.

Chapter 5, titled “Summary and Conclusions,” provides a summary of the test results, conclusions from the evaluations of QBA layer performance trends, and the case study lessons learned as recommendations. This chapter also discusses recommendations for improvements in future implementation projects with QBA materials for optimized performance, as well as some recommendations for future research.

CHAPTER 2: PROJECT DESCRIPTION

SITE LOCATION AND DESCRIPTION

This project is carried out as part of the removal and replacement of structure number (SN) 046-0087 on Larry Power Road over I-57 in Bourbonnais Township in Kankakee County, Illinois. The project limits extend from approximately 650 ft west of existing structure SN 046-0087 over I-57 to approximately 800 ft east of the existing structure. The project is 1.2 miles (1.9 km) north of Kankakee (see Figure 4). The construction work involves removing and replacing the existing four-span bridge structure. The replacement bridge structure consists of two-span continuous, composite, wide-flange steel beams supporting a reinforced concrete deck. The new deck is 51 ft 11 in. (15.8 m) wide and provides a three-lane roadway section with a 10 ft (3 m) wide shared-use path on the north side of the deck. The length of the new structure is 215 ft (65.5 m) back to back of the abutments. The profile grade of Larry Power Road is to be raised approximately 2.25 ft (0.686 m) to provide clearance over I-57. Larry Power Road improvements consist of pavement removal and replacement, curb and gutter, multiuse path, storm sewer, guardrail removal and replacement, seeding, and pavement marking, among other items.

Figure 4. Illustration. Diagram. Larry Power Road project site over I-57 in Kankakee County, IL.

The project detailed in this report is involved mainly with the construction of subsurface layers, i.e., ASI layers, on the road leading to the main bridge structure (east and west of the bridge). The construction on these roads involves widening the roadway to accommodate three lanes: westbound, eastbound, and a shared middle lane, with curbs on both sides of the roadway. The roads will have a 12 in. (305 mm) ASI layer (including a 3 in. or 76 mm capping layer) topped with 10.75 in. (273 mm) of HMA. The immediate bearing value (IBV), which corresponds to the unsoaked California bearing ratio tested in a 4 in. (102 mm) diameter mold, of the existing natural subgrade is 3% on average, which necessitates using an ASI layer as per IDOT's *Subgrade Stability Manual* (IDOT 2005). Conventional ASI layers were constructed on the east side of the bridge, while layers of PCR mixed with QB were constructed on the west side of the bridge. Figure 5 shows the proposed typical cross section of the

Larry Power Road for construction. An aggregate subgrade improvement of 12 in. (special), as indicated in the project plan, utilizes a special provision using mixes of PCR and QB.

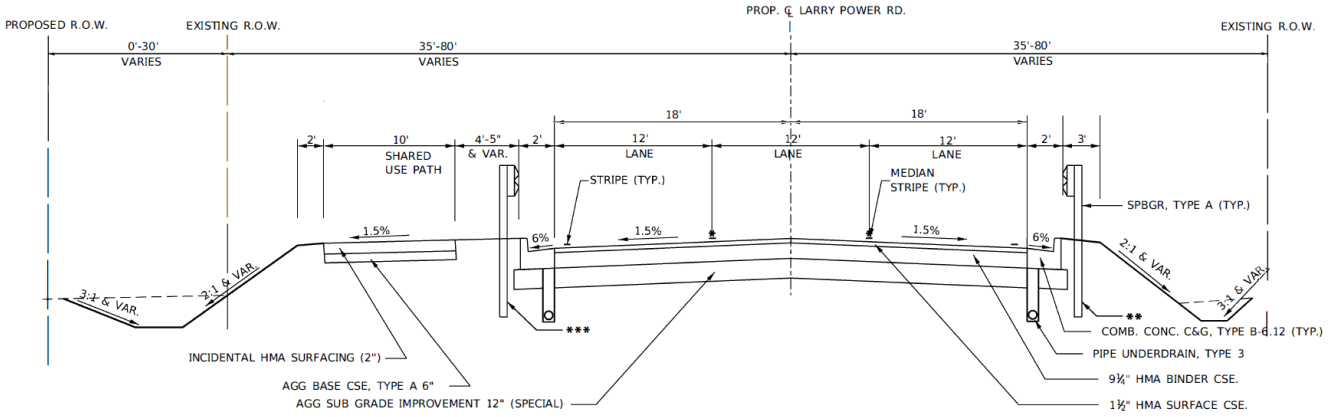

Figure 5. Illustration. Proposed Section 1 of Larry Power Road with 12 in. ASI (special)—Stations 2360+00 to 2366+05.

The construction provides the opportunity to investigate proper construction methods and study effects of the property variation such as QB content and construction methods on constructability and performance. Pavement performance data collected from the project site are to be closely monitored from the field sections during the construction and traffic-use phases. The constructability, longevity, and overall field performance trends of aggregate subgrade improvements with QB subjected to real traffic loads and environmental conditions are also to be investigated. The successful subgrade improvement application with QB is being evaluated for possible incorporation into IDOT's standard practices for pavement construction and rehabilitation.

RESEARCH SCOPE

This field construction project will monitor the construction and performance of aggregate subgrade layers with QB. Anticipated results include a full evaluation of the best construction practices of subgrade improvements with QB, collection of field performance data and pavement responses, and recommendation of improvements and best practices from the UIUC packing box laboratory studies. This project is intended to identify and propose solutions for any anticipated issues with the use of QB in aggregate subgrade improvements such as segregation, handling difficulties, compaction challenges, and performance issues.

QUARRY BY-PRODUCT AGGREGATE SPECIAL PROVISION

A special provision titled "Aggregate Subgrade Improvement 12 in. Special" was added to the "Notice to Bidders, Specifications and Proposal" document for Contract No. 66961 by IDOT. This letting covers the construction of QBA layers at the west side of the bridge at Larry Power Road over I-57. The special provision supplements IDOT's (2016) *Standard Specifications for Road and Bridge Construction*, adopted April 1, 2016. A copy of the special provision can be found in Appendix A. Note that the special provision defines QBA as a mixture of surplus quarry stone sand and primary crushed

stone, which is essentially the same as a mixture of QB and PCR for the terminology used throughout this report.

The main points covered in this special provision, which are of direct influence on the tasks and deliverables of this project, are as follows:

- **Materials description**:
    - Capping material: Capping material shall consist of coarse aggregates. The 3 in. (75 mm) layer of capping aggregate shall consist of sound durable particles reasonably free of deleterious materials and be gradation CA 6 or CA 10. Alternatively, reclaimed asphalt pavement (RAP) having 100% passing the 1.5 in. (37.5 mm) sieve and being well graded may be used as capping aggregate.
    - Quarry by-product aggregates: Note 4 in the special provision states the following:

      [QBA] shall consist of a mixture of surplus quarry stone sand and primary crushed stone. The surplus quarry stone sand and primary crushed stone shall be combined in the presence of the Engineer with 25% to 50% by weight surplus quarry stone sand to create the quarry by-product aggregate. Mixing with loaders will be permitted provided the weights of materials being mixed can be verified and the resulting stockpile is evenly mixed and free from segregation. The surplus quarry stone sand shall be defined as surplus materials from the aggregate production process and shall be 100% passing the 3/8 in. (9.5 mm) sieve. The primary crushed stone shall be defined as the aggregate resulting after processing through one crusher and shall be 100% passing the 6 in. (150 mm) sieve. The gradation of the combined material shall be 100% passing the 6 in. (150 mm) sieve and 8% to 12% passing the No. 200 sieve. Quarry by-product aggregate shall be free of objectional deleterious material. The quarry by-product aggregate shall not be permitted to segregate during mixing, stockpiling, transporting, or placing. In the event segregation is not prevented during mixing, stockpiling, transporting, or placing, then all mixing shall be performed at the job site at the point of placement.
- **Soil preparation**: The stability of the soil shall be according to IDOT's *Subgrade Stability Manual* for the aggregate thickness specified.
- **Placing aggregate**: The maximum nominal thickness of quarry by-product aggregate placed in a single lift shall be 24 in. (600 mm).
- **Capping aggregate**: The top surface of the aggregate subgrade improvement using quarry by-products shall consist of a minimum 3 in. (75 mm) of capping aggregate.
- **Compaction**: All aggregate lifts shall be compacted to the satisfaction of the engineer. If the moisture content of the material is such that compaction cannot be obtained, sufficient water shall be added so that satisfactory compaction can be obtained.

DESCRIPTION OF FIELD TEST SECTIONS

Four test sections were constructed in the field: two QBA aggregate sections and two ASI sections with primary crushed rocks. The two QBA sections were constructed on the west side of the bridge crossing I-57 on Larry Power Road, while the other two conventional ASI sections were constructed on the east side of the bridge. (See Figure 6, which shows the stations and location of each test section.) Note that the conventional sections are still considered control sections for comparison purposes, even though the rock sizes and IDOT gradation numbers do not closely match those of the large PCR used in the QBA test sections. The reason is because these conventional sections are the baseline for the state of practice by IDOT, which the experimental and performance aspects of QBA are compared to. For the QBA sections, the same materials were used for both sections, but the mixing ratio of QB and the PCR were different (45% QB vs. 31% QB for QBA_M1 and QBA_M2, respectively). For the conventional sections, a RAP capping material was used for section RCA_1, while a virgin capping material was used for PCR_1 section.

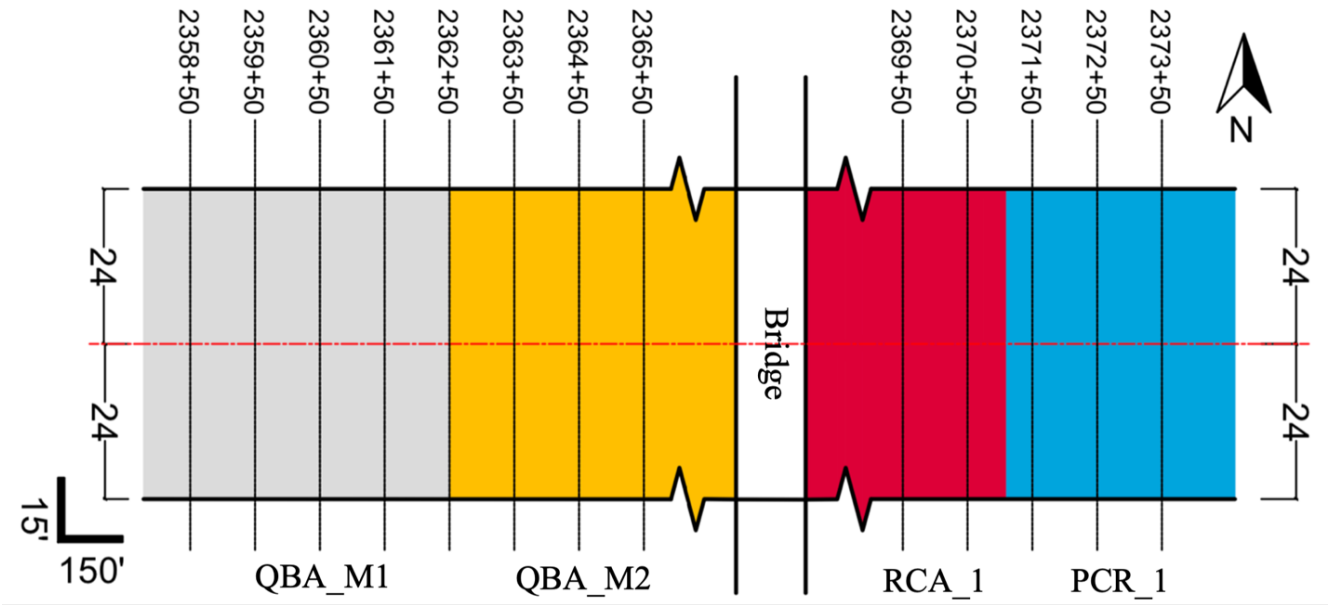

Figure 6. Illustration. Test section locations relative to the bridge over I-57.

Table 1 gives the IDOT gradation numbers of the materials utilized in constructing the test sections, while Table 2 provides the detailed description of the test sections. The conventional sections on the east side of the bridge conformed to IDOT's CS02 gradation, while the PCR in the QBA material, called 3×1 aggregate, more closely followed IDOT's RR 01 grain size distribution requirements. The virgin and RAP capping materials used for all four test sections followed IDOT's CA 6 grain size distribution requirements.

Table 1. Selected IDOT Gradation Bands

	Sieve size and percent passing									
Gradation	**6″**	**4″**	**3″**	**2″**	**1.5″**	**1″**	**0.5″**	**#4**	**#16**	**#200**
CS 02	100	80 ± 10		25 ± 15						
RR 01			100		53 ± 23					
CA 6					100	95±5	75±15	43±14	25±15	8±4

Table 2. Description of Field Test Sections

Section	Location	Description of aggregate subgrade improvement (ASI)
QBA_M1	West side of bridge	Quarry by-product aggregate (QBA) with higher QB content—55% 3×1 primary crushed rocks (PCR) and 45% QB. Virgin CA 6 capping material
QBA_M2	West side of bridge	QBA with lower QB content—69% 3×1 PCR and 31% QB. Virgin CA 6 capping material
RCA_1	East side of bridge	Recycled Concrete CS02 Aggregates. RAP CA 6 capping
PCR_1	East side of bridge	Virgin CS02 PCR. Virgin CA 6 capping

CHAPTER 3: MATERIAL EVALUATION—LAB

Prior to the field construction, materials were shipped from the Vulcan Lehigh quarry in Kankakee County, Illinois, for characterization at the Advanced Transportation Research and Engineering Laboratory (ATREL). Primarily, materials used for the construction of quarry by-product aggregates (QBA) on the west side of the bridge were characterized. Bags of materials were shipped to ATREL for the large primary crushed rocks and the quarry fines, as well as mixtures of materials mixed at the quarries. Mixes of 1:1, 2:1, and 3:1 PCR to QB ratios by weight were considered. Note that mixes by weight (in lieu of volume) were considered to facilitate proportioning at the quarry by using scales.

GRAIN SIZE DISTRIBUTION

Grain size distributions were determined for the 3×1 PCR aggregates and the QB material from Vulcan Lehigh quarry used to construct the QBA layers on the west side of the Larry Power Road bridge over I-57. Initially, two quarry mixes of the QBA aggregates were shipped to ATREL and sieved, but the results for these mixes are not of interest in this report because the mixing ratios were subsequently changed after recommendations following the box packing studies to further reduce the QB amounts. Alternatively, the as-built mixes of QBA_M1 and QBA_M2 were sampled in the field, and those samples were sieved after construction. Chapter 4 presents the results for the as-built grain size distributions. This section presents the grain size distributions of the individual materials and the considered QBA mixes.

Grain Size Distribution of 3×1 PCR Aggregates

The particle size distribution of the large 3×1 PCR aggregates was determined by dry sieve analyses in accordance with ASTM C136/C136M (2019). Sieve analysis tests on the PCR material were also conducted at the quarry. Figure 7 presents the grain size distribution of the PCR aggregates, which shows that the gradations determined at the quarry and ATREL closely match. The nominal maximum aggregate size for the 3×1 PCR material is 3 in. (76 mm), and the gradation falls within IDOT's RR 01 gradation band.

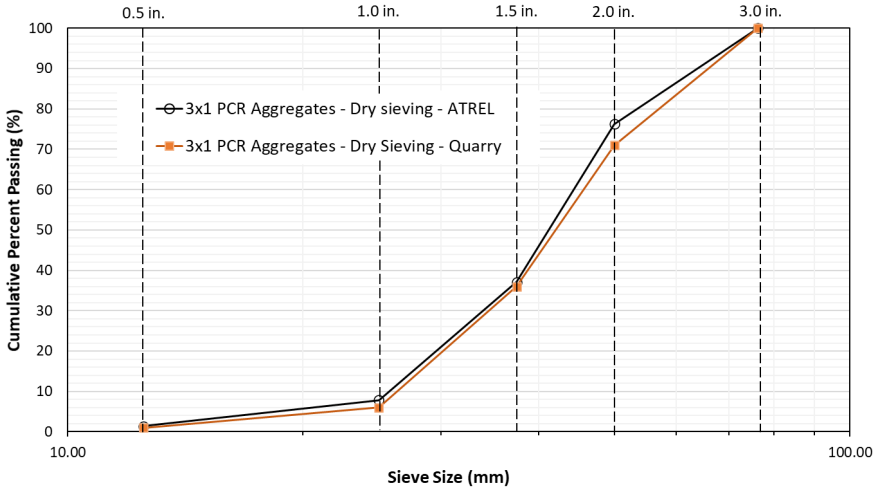

Figure 7. Graph. Grain size distribution of 3×1 PCR aggregates.

Grain Size Distribution of Quarry By-product Material

The particle size distribution of the QB material was determined at the quarry and in ATREL by washed sieving in accordance with ASTM C117 (2017). Dry sieving in accordance with ASTM C136 standard was also conducted at ATREL. Figure 8 presents the grain size distribution of the QB material. The QB material is relatively well graded and all aggregates are smaller than 3/8 in. (9.5 mm) in size. The fines content, i.e. materials passing the No. 200 sieve (less than 0.075 mm in size), is 22% in accordance with washed sieving, which is relatively high. Further, the washed gradations determined at the quarry and ATREL are in close agreement.

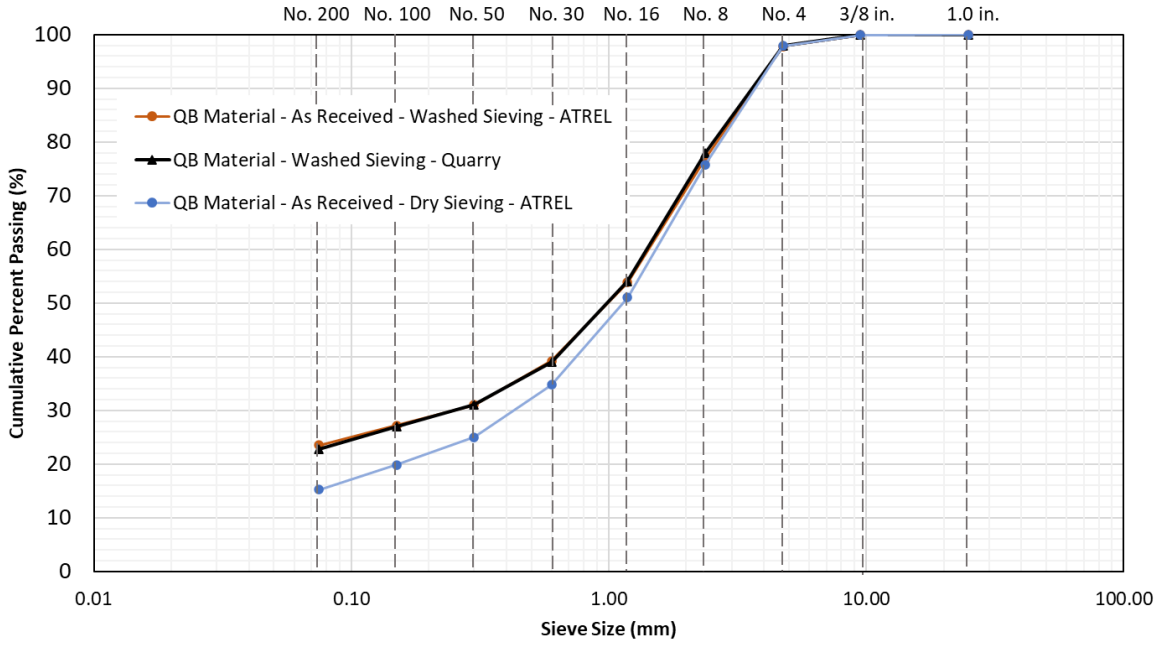

Figure 8. Graph. Grain size distribution of QB material (washed and dry gradations).

Grain Size Distribution of Quarry By-product Aggregate Mixes

Based on the gradation curves presented for the 3×1 PCR aggregates and the QB material, the grain size distribution of three mixes of QBA materials were determined and plotted in Figure 9. The three mixes are a 1:1 mix of PCR:QB (50% PCR aggregates and 50% QB by weight), a 2:1 mix (67% PCR and 33% QB), and a 3:1 mix (75% PCR and 25% QB). The No. 4 sieve (4.75 mm) was designated as the separation between PCR aggregates (larger than No. 4 sieve) and the QB (passing No. 4). Thus, Figure 9 shows that the percent passing No. 4 sieve were 50%, 33%, and 25% for the 1:1, 2:1, and 3:1 mixes, respectively. Note that the 1:1 and 2:1 mixes are similar to what was constructed in the field, while the 3:1 mix was found to contain the optimum QB content if the contact between large aggregates is maximized for the largest shear strength and load-carrying capacity. The three mixes were reproduced in the laboratory to visually illustrate the effect of QB content on the contact between the large aggregates.

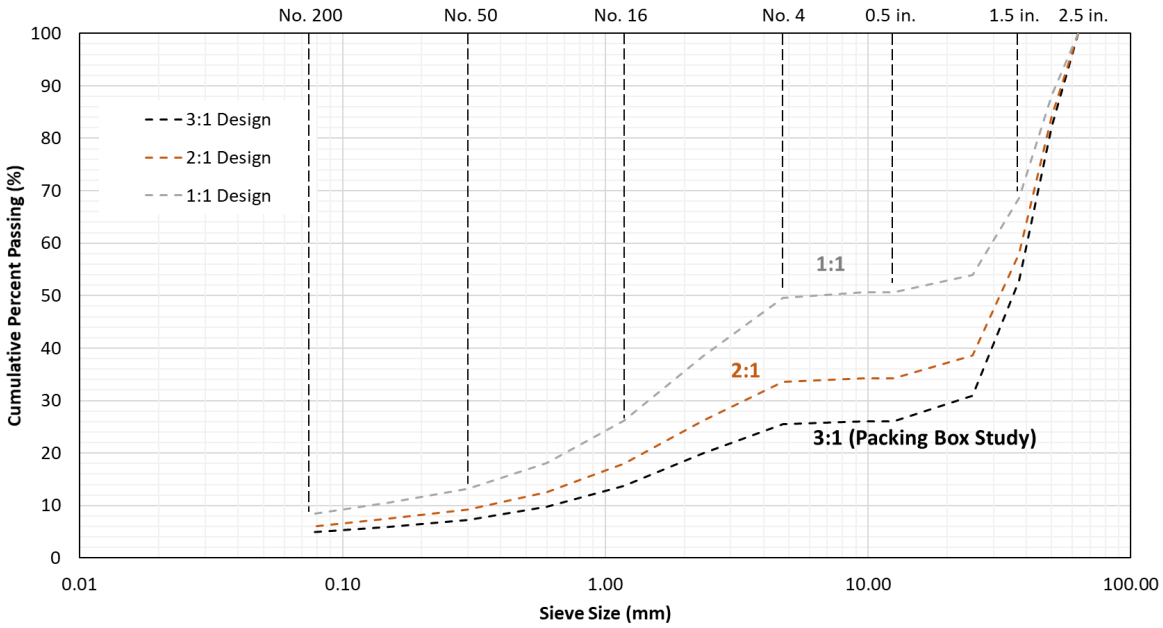

Figure 9. Graph. Proposed grain size distributions of different QBA mixes.

SPECIFIC GRAVITY AND ABSORPTION OF PCR AGGREGATES

Knowing the specific gravity of the large 3×1 PCR aggregates was deemed necessary prior to conducting the packing box studies in order to estimate the porosity and voids' content. The bulk specific gravity of the 3×1 PCR aggregate material was measured as per ASTM C127 (2015), which estimates both specific gravity and percent absorption according to the equations in Figure 10 and Figure 11, respectively:

$$\text{Relative density (specific gravity) (OD)} = \frac{A}{(B-C)}$$

Figure 10. Equation. Calculating relative density (specific gravity).

where *A* is the mass of an oven-dry test sample in air (g), *B* is the mass of a saturated surface-dry test sample in air (g), and *C* is the apparent mass of a saturated test sample in water (g).

$$\text{Absorption (\%)} = \frac{(B-A)}{A} x100$$

Figure 11. Equation. Calculating percent absorption.

where *A* is the mass of an oven-dry test sample in air (g), and *B* is the mass of a saturated surface-dry test sample in air (g).

Based on a representative 3×1 PCR sample of the appropriate size, the specific gravity of the 3×1 PCR aggregates is 2.63, while the percent absorption was determined to be 1.7%.

PACKING BOX STUDIES

Prior to the field construction of sections utilizing 3×1 PCR and QB, a laboratory investigation was conducted to ascertain the optimized blend of large PCR and QB. The customized compaction steel box (the UIUC packing box) with dimensions of 24 in. (610 mm) × 24 in. × 21 in. (530 mm) in height was utilized. The goal was to identify the maximum quantity of QB that could be added to fill the voids in between the PCR while they remained in contact with one another.

As a first step, tests for the compaction of the large 3×1 PCR were conducted to measure the void ratios or porosities using the equations presented in Figure 12, Figure 13, and Figure 14. Three repeat tests were conducted for packing the PCR in the box. For each test, the heights of the loose and compacted rocks were measured at nine locations (center, midpoint of each face, and each corner), and averaged for density calculations. To minimize variability, the same large aggregates were used for all tests. The rocks were handled with care to eliminate breakage that might result in changing how they pack together and with the QB aggregates. The average void ratio and porosity values of 76.1%, and 43.3%, respectively, were calculated using the specific gravity of the 3×1 rocks determined earlier and based on the packing arrangement of the PCR in the box (with no particle crushing or breakage). Based on these calculations, the maximum possible QB quantity to be used was determined to be 43.3% of the weight of the large aggregate subgrade rocks (which is equivalent to a mix of 69.8% PCR and 30.2% QB if all voids could be filled).

Given the challenge of filling all voids, a fourth test was conducted for a QBA mix to determine the maximum QB that could fill the voids without losing rock-to-rock contacts. To achieve this goal, the PCR were placed first in two lifts, and the QB was added from the surface of each lift and driven into the voids by a vibratory action from a lab-sized vibratory roller compactor. Based on this last test, a mix of 75% PCR and 25% QB (3:1 mix) was deemed as the optimized mix. Table 3 gives a summary of the four packing box studies, and Figure 15 shows photos of the tests. The last column in Table 3 lists the surface moduli calculated using a lightweight deflectometer (LWD). The LWD results, which may have been influenced by the rigid box walls, are given as a check of test uniformity and to show the trend of increasing stiffness when QB is used to fill the voids. Note that the method used to prepare the QBA mix in this test is different from the construction method in the field, where the PCR aggregates and QB were mixed at the quarry before construction. Nevertheless, this test was essential to understand the effect of QB content on performance.

$$V_s = \frac{M_s}{G_s * \rho_w}$$

Figure 12. Equation. Calculating volume of solids.

where V_s is the volume of the solids, M_s is the mass of the solids, and ρ_w is the density of water.

$$Porosity\,(\%) = \phi = \frac{V_v}{V_T} x100\%$$

Figure 13. Equation. Calculating porosity (%).

where V_v is the volume of the voids (total volume minus solid volume) and V_T is the total volume.

$$Void\ Ratio\,(\%) = e = \frac{V_v}{V_s} x\,100\%$$

Figure 14. Equation. Calculating void ratio (%).

where V_v is the volume of the voids (total volume minus solid volume) and V_s is the volume of the solids.

Table 3. Summary of Packing Box Test Matrix

Test No.	Materials and Test Description	Percentage of QB (%)	Number of Lifts	Density (pcf)	Porosity (%)	Void Ratio (%)	Composite Surface Modulus (MN/m^3)
1	3×1 PCR	0	2	92.8	43.5	76.8	22.2
2	3×1 PCR	0	2	93.3	43.2	75.9	23.6
3	3×1 PCR	0	2	93.4	43.1	75.7	25.4
4	75.6% 3×1 PCR + 24.4% QB	24.4	2	119.4			37.2

(A) Packing of 3×1 PCR (Test No. 1–3) (B) Packing of 3×1 PCR and QB (Test 4)

Figure 15. Photos. Packing box studies for 3×1 rocks and the 3:1 QBA mix.

PAN ILLUSTRATION FOR QUARRY BY-PRODUCT CONTENT

In an attempt to visualize the packing of the PCR with QB when randomly mixed and placed, several demonstrations were conducted by placing materials in a shallow pan with dimensions of 24 in. × 24 in. × 4 in. for length, width, and height, respectively (1 in. = 2.54 cm). The need for these simulations was to better simulate and understand the field construction method, where the PCR and QB would be premixed at the quarry, shipped by trucks, and then dumped and spread. Further, this illustration helps to visualize the final packing of the mix and identify the recommended QB content that can act as a filler of the voids, while at the same time keeping the PCR in full contact with one another for a higher load-bearing capacity. The large 3×1 PCR act as the primary structure that provides strength to the mix, while the smaller QB particles act as the secondary structure that fills the voids and provide stability (reducing movements and deformations).

Three mixes of large 3×1 PCR aggregates and QB were constructed in the pan, with two repetitions per mix. These mixes are referred to as 1:1, 2:1, and 3:1 QBA mixes, which had large PCR contents of 50%, 67%, and 75%, respectively, and QB contents of 50%, 33%, and 25%, respectively. Mostly, materials were placed to a maximum height of 3 in. (76 mm) inside the pan, which is the nominal maximum aggregate size for the large 3×1 PCR as determined by sieve analysis. The images of the different trials are shown in Figure 16, which captures the top view of each mix.

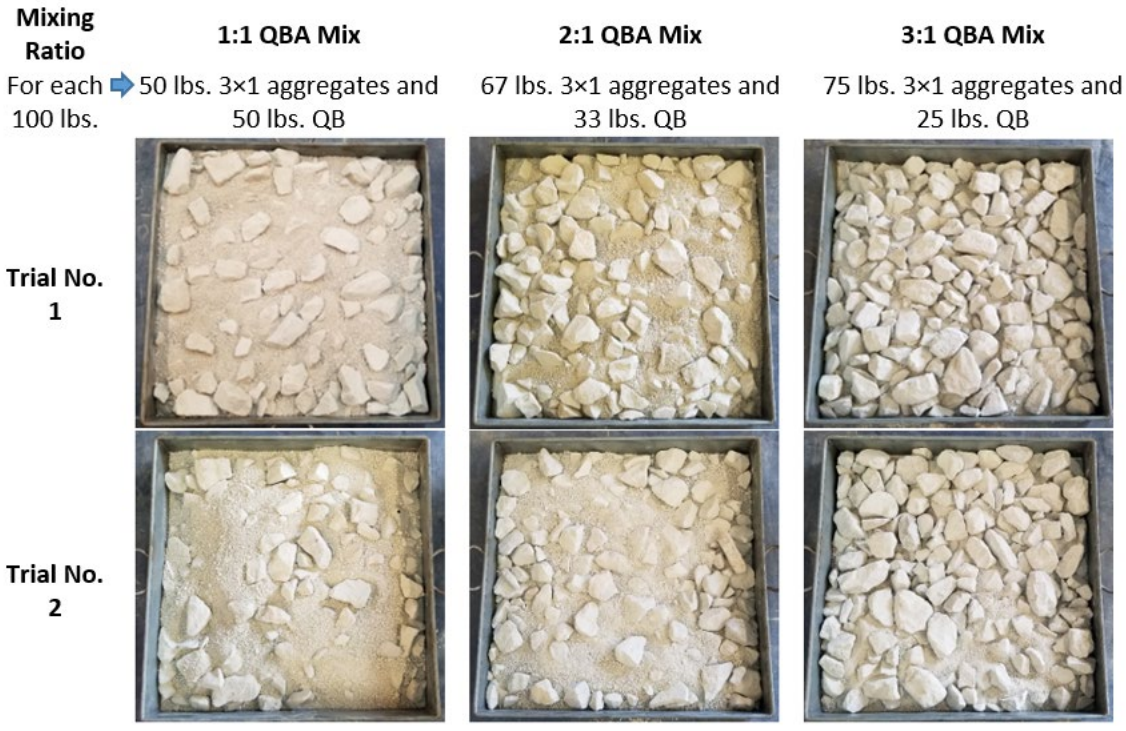

Figure 16. Illustration. Packing of QBA mixes with different mixing ratios.

A 1:1 mix of 3×1 PCR and QB produce a mix with large aggregates floating in QB and barely any contact between the large aggregates. A 2:1 mix provides more rock-to-rock contacts, but most of the particles are still floating in QB, reducing the shear strength. In contrast, a 3:1 mix provides more

contact between the large particles, and most of the 3×1 PCR are in contact. Note that even with the 3:1 mix, some localized fine pockets (QB) can be formed due to nonuniformity and segregation (which is clearer from Trial 2 with the 3:1 mix). However, most of the large particles will remain in contact, thus providing enough strength.

CHAPTER 4: FIELD CONSTRUCTION AND EVALUATION

This chapter presents details on the construction and sampling of the quarry by-product aggregate (QBA) materials in the field, as well as the data and interpretation from conducted field testing and evaluation. The proper construction and compaction of the QBA materials was evaluated using dynamic cone penetrometer (DCP) and lightweight deflectometer (LWD) on top of the natural subgrade and the aggregate subgrade improvement (ASI) capping layers. Falling weight deflectometer (FWD) on top of the capping layer and hot-mix asphalt (HMA) was also used to check layer stiffness and load-carrying capacity.

CONSTRUCTION

Construction of subgrade improvements with QBA at Larry Power Road in Bourbonnais Township took place on July 27, 2020. Selected construction and testing photos are presented in Appendix B. The material was plant mixed using loaders at the Vulcan Lehigh quarry in Kankakee County, Illinois, and brought to the construction site using trucks. Truck loads were dumped near the construction location and spread using a bulldozer. Visual inspection of the truck loads and videos/images collected for the stockpiles and the spread material did not show evidence of severe material segregation. The segregation levels were in a typical range to what is normally seen for dense-graded aggregate materials. The spread of the material with a bulldozer also helped with remixing and provided more uniformity for the placed mixes. Figure 17 shows part of the construction activities for constructing the QBA_M1 mix having 55% PCR and 45% QB in composition.

Figure 17. Photo. Placement and spreading of QBA_M1 material in the field.

Figure 18 shows representative images of the QBA_M1 and QBA_M2 mixes after placement and before compaction. These mixes were compacted using a vibratory roller, with a sufficient number of passes to ensure proper placement. Note that IDOT requirements for ASI layers do not specify a target density or a certain number of passes (compactive effort) for ASI layers, but these layers should be compacted to the satisfaction of the engineer. The nominal thickness of the QBA layers was 9 in. (229 mm). A 3 in. (76 mm) densely graded virgin crushed stone capping layer was placed and compacted on top of the QBA material. Similar construction activities were also conducted on the east side of the bridge, except that a conventional CS02 aggregate material was used instead of the QBA materials, and both virgin crushed stone and RAP were used as capping materials. The ASI layers were topped with 10.75 in. (273.1 mm) of HMA: a 9.25 in. (235 mm) binder course and a 1.5 in. (38.1 mm) surface course.

(A) QBA_M1 (45% QB, 55% PCR) (B) QBA_M2 (31% QB, 69% PCR)

Figure 18. Photo. Comparison of QBA_M1 and QBA_M2 after placement and before compaction.

FIELD SAMPLING OF QUARRY BY-PRODUCT AGGREGATE MATERIALS

Representative field samples from QBA_M1 and QBA_M2 mixes were collected from truck dumps during construction. Several bags were collected for each material and transported back to ATREL for sieving to determine the as-delivered gradations. For each mix, four bags were randomly selected and separated into two samples with two bags each. Sieving was conducted in accordance with ASTM C136 (2019) using a proper sample size and a Gilson H-4276 sieve shaker equipment.

Figure 19 shows the as-delivered gradations of the two samples for QBA_M1. The gradation has 45.5% QB-sized materials passing No. 4 sieve (4.75 mm) and 54.5% of PCR. The gradation of this material more closely resembles a 1:1 mix. The gradation of the two randomly selected samples were identical. Figure 20 presents the gradation of the QBA_M2 mix. The as-delivered gradation has, on average, 30.9% QB-sized materials and 69.1% PCR. The two randomly selected samples had more variability than the QBA_M1 mix, but the difference in material percentage retained on any sieve size was no more than 4% for both samples. The QBA_M2 material gradation more closely resembles a 2:1 mix.

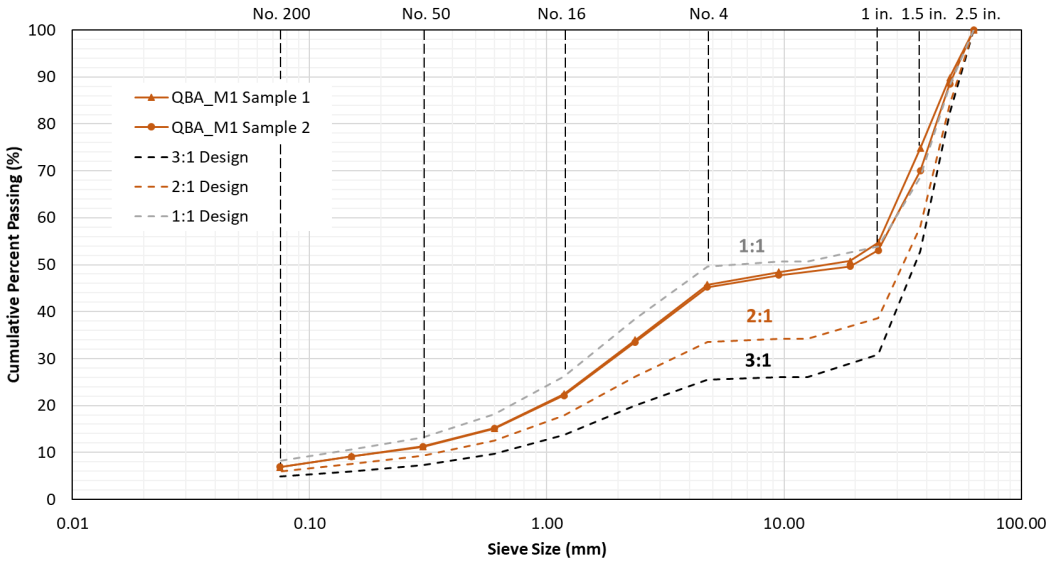

Figure 19. Graph. Grain size distributions of field samples collected from QBA_M1 mix.

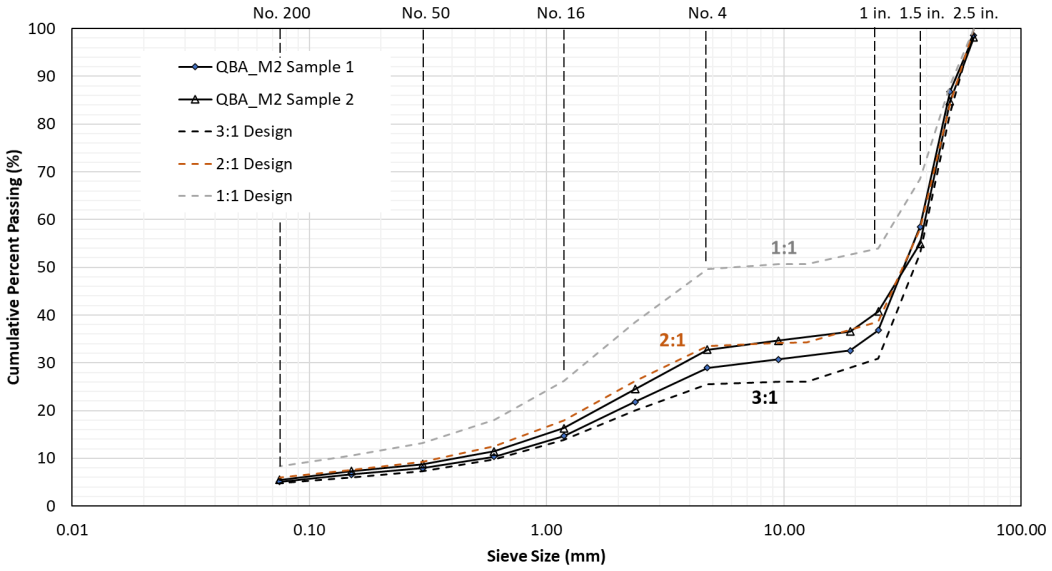

Figure 20. Graph. Grain size distributions of field samples collected from QBA_M2 mix.

FIELD EVALUATION—DYNAMIC CONE PENETROMETER

DCP tests were conducted on top of the natural subgrade and on top of the capping layer for all sections on the west and east sides of the bridge. When DCP tests were conducted on top of the capping layers, the penetration depth at each testing point was enough to cover the depth of the ASI layer and the top part of the underlying prepared subgrade. (These data points were mostly taken closer to the curb—6 ft (1.83 m) from the curb—in the vehicle's wheel path of the traffic lane in both

directions.) For all testing points, the depth of the ASI layer was assumed to be 12 in. (305 mm) unless otherwise evident from the data that a slightly thicker/thinner layer was constructed.

The IBV was back-calculated from the penetration rate, PR (in/blow) of the DCP, to estimate the strength profile with depth at each DCP location. Figure 21 gives the IDOT equation for calculating IBV (%). Note that this equation was developed and calibrated for low-strength subgrade soils with relatively low IBV number. Figure 22 shows an example of the DCP profile at one station in each section. The DCP profiles for the natural subgrades for all stations are presented in Appendix C and Appendix D. Note that different DCP/IBV profiles are expected at different locations because of construction and soil-type variability. In some locations with poor muddy soils, IDOT engineers confirmed that soil was removed and replaced, further increasing the variability in subgrade soil conditions. Overall, some spots along the depth had low IBV numbers of three or less, and these low values necessitated the use of an additional aggregate subgrade layer of 12 in. (305 mm) as a subgrade remediation action.

$$IBV(\%) = 10^{(0.84-1.26*LOG(PR))}$$

Figure 21. Equation. Calculating IBV (%) from DCP penetration rate in inches per blow.

where *PR* is the penetration rate in inches per blow (in./blow).

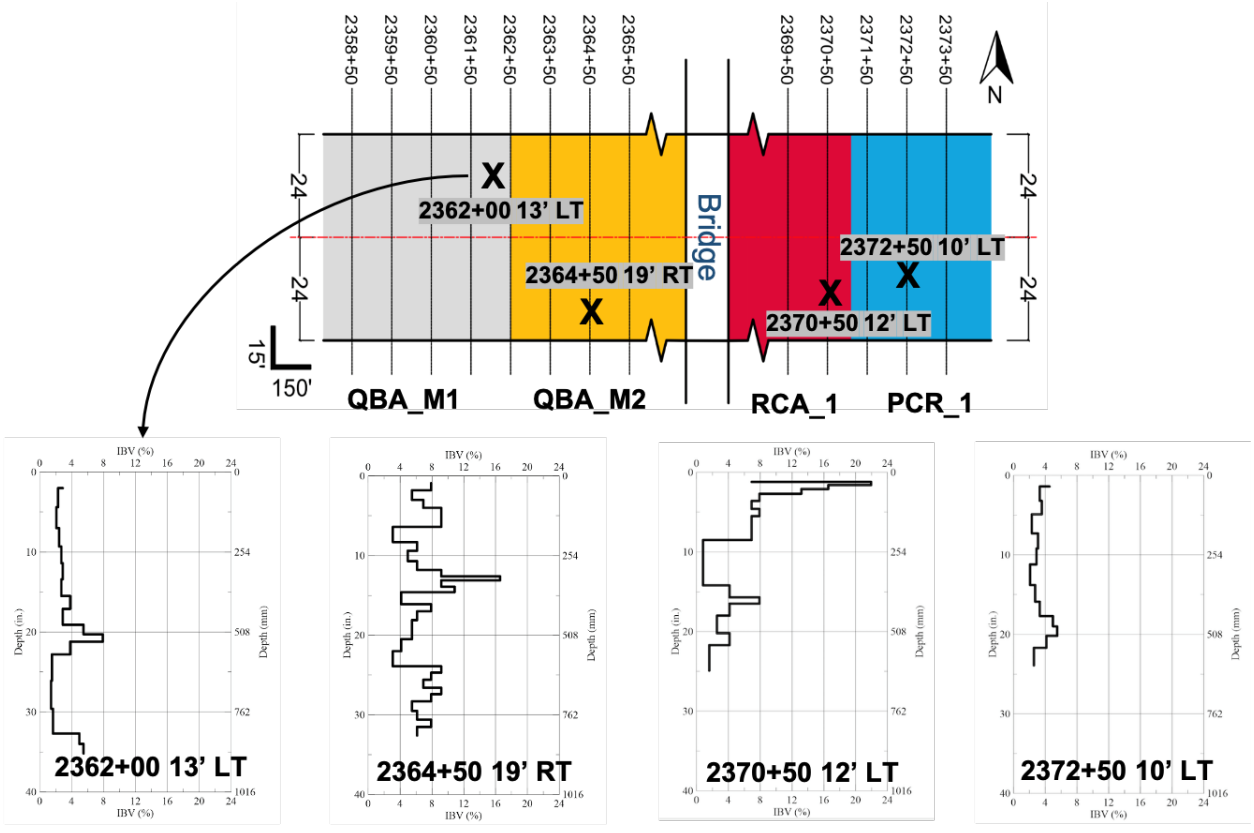

Figure 22. Graph. Sample DCP depth profiles for the prepared natural subgrade under all sections.

Figure 23 shows a summary of the average subgrade IBV at different locations on the west side of the bridge, where the QBA layers were constructed, and Figure 24 presents a summary of the average IBV at the sample locations on the east side of the bridge, where conventional ASI layers were constructed. Note that the high IBV values are part of the prepared natural subgrade because they continue to high depths in the DCP profile. The higher values are mostly toward the curbs of the roadway, where the road widening work necessitated bringing and compacting borrowed soil materials to create a more stable subgrade compared to the existing material. Figure 25 presents a box plot summary and comparison of the prepared subgrade IBV in the four test sections. The whiskers show the maximum and minimum values (excluding outliers), while the boundaries of the box present the 25th and the 75th quartiles (upper and lower quartiles) of the values. It is evident that the natural prepared subgrade under the QBA_M1 ASI improvement with the higher QB content (45%) has the lowest and the least variable subgrade IBV, followed by the RCA_1 section with conventional CS02 ASI and RAP capping. The natural subgrade soil under the QBA_M2 and PCR_1 sections is stronger and has higher variability. On average, the median IBVs of the prepared subgrade under sections QBA_M1, QBA_M2, RCA_1, and PCR_1 are 8.4%, 12.9%, 8.6%, and 17.7%, respectively, and excluding outliers. The DCP profiles in the areas closest to the curb were measured following a period of drought, so the use of aggregate subgrade layers is justified on top of this soil, where the strength can drop significantly because of moisture intrusion.

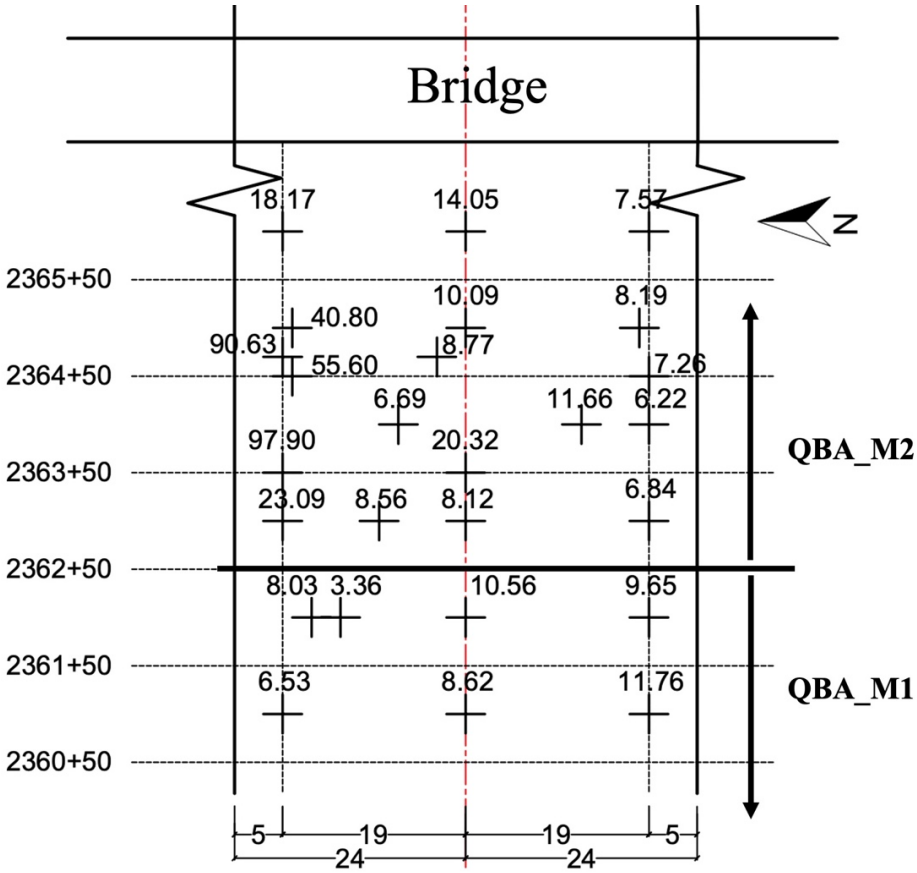

Figure 23. Plot. Achieved IBV(%) in the prepared natural subgrade (west side of bridge).

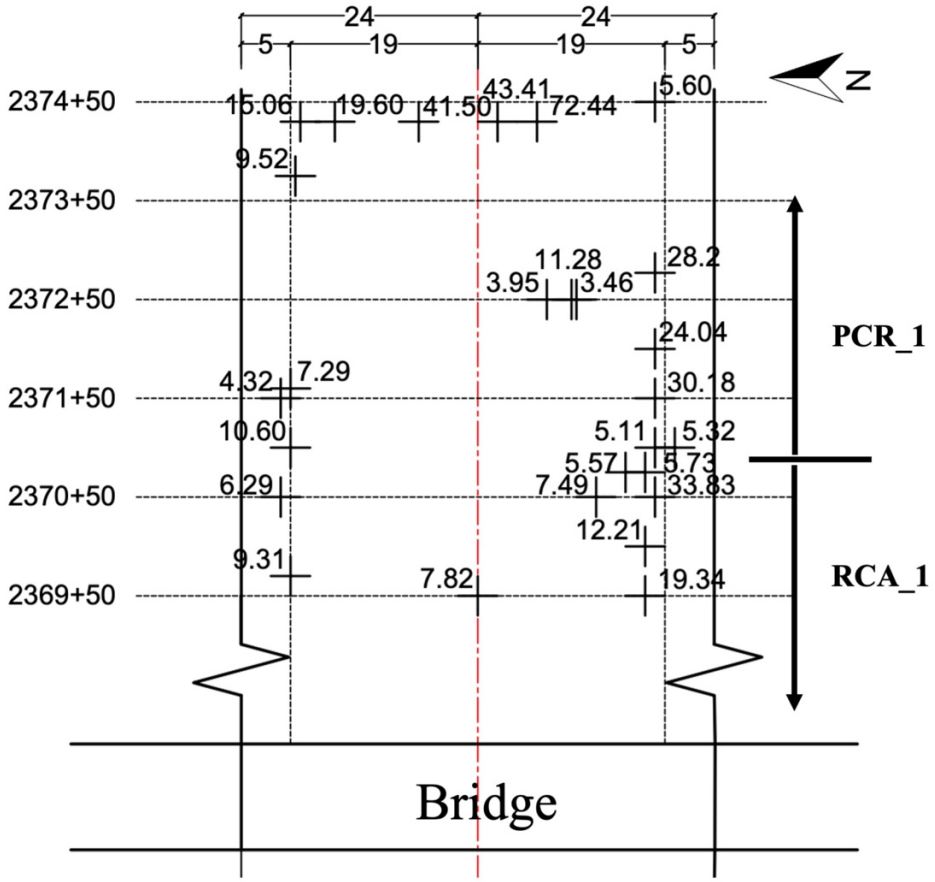

Figure 24. Plot. Achieved IBV(%) in the prepared natural subgrade (east side of bridge).

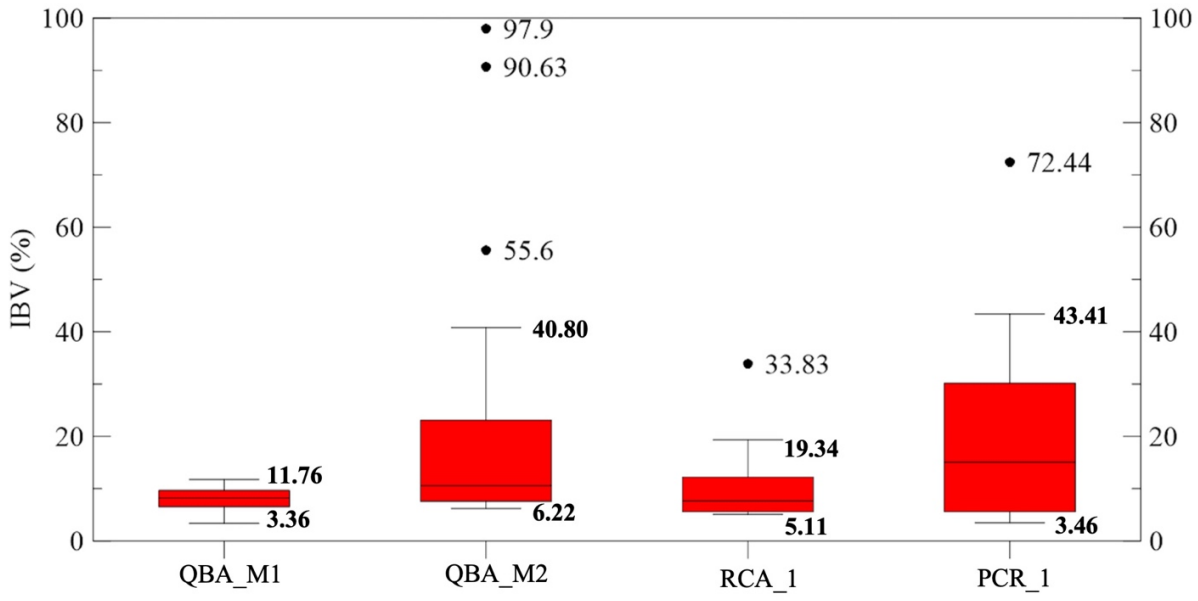

Figure 25. Diagram. Summary of average DCP (IBV) results for prepared natural subgrade.

The DCP profile in the ASI layers, consisting of 3 in. (75 mm) of capping layer underlain by 9 in. (229 mm) of QBA or conventional CS02 materials, was also evaluated at selected points in each section. Figure 26 presents a sample of the IBV profiles calculated from DCP penetration rates for the different sections. The full data for DCP profiles collected on top of capping layers is presented in Appendix E and Appendix F. Note that IDOT's DCP/IBV equation presented in Figure 21 was applied for these stiffer materials to calculate the strength profile from DCP penetration rates. For calculation purposes, a 12 in. (305 mm) nominal thickness was used to average and report the IBV numbers. Further, because 0.1 in. (2.5 mm) is the smallest increment that could be practically recorded for DCP penetration in the field, the upper IBV value was limited to 125.9% at any point, which is equivalent to a 0.1 in. penetration when the equation in Figure 21 is used.

Figure 27 shows a summary of the average IBV of the ASI layers at different locations on the west side of the bridge, where the QBA layers were constructed. The average IBV numbers for the QBA_M1 mix ranged between 77% and 111%, and between 48% and 98% for the QBA_M2 section with lower QB content (45% vs. 31% QB content, respectively). The opposite trend was expected for these two sections because the QBA_M2 section has more PCR content and is expected to have a higher average IBV. Nevertheless, the average IBV of this QBA_M2 section (71%) still indicates a relatively strong mix. The lower IBV for this section compared to the QBA_M1 section is not fully understood. Figure 28 presents the average IBV numbers for the conventional ASI sections on the east side of the bridge. The IBV numbers for the RCA_1 section with RAP capping material ranged between 53% and 75%, and ranged between 45% and 96% for the PCR_1 section with virgin capping material. These values also indicate strong mixes were constructed. When the average IBVs are considered, the PCR_1 section with virgin crushed stone capping material had slightly higher IBV numbers than the RAP section, but the two sections were comparable. Note that the DCP profiles for the four sections were taken in the vehicle wheel path, i.e., approximately 9 in. or 229 mm from the curb, in the driving lane and in both directions.

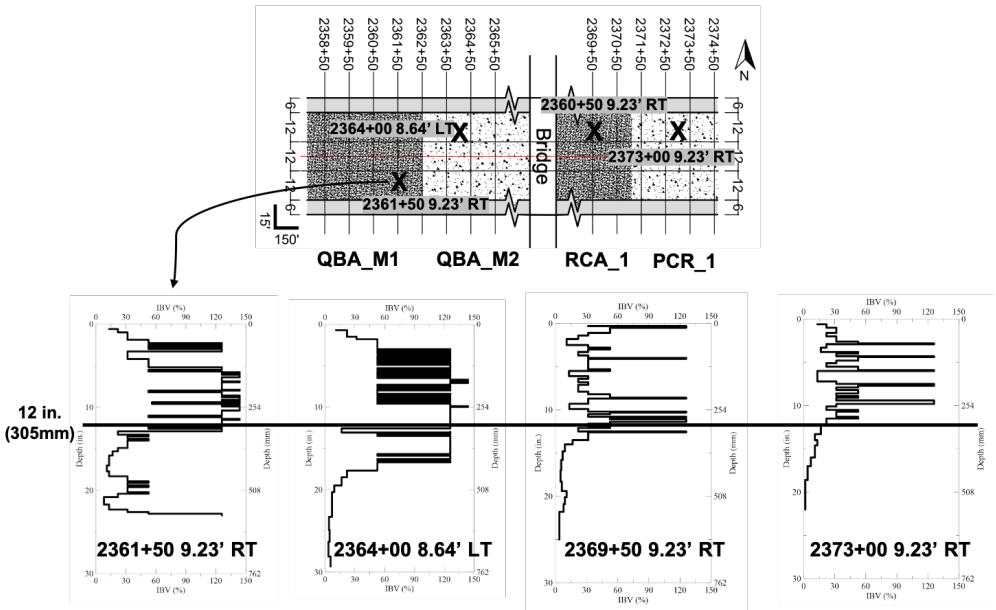

Figure 26. Graph. Sample DCP depth profiles on top of ASI capping layers.

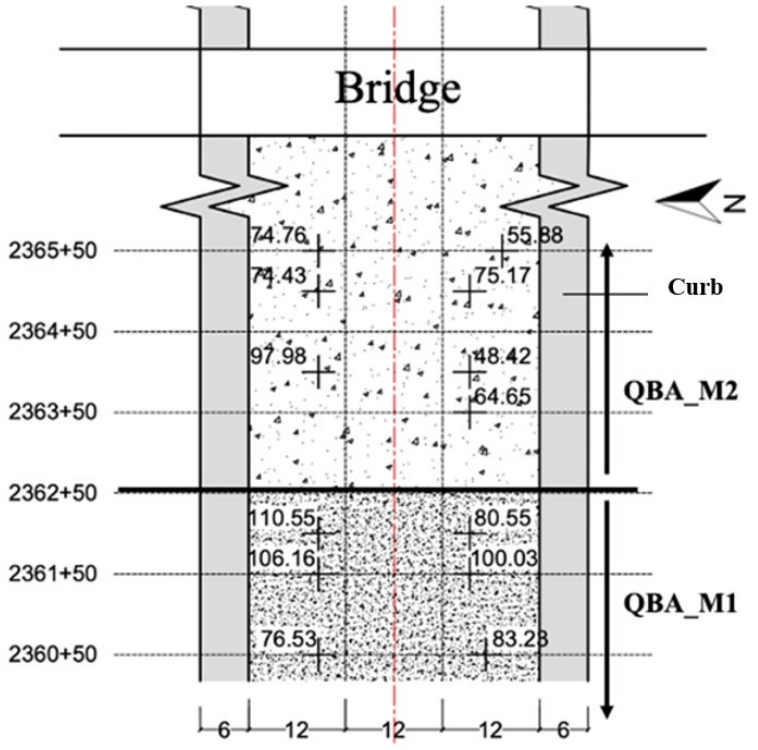

Figure 27. Plot. Achieved average IBV(%) in the ASI layers (west side of bridge).

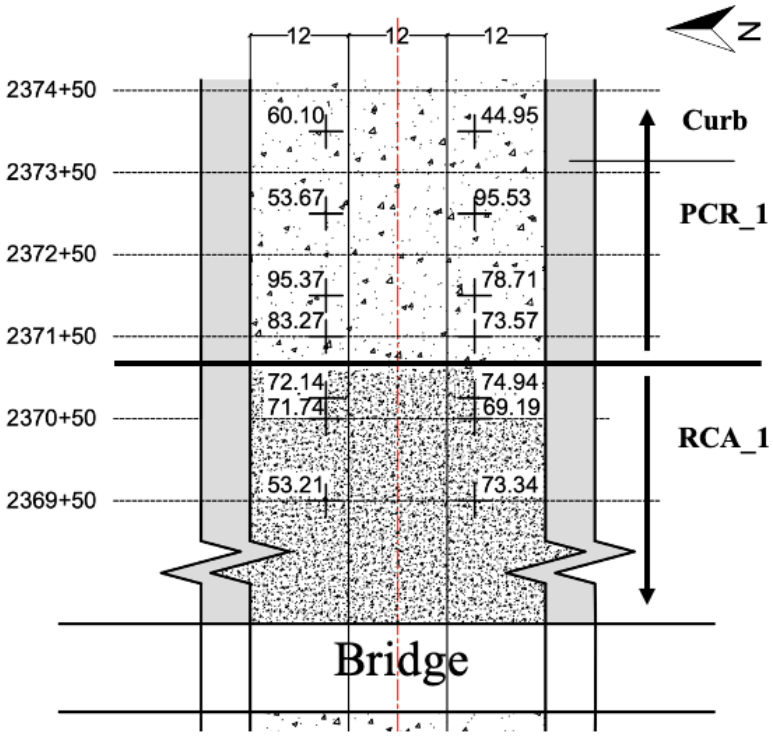

Figure 28. Plot. Achieved average IBV(%) in the ASI layers (east side of bridge).

Figure 29 presents the box-and-whisker plots to compare the range of IBV numbers of the ASI and capping layers of the four test sections. It is evident from these plots that the DCP profiles within each section show some variability, with the RCA_1 section showing the least variability. On average, the median IBVs of the ASI layers in sections QBA_M1, QBA_M2, RCA_1, and PCR_1 are 92%, 74%, 72%, and 76%, respectively, and exclude outliers, where the latter three sections have fairly similar average IBV numbers. The DCP profiles were measured following a period of drought, so the values measured for the sections with QBA could become slightly lower in the incident of moisture inclusion.

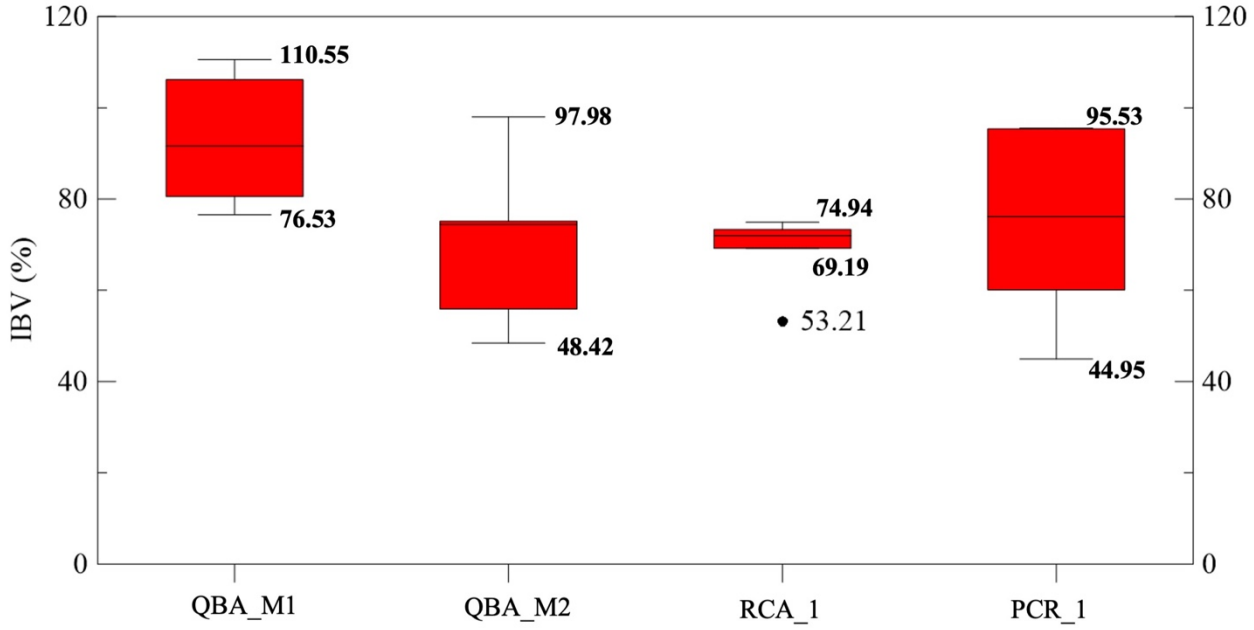

Figure 29. Diagram. Summary of average DCP (IBV) results for the different ASI layers.

FIELD EVALUATION—LIGHTWEIGHT DEFLECTOMETER

To evaluate the quality of the constructed test sections, the composite surface moduli on top of the prepared subgrade, QBA layers, and capping layers on both sides of the bridge were measured using a lightweight deflectometer (LWD). A minimum of six LWD drops, including three seating drops, were carried out at each measuring point. To ensure the uniformity of the surface, a thin layer of sand was placed at the locations of LWD drops. This was especially necessary on top of the QBA layers and capping layers, where the surface elevation could vary widely. All measurements were taken using a Zorn LWD, with a falling weight of 11 lb (5 kg) and a drop height of 14.8 in. (0.375 m).

Figure 30 presents the summary results from LWD testing on top of the prepared subgrade on the west side of the bridge. The average surface modulus of the subgrade under the QBA_M1 section is 1.3 ksi (8.9 MN/m^2) compared to 4.8 ksi (33.1 MN/m^2) for the QBA_M2 section with lower QB content. Note that the back-calculated LWD moduli are low, but the LWD data were mostly used to assess construction uniformity, while layer moduli are later calculated more reliably using falling weight deflectometer (FWD) data. Figure 31 presents the FWD results on top of the QBA materials before the placement of the capping layer. The QBA_M1 section had a significant increase in stiffness

upon the addition of the aggregate subgrade layer (average surface moduli of the QBA_M1 and QBA_M2 sections before placement of capping layer are 3.5 ksi [23.9 MN/m^2] and 5.0 ksi [34.7 MN/m^2], respectively). Full LWD results on top of subgrade are presented in Appendix G.

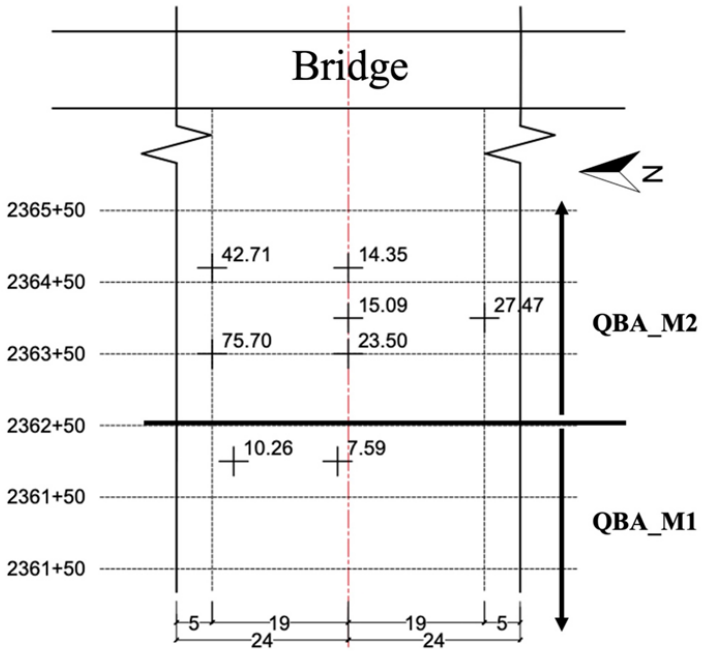

Figure 30. Plot. Subgrade moduli in MN/m^2 measured with LWD for sections west of the bridge. (1 ksi = 6.89 MN/m^2)

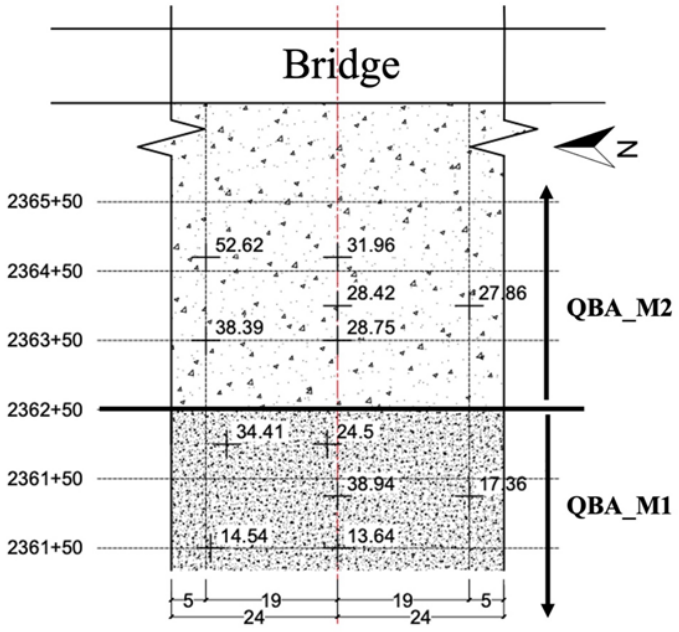

Figure 31. Plot. Composite surface moduli in MN/m^2 on top of QBA mixes, measured with LWD. (1 ksi = 6.89 MN/m^2)

Figure 32 presents the surface moduli measured by LWD on top of the virgin capping layer for the QBA_M1 and QBA_M2 sections on the west side of the bridge. For the QBA_M1 section with higher QB content of 45%, the surface moduli ranged between 2.8 ksi (19.0 MN/m^2) and 9.9 ksi (68.6 MN/m^2) with an average of 6.1 ksi (42.4 MN/m^2). For the QBA_M2 section with lower QB content of 31%, the surface moduli ranged between 4.2 ksi (29.1 MN/m^2) and 10.8 ksi (74.3 MN/m^2) with an average of 6.8 ksi (46.9 MN/m^2). Thus, the two sections have, on average, similar surface moduli with some variability resulting from the variability naturally inherent in construction. The two sections are expected to perform similarly because the placement of the ASI layer with virgin crushed stone capping aggregate evened out the differences in section stiffnesses compared to the discrepancies in the underlying prepared subgrade layer. In comparison, Figure 33 presents the surface moduli on top of the capping layers for the conventional ASI layers on the east side of the bridge. The surface moduli for the RCA_1 section with a RAP capping ranged between 8.1 ksi (55.7 MN/m^2) and 11.3 ksi (78.1 MN/m^2), excluding one outlier, with an average of 9.5 ksi (65.8 MN/m^2), while that for the PCR_1 section with a virgin capping ranged between 4.2 ksi (28.9 MN/m^2) and 17.6 ksi (121.3 MN/m^2) with an average of 9.7 ksi (67.2 MN/m^2). Despite having high variability, both sections had, on average, similar surface moduli and are expected to perform similarly after the placement of the thick HMA layer.

Figure 34 presents a side-by-side comparison of the surface moduli measured on top of the capping layers for the four sections. The full LWD data on top of QBA and on top of the capping layers on both sides of the bridge is presented in Appendix H and Appendix I. The conventional PCR layers on the east side of the bridge had higher surface moduli, while the QBA_M1 and QBA_M2 sections had significantly lower surface moduli. These results are expected because the conventional sections have full contact between the large-sized particles, leading to higher loading capacity, strength, and stiffness, while the presence of high QB content can separate the large rocks and lead to lower strength and stiffness. Nevertheless, it will be shown later in this chapter that the presence of HMA on top of the QBA layers reduced these differences and led to similar FWD deflections, indicating that QBA layer construction is a sustainable and effective construction practice, which can have more prominent long-term effects such as reducing permanent deformation and increasing ASI layer stability.

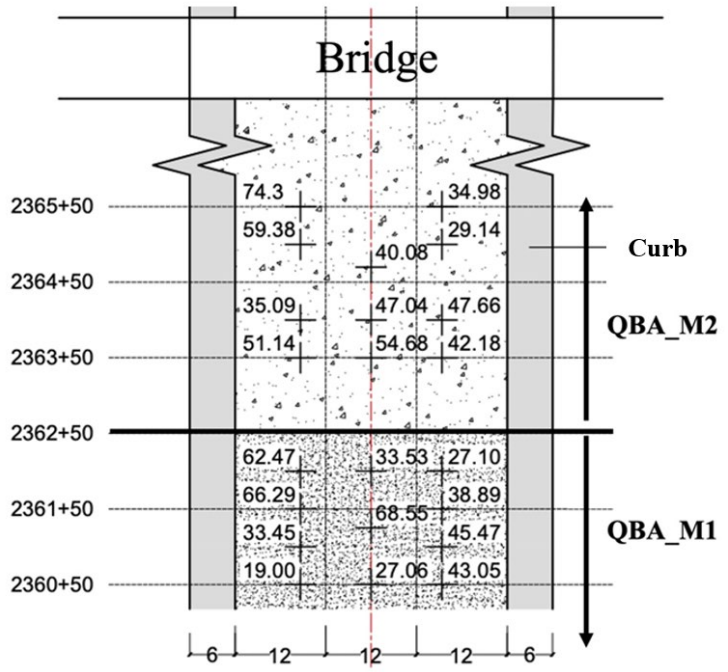

Figure 32. Plot. Composite surface moduli in MN/m^2 on top of capping layer for QBA sections on the west side of the bridge. (1 ksi = 6.89 MN/m^2).

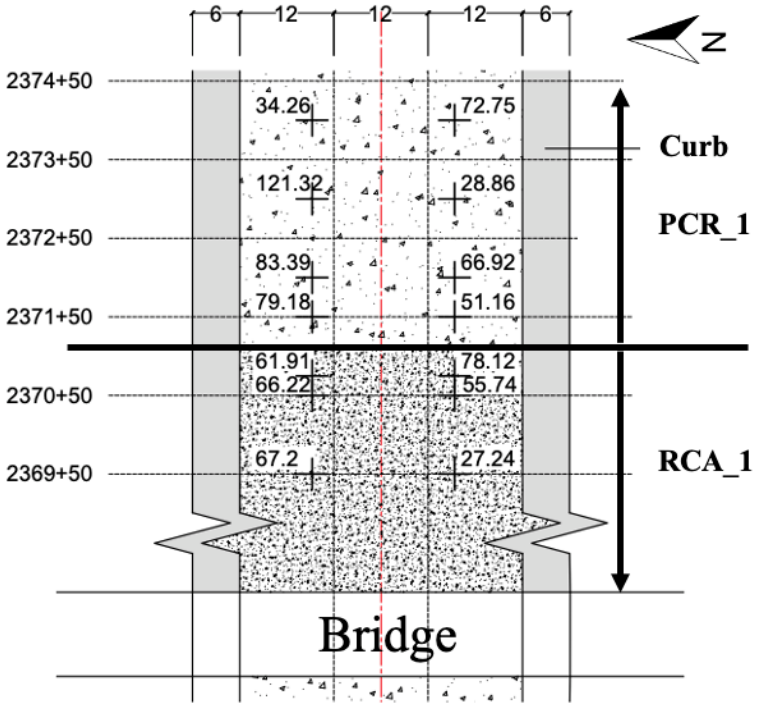

Figure 33. Plot. Composite surface moduli in MN/m^2 on top of capping layer for conventional ASI sections on the east side of the bridge. (1 ksi = 6.89 MN/m^2).

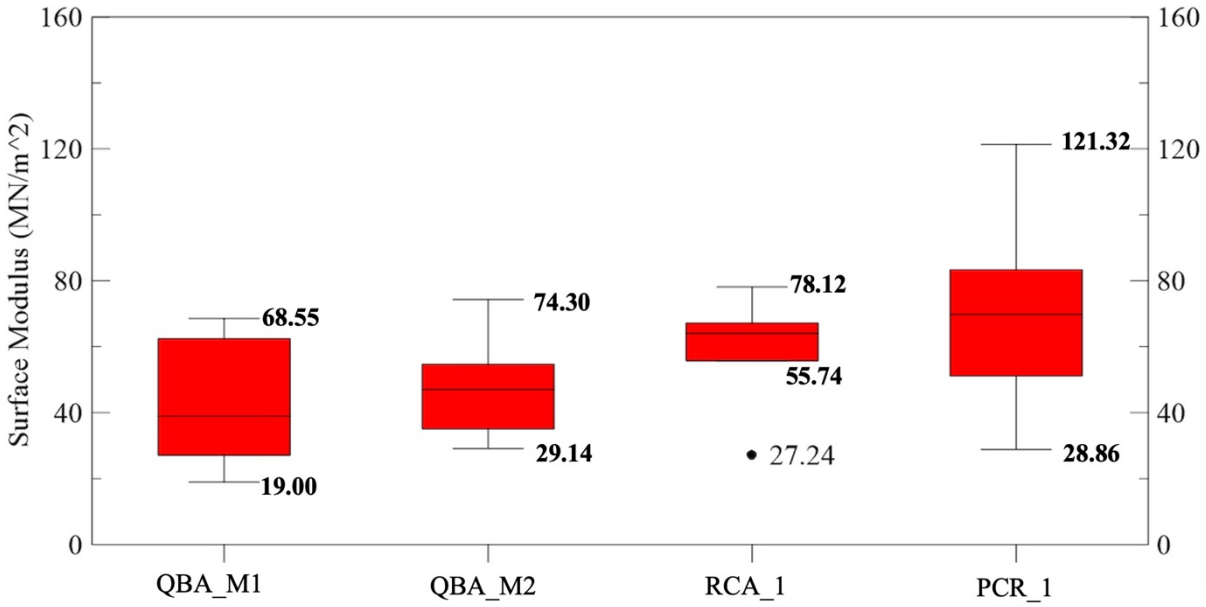

Figure 34. Diagram. Summary of LWD composite surface moduli on top of capping layers (1 ksi = 6.89 MN/m^2).

Table 4 presents a summary of the average LWD and DCP results on top of the capping layers for all sections. All trends and values are within expectations given the composition of the different sections, except for the high IBV of the QBA_M1 section, which is not fully understood but could be due to a sampling issue and could be resolved if more DCP data points were taken in that section.

Table 4. Average DCP and LWD Results on Top of Capping Layers

Section / Field Test	IBV (%) by DCP	Surface Modulus (MN/m^2) by LWD*
QBA_M1	92.8	42.3
QBA_M2	70.2	46.7
RCA_1	72.3	65.8
PCR_1	73.2	67.2

* 1 ksi = 6.89 MN/m^2

FIELD EVALUATION—FALLING WEIGHT DEFLECTOMETER

The analyses and interpretations of falling weight deflectometer (FWD) data can be divided into two broad approaches: (1) forward analysis methods, which calculate pavement responses, and (2) back-calculation methods, which predict pavement responses (Smith et al. 2017). This section presents the results of FWD tests conducted on top of the capping layers and on top of the HMA after paving and before opening to traffic. The deflections on top of the capping aggregates are first compared to draw conclusions on the stability and stiffness of the constructed ASI layers. For FWD tests on top of HMA,

common deflection basin parameters were first calculated to compare the structural integrity of the four sections. Then, the modulus of each constructed layer is calculated using two popular and commercially available back-calculation programs: PCASE by US Army Corps of Engineers Engineer Research and Development Center (ERDC) and ELMOD by Dynatest (formerly).

Falling Weight Deflectometer Tests on Top of Capping Layers

FWD tests were conducted by Applied Pavement Technology (APTech) on top of the capping aggregates. At each drop location, FWD tests were conducted by dropping three different load levels to induce variable stress states in pavement layers and detect the surface deflections from seven geophones that are set 12 in. (305 mm) apart, including a center geophone directly under the load drop location. The complete data covering all deflection basins from the conducted tests are presented in Appendix J for the QBA_M1 and QBA_M2 test sections on the west side of the bridge and in Appendix K for the RCA_1 and PCR_1 sections on the east side of the bridge. The load level for each drop is also listed in the appendices. FWD tests were conducted at an average ambient temperature of 83°F (28°C) and a surface temperature of 89°F (32°C). The standard deviation in temperature was ±1°F (±0.56°C).

For comparative purposes, the FWD deflections were normalized from the three drops to a 12 kip (53 kN) load level, applying a uniform pressure of 107 psi (735 kPa) over a circular area with a radius of 5.9 in. (150 mm). A 12 kip load was selected instead of the standard 9 kip (40 kN) load level because some load levels applied on the east side of the bridge were higher than the standard 6, 9, and 12 kip load levels (1 kip = 4.44 kN) due to difficulties with running the FWD on top of the nonuniform capping layer surfaces. The 12 kip (53 kN) data were more readily available for all testing locations and was selected for comparison. Further, the FWD data on top of the capping aggregates was carefully checked to eliminate odd and nondecreasing data points to ensure they were not included in the analysis. Note that Appendix J and Appendix K only show the accepted data points after eliminating nondecreasing deflection basins. The main cause of nondecreasing deflections could be attributed to surface irregularities affecting the loading plate or sensors, as all tests were performed on top of the capping aggregate layer. Additionally, the area experienced rain in the days before testing, which could have contributed to soft conditions in the deeper layers. On the east side of the bridge, 73 out of 144 drops had at least one nondecreasing point. On the west side of the bridge, 82 out of 108 drops had the same behavior. In both cases, most of these differences were observed for the far-out sensors, which tend to relate to the stiffness of deeper layers. Note that several data points also had deflection levels exceeding the center geophone capacity, and these data points were also eliminated from the analysis.

Using FWD deflection basin data on top of the capping aggregate layers and eliminating all data points exceeding FWD geophone capacity or showing a nondecreasing trend, a summary of FWD center deflections (D_0) in mils is given in Figure 35 for the individual data points. Figure 36, in contrast, shows a box-and-whisker plot comparison of the distribution of FWD deflection in the four field test sections. The data shown in both figures are normalized to a 12 kip (53 kN) load level. The FWD center deflections varied the most for sections QBA_M2 with lower QB content (31%) and section PCR_1 with conventional ASI and virgin capping. The least variability was seen for section RCA_1 with conventional ASI and RAP capping. Despite this variability, sections QBA_M2, RCA_1, and

PCR_1 had relatively similar median and average FWD center deflections (average deflections of 74, 56, and 64 mils, respectively, and median deflections of 61, 55, and 51 mils, respectively). The QBA_M1 section had the highest FDW center deflection (average 112 mils and median 116 mils), which is significantly higher than those for the other three sections. When a high load level was used to induce high stress states in the pavement, the QBA_M1 section with the higher QB content of 45% showed the weakest behavior and least stiffness with the QB separating the large PCR aggregates and creating weak shear planes. For the other QBA section (QBA_M2) with 31% QB content, the FWD center deflections were slightly higher but not statistically different than those for the conventional sections and, thus, is expected to have good field performance.

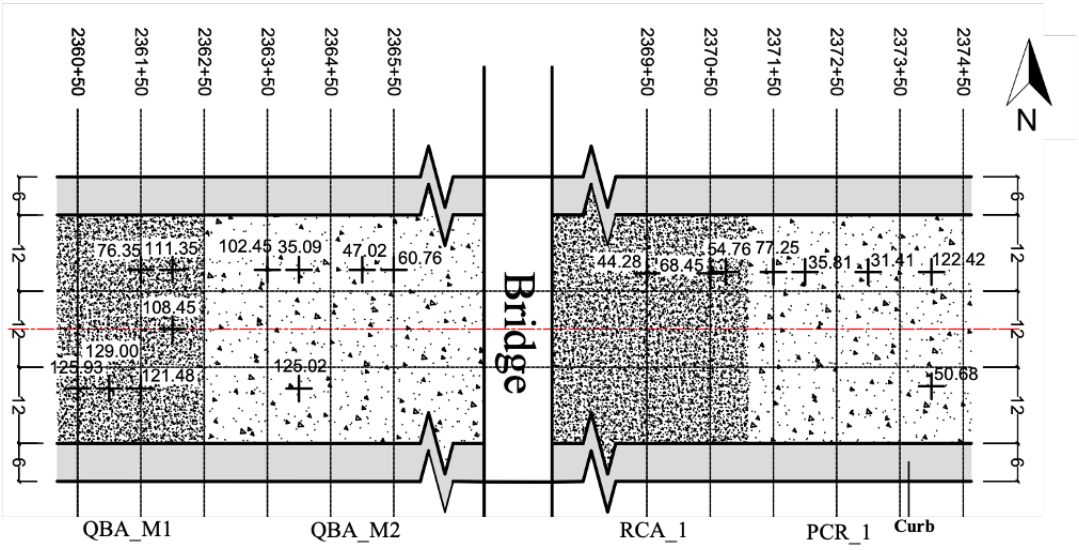

Figure 35. Plot. FWD surface deflections (mils) of center geophone (D_0) on top of capping layer, normalized to a 12 kip (53 kN) load level.

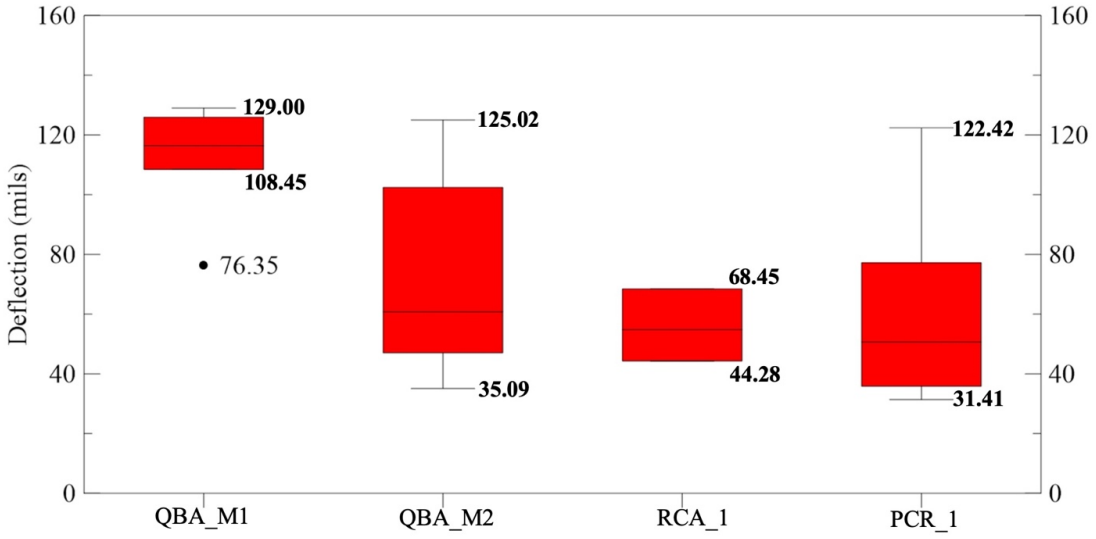

Figure 36. Diagram. Summary of FWD surface deflections (mils) of center geophone (D_0) on top of capping layer, normalized to a 12 kip (40 kN) load level.

Falling Weight Deflectometer on Top of Hot-mix Asphalt—After Construction

FWD tests were conducted by APTech after the construction of the 10.75 in. (273 mm) HMA binder and surface course layers and before opening the road to traffic. At each drop location, FWD tests were conducted by dropping four load levels (6, 9, 12, and 15 kips; 1 kip = 4.44 kN) to induce variable stress states in pavement layers and detect the surface deflections from seven geophones set 12 in. (305 mm) apart, including a center geophone directly under the load drop location. Four load levels were used to offer additional data for more closely matching the loading levels obtained during the first round of testing, when the site was unpaved. The complete data for all deflection basins from the conducted tests are presented in Appendix L for the QBA_M1 and QBA_M2 test sections on the west side of the bridge and in Appendix M for the RCA_1 and PCR_1 sections on the east side of the bridge. The load level for each drop is also listed in the appendices. FWD tests were conducted at an average ambient temperature of 50.5°F (10.3°C) and a surface temperature of 53.5°F (11.9°C). The standard deviation in surface temperature was ±3.5°F (±1.94°C).

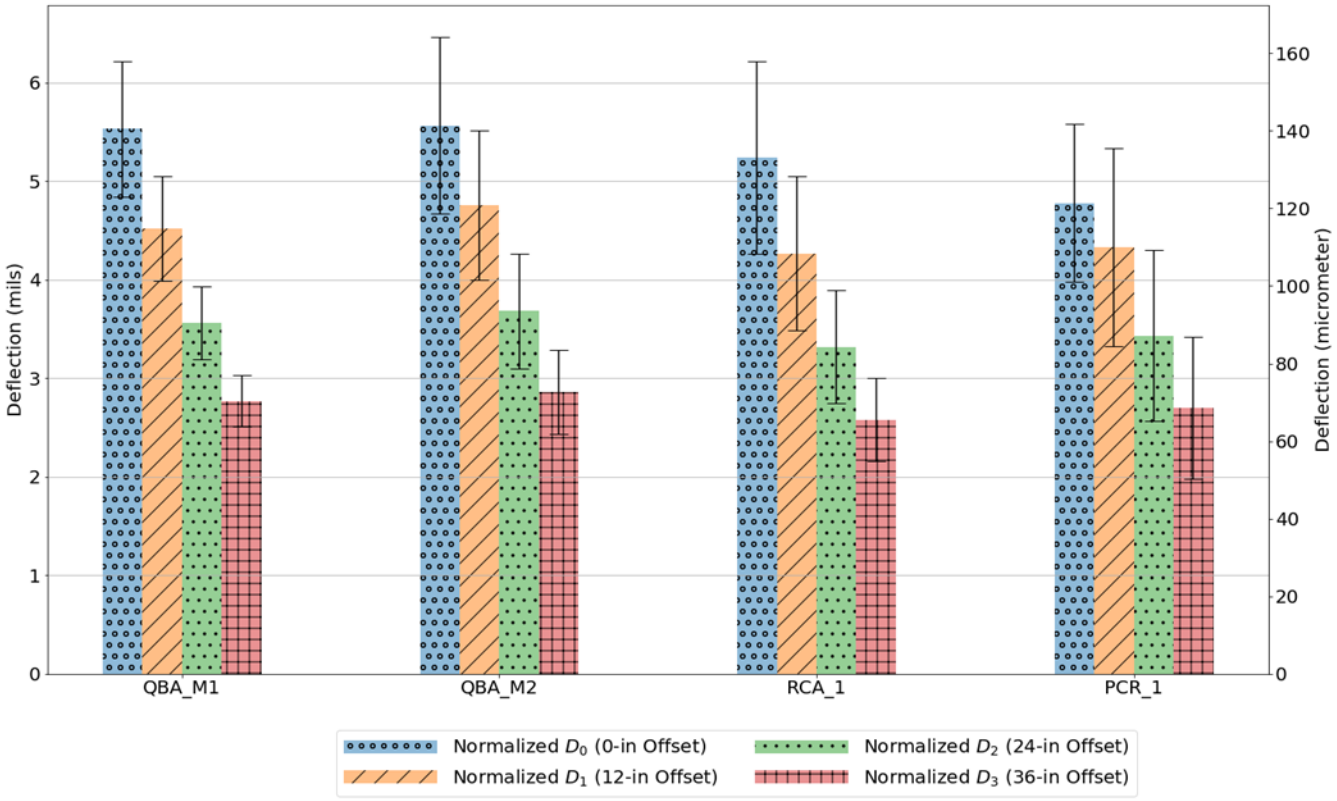

Figure 37. Chart. Recorded average FWD deflections for sensors D_0–D_3.

For comparative purposes, the deflection basins from the three drops at each drop location were normalized to the standard 9 kip (40 kN) equivalent single-axle load, applying a uniform pressure of 80 psi (551 kPa) over a circular area with a radius of 6 in. (152 mm). None of the 140 total drops showed a nondecreasing deflection trend. The average data (and one standard deviation) for the first four sensors (D_0–D_3) are plotted in Figure 37. For all sections, these measured deflections are considered relatively low and are typical of very stiff sections, e.g., full-depth HMA pavements or

pavements with stabilized base/subbase layers, indicating high structural capacity. The main reason for the low deflections can be attributed to the thick HMA layer topping the ASI layers. Further, all four sections have comparable FWD deflections, indicating similar structural capacity. In particular, the D_2 and D_3 geophones offset at 24 in. (610 mm) and 36 in. (914 mm), respectively, from the load drop location showed fairly similar deflections, indicating that the subsurface ASI layers likely have comparable stiffnesses after paving. Note that conclusions cannot be drawn solely based on single deflection values, so some common deflection basin parameters were calculated and compared to draw more accurate conclusions about any differences in the deflections/stiffnesses of the QBA and conventional sections.

Deflection Basin Parameters

Initially, before the FWD deflections were thoroughly analyzed, seven of the commonly known and used deflection basin parameters were calculated from the measured FWD deflections on top of the HMA layer. The deflection basin parameters were used to assess/compare the overall structural adequacies of the different test sections with and without QB and draw conclusions about the effects of adding the QB in the ASI layer on pavement responses. For the purpose of these analyses, the innermost geophone of the FWD equipment located under the load drop location is referred to as D_0 (also known as the maximum center deflection), while the other six geophones spaced 12 in. (305 mm) apart are referred to as D_1 to D_6.

First, parameters that indicate strength properties of individual pavement layers were investigated. These parameters are surface curvature index (SCI), base damage index (BDI), and base curvature index (BCI). Figure 41 shows the calculated parameters from the averaged and normalized FWD deflections in each test section. SCI is an indication of the stiffness of the upper portion of the pavement structure, particularly the HMA layer. BDI, in contrast, indicates the strength of the intermediate base/subbase layers, while BCI is an indication of the stiffness of the lowermost subgrade conditions (Horak 1987; Hoffman 1980; Hossain and Zaniewski 1991; Talvik and Aavik 2009). Figure 38, Figure 39, and Figure 40 give the equations for SCI, BDI, and BCI, respectively. Based on Figure 41, the test sections constructed with conventional ASI layers and with QBA of different mix ratios have comparable FWD deflection basin parameters and are expected to have similar structural capacities. The relatively low values of SCI, BDI, and BCI are indicative of the thick HMA layer, which is likely the reason all sections are expected to have similar structural capacities.

SCI, measured in units of mils (μm), is calculated as the difference between maximum center deflection (D_0) and the deflection at D_1, located 12 in. (305 mm) from the center deflection, using the following equation:

$$SCI = D_0 - D_1$$

Figure 38. Equation. Calculating surface curvature index from FWD deflections.

BDI, measured in units of mils (μm), is calculated as the difference between the second deflection sensor (D_1) and the third deflection sensor (D_2) using the following equation:

$$BDI = D_1 - D_2$$

Figure 39. Equation. Calculating base damage index from FWD deflections.

BCI, measured in units of mils (μm), is calculated as the difference between the third deflection sensor (D_2) and the fourth deflection sensor (D_3) using the following equation:

$$BCI = D_2 - D_3$$

Figure 40. Equation. Calculating base curvature index from FWD deflections.

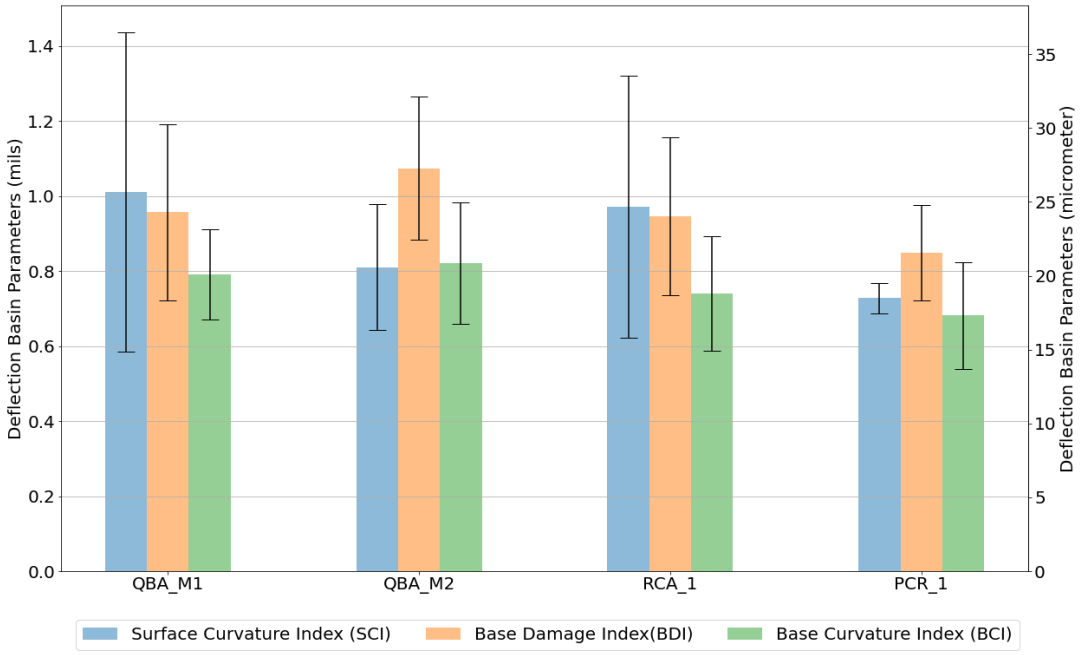

Figure 41. Chart. FWD deflection basin parameters (average values): SCI, BDI, and BCI.

Next, the shape factor parameters F1 and F2 were calculated. These parameters identify the relative differences among pavement layer properties (Hoffman 1980; Hoffman and Thompson 1981; Hossain and Zaniewski 1991). Generally, given similar thicknesses of the pavement structure, a higher value of shape factor F1 is an indication of a lower E_1/E_2 ratio, i.e., the ratio of the modulus of the top HMA layer and the underlying ASI layer. In contrast, shape factor F2 is more sensitive to the thickness of the top layer(s), and its value increases as the thickness decreases. Figure 42 and Figure 43 give the equations of F1 and F2 shape factors, respectively. Based on Figure 44, the test sections are expected to have fairly similar HMA layer thickness (same F2 values). Because HMA thickness at each FWD drop location is not available from cores, the nominal (design) HMA thickness will be assumed during back-calculation. This assumption is fairly accurate given the F2 shape factor values are similar for all sections. Values of F1 shape factor are also very similar for the different sections. They are slightly lower for sections QBA_M2 and PCR_1, indicating that these sections may have slightly higher

stiffness of the ASI layers, E_2, assuming the HMA layer stiffness, E_1, is the same for all sections (to be verified with back-calculation).

The dimensionless shape factor F1 calculates the relative difference between the first and third sensor deflections (D_0 and D_2, respectively) normalized to the deflection of the second sensor (D_1) using the following equation:

$$F1 = \frac{D_0 - D_2}{D_1}$$

Figure 42. Equation. Calculating F1 shape factor from FWD deflections.

The dimensionless shape factor F2 calculates the relative difference between the second and fourth sensor deflections (D_1 and D_3, respectively) normalized to the deflection of the third sensor (D_2) using the following equation:

$$F2 = \frac{D_1 - D_3}{D_2}$$

Figure 43. Equation. Calculating F2 shape factor from FWD deflections.

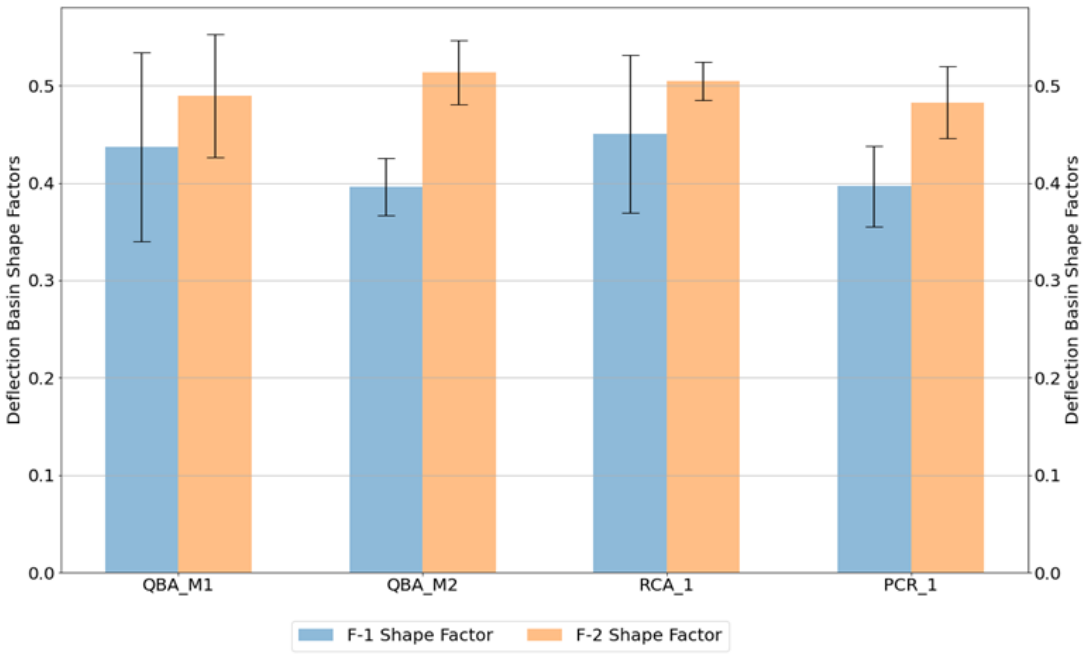

Figure 44. Chart. FWD deflection basin parameters (average values): shape factors F1 and F2.

Finally, the AREA parameter and the area under pavement profile (AUPP) were calculated according to the equations of Figure 45 and Figure 46, respectively. The AREA parameter combines multiple measured deflections into one value, minimizing the contribution of malfunctioning sensors, if any (Hoffman 1980). Higher AREA values generally indicate better structural integrity. The AUPP

deflection basin parameter is complementary in definition to the AREA profile, and a lower AUPP is typically indicative of a higher pavement stiffness and better integrity. According to Figure 47 and Figure 48, all four sections have similar structural integrity, but sections QBA_M2 and PCR_1 with lower QB content and conventional ASI section with virgin capping, respectively, are expected to be slightly stronger with higher load carrying capacity and stiffness.

AREA parameter, measured in units of inches (mm), calculates the area of deflection basin over a radial distance of 36 in. (914 mm) from the center of the load plate, normalized with respect to D_0 sensor deflection. It is calculated using the following equation:

$$AREA = \frac{6[D_0 + 2D_1 + 2D_2 + D_3]}{D_0}$$

Figure 45. Equation. Calculating AREA parameter from FWD deflections.

AUPP, measured in units of mils (μm), calculates the area beneath the deflection basin over a radial distance of 36 in. (914 mm) from the center of the load plate.

$$AUPP = \frac{5D_0 - 2D_1 - 2D_2 - D_3}{2}$$

Figure 46. Equation. Calculating AUPP from FWD deflections.

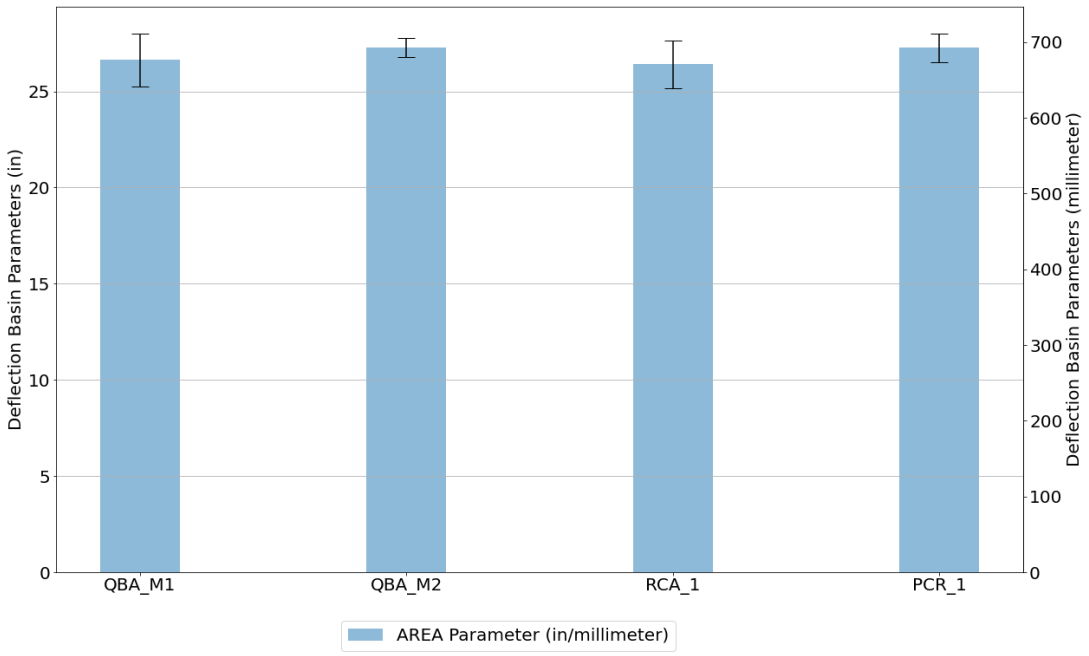

Figure 47. Chart. FWD deflection basin parameters (average values): AREA parameter.

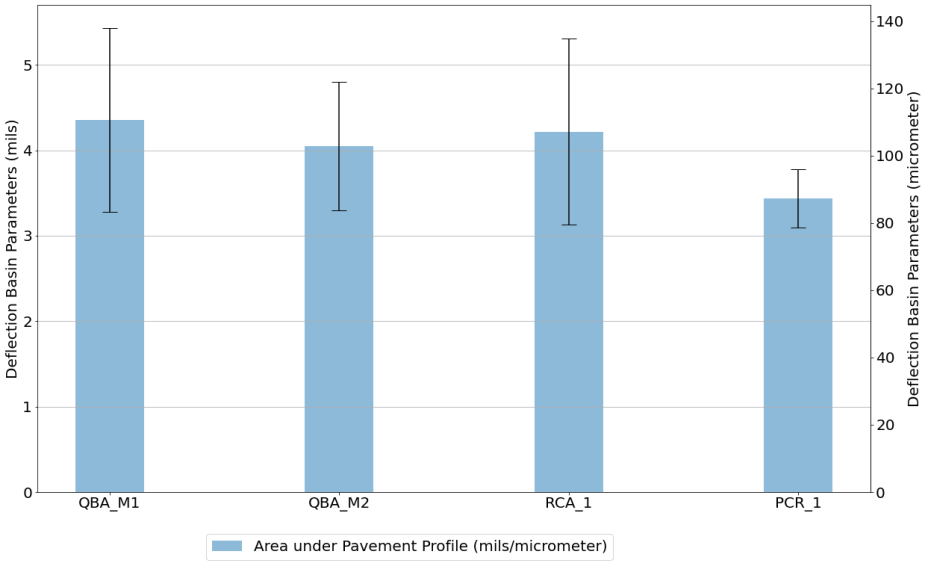

Figure 48. Chart. FWD deflection basin parameters (average values): Area under pavement profile.

Falling Weight Deflectometer Back-calculation from Deflection Data on Top of Hot-mix Asphalt

The FWD back-calculated moduli were estimated using two programs: PCASE and ELMOD software. PCASE stands for Pavement-Transportation Computer Assisted Structural Engineering, which is the US Army Engineer Research and Development Center pavement evaluation and design software. ELMOD software was developed by Dynatest company to perform back-calculation of pavement layer resilient moduli using their FWD equipment. Both software programs have been widely used for the analyses of FWD data (Pierce et al. 2017; Smith et al. 2017; Priddy et al. 2015). PCASE used the sum of squares of absolute error as the convergence scheme, while ELMOD uses the relative error of five sensors (Pierce et al. 2017). Table 5 lists some commonly used back-calculation programs.

Table 5. Some Commonly Used Back-calculation Programs

Program Name	Pavement Type	Max. No. of Layers	Convergence Scheme
BAKFAA	Flexible/rigid	Five	Sum of squares of absolute error
BOUSDEF 2.0	Flexible	At least four	Sum of percent errors
ELMOD®/ ELCON 5	**Flexible/rigid**	**Four (exclusive of rigid layer)**	**Relative error of five sensors**
EVERCALC©	Flexible	Three (exclusive of rigid layer)	Sum of absolute error
MODULUS 6.0	Flexible	Four plus rigid layer	Sum of relative squared error
PCASE 2.08	**Rigid/flexible/composite**	**Five**	**Sum of squares of absolute error**
WESDEF	Flexible	Four + rigid layer	Sum of squares of absolute error

Adapted from Pierce et al. (2017)

For back-calculation purposes, the following assumptions were made. First, the 1.5 in. (38 mm) surface course and the 9.25 in. (235 mm) binder course layers were combined into one layer for calculation purposes. The nominal design thickness of 10.75 in. (273 mm) was assumed at all locations because as-built thicknesses were not available from cores or GPS coordinates. Second, the 9 in. (229 mm) QBA/CS 02 layer and the 3 in. (76 mm) capping layer were combined into one layer for back-calculation purposes. A 12 in. (305 mm) nominal design thickness was assigned for all drop locations due to lack of as-built layer thicknesses. Program defaults for selection of the drop to be included in the analysis was also made. For PCASE, modulus is calculated per station per drop. The drop at one station with the smallest error is selected as the representative one. For ELMOD, the deflection basin fit method still utilizes Odemark-Boussinesq methods, but an additional iteration process utilizes the convergence criteria based on the degree of fit between the overall measured and calculated deflection basins. Modulus is calculated per drop at each station, then an average value is calculated per section per drop. Lastly, assumptions were made for the seed moduli of the various layers to fit the expected layer moduli. For the HMA layer, the modulus is expected to range from 875,000 psi (6033 MPa) for a 60°F (16°C) to a 1,270,000 psi (8,756 MPa) for a 50°F (10°C) temperature (Pierce et al. 2017).

Table 6 and Table 7 present the back-calculation results obtained using PCASE and ELMOD 6, respectively. In comparison, the back-calculated HMA and ASI layer moduli are higher by PCASE than ELMOD 6, while the back-calculated subgrade moduli obtained from PCASE are generally lower. Knowing the pavement structure and the expected stiffnesses of the constructed pavement layers, the results obtained by PCASE seem more reasonable and reliable. Regardless, the layer moduli calculated by both programs follow the same trends for all layers: HMA layer moduli is lowest for QBA_M2; subgrade moduli is highest for PCR_1 and lowest for QBA_M1/QBA_M2; and the ASI layers' stiffness is, on average, the strongest for RCA_1/PCR_1 sections, followed by QBA_M2, and the lowest for QBA_M1 section. The back-calculated layer moduli for the ASI layers is also in full agreement with the magnitudes of FWD center deflections on top of the capping layers discussed earlier in this chapter.

Generally, given these results, it can be concluded that the presence of 31% QB in the QBA_M2 mix, which is higher than the maximum percentage of 25% recommended by the packing box study, slightly reduced the structural integrity of the ASI layer with QBA. The increase in the QB content to 45% in the QBA_M1 caused a further reduction in the stiffness and layer moduli as more QB is available to separate the large rock contact points and reduce the shear strength of the mix. If individual FWD drop locations are considered, and the range (min., max.) moduli are taken into consideration, it can be realized that for the QBA_M2 mix, with the lower QB content of 31%, the back-calculated ASI layer moduli is within the same range as RCA_1 and PCR_1 mixes, and even higher at some drop locations. It can be concluded that the QBA_M2 mix is adequate as an ASI layer. For the QBA_M1 with higher QB content of 45%, the ASI layer moduli are consistently lower for most locations. Given that a thick HMA layer is overlaying the ASI sections, all sections are expected to perform well because the ASI layer is buried deep in the pavement and will receive relatively low stress states from moving traffic. The designs with QBA are deemed sustainable and adequate for the purpose of this project and are expected to show good performance. In cases where the ASI layers are expected to receive higher stress states, i.e., in flexible pavement sections with lower HMA

thicknesses, the use of QBA layers as a sustainable design that consumes large volumes of QB is also recommended, but the QB content shall not exceed 25% in order to maintain contact between the large aggregates. If these QBA layers are well designed to minimize loss of contacts between the large particles, then the QBA layers can also benefit from higher stability and lower layer deformation, as the QB fines pack inside the voids and increase the structural capacity of the designed ASI layers with QBA.

Table 6. PCASE Back-calculation Results (after Construction)—Layer Moduli (Average and Range of Values)

Section / Layer	HMA Modulus (ksi)	Aggregate Subgrade Improvement Modulus (ksi)	Prepared Subgrade Modulus (ksi)
QBA_M1	1342 (1279–1472)	37.3 (22.5–54.8)	18.7 (13.5–22.0)
QBA_M2	1326 (859–1564)	44.7 (20.4–80.0)	19.3 (15.0–23.8)
RCA_1	1407 (1227–1730)	52.6 (26.0–76.4)	20.2 (15.8–22.0)
PCR_1	1390 (1217–1511)	56.0 (22.5–81.1)	21.1 (12.5–24.4)

1 ksi = 6.895 MPa

Table 7. ELMOD 6 Back-calculation Results (after Construction)—Layer Moduli (Average and Range of Values)

Section / Layer	HMA Modulus (ksi)	Aggregate Subgrade Improvement Modulus (ksi)	Prepared Subgrade Modulus (ksi)
QBA_M1	1200 (1104–1273)	30.4 (21.8–37.7)	24.6 (18.1–35.6)
QBA_M2	1081 (864–1278)	35.3 (25.6–72.8)	24.2 (14.6–36.0)
RCA_1	1204 (1146–1269)	40.8 (29.1–55.2)	27.2 (22.8–32.9)
PCR_1	1228 (1142–1362)	39.7 (23.4–61.1)	30.1 (14.5–40.4)

1 ksi = 6.895 MPa

Falling Weight Deflectometer on Top of HMA—200 Days after Opening to Traffic

The third FWD tests were conducted on May 4, 2021, after the newly constructed road remained open to traffic for about 200 days. FWD tests were scheduled to be conducted by dropping three load levels (6, 9, and 12 kips; 1 kip = 4.44 kN) to induce variable stress states in pavement layers. However, at most test locations, three load levels closer to 9, 12, and 15 kips (1 kip = 4.44 kN) were conducted. At most test locations, three duplicate tests were conducted, and the results obtained from the three

duplicate tests were very similar. The complete data for all deflection basins from the conducted tests are presented in Appendix N for the QBA_M1 and QBA_M2 test sections on the west side of the bridge and in Appendix O for the RCA_1 and PCR_1 sections on the east side of the bridge. The load level for each drop is also listed in the appendices. FWD tests were conducted at an average ambient temperature of 62.5°F (16.9°C) and an average surface temperature of 74.5°F (23.6°C). The standard deviation in surface temperature was ±0.7°F (±0.4°C).

For comparison purposes, the deflection basins at each drop were normalized to the standard 9 kip (40 kN) equivalent single-axle load, applying a uniform pressure of 80 psi (551 kPa) over a circular area with a radius of 6 in. (152 mm). None of the 333 total drops showed an abnormal or a nondecreasing deflection trend. The average data (and one standard deviation) for the first four sensors (D_0–D_3) are plotted in Figure 49. For all sections, these measured deflections are considered relatively low and are typical of very stiff sections, e.g., full-depth HMA pavements or pavements with stabilized base/subbase layers, thus indicating high structural capacity. Generally, lower deflections are measured after the road was first opened to traffic, which indicates the shakedown and stiffening of pavement structure in time. The sections having RCA_1 and PCR_1 constructed with conventional ASI layers generally had slightly lower deflection basins compared to the sections with QBA_M1 and QBA_M2 ASI layers. Still, it is hard to draw the conclusion solely based on single deflection values, and the deflection basin parameters were calculated and compared next.

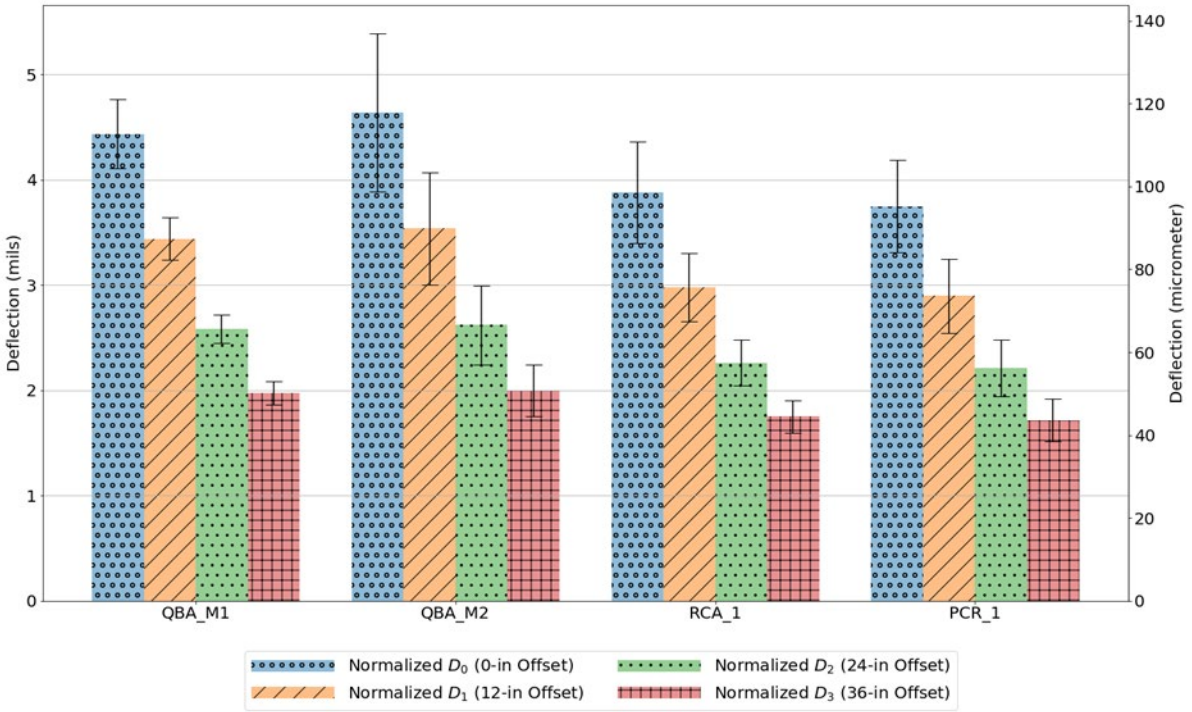

Figure 49. Chart. Recorded average FWD deflections for sensors D_0–D_3 (after traffic).

Deflection Basin Parameters

Like the analysis applied on FWD results obtained before the road was opened to traffic, deflection basin parameters including surface curvature index (SCI), base damage index (BDI), and base

curvature index (BCI) are computed. The definitions, calculations, and pavement structure properties indicated by the three parameters were discussed in the previous section. Figure 50 shows the calculated parameters from the averaged and normalized FWD deflections in each test section. Based on Figure 50, the test sections constructed with conventional ASI layers and with QBA of different mix ratios have comparable FWD deflection basin parameters and are expected to have similar structural capacities. The test results also follow the same trends observed in the FWD results from the time before opening the road to traffic.

The shape factor parameters F1 and F2 were also calculated. Figure 42 and Figure 43 present the equations of F1 and F2 shape factors, respectively. As discussed in the previous sections, generally when given similar thicknesses of the pavement structure, a higher value of shape factor F1 is an indication of a lower E_1/E_2 ratio, which is the ratio of the modulus of the top HMA layer and that of the underlying ASI layer. In contrast, shape factor F2 is more sensitive to the thickness of the top layer(s), and its value increases as the thickness decreases.

The calculated shape factors are plotted in Figure 51, and because shape factors are normalized, it is reasonable to compare the factors calculated before and after the road was opened to traffic. Based on Figure 51, the similar F2 factor among the four sections validates the assumption that the test sections had similar HMA layer thicknesses and the nominal (design) HMA thickness used for back-calculation. The increase in F2 factor after traffic is mainly due to the lower HMA modulus because these tests were conducted at a higher ambient and surface temperatures compared to the case when FWD tests were conducted before opening the road to traffic (average ambient temperature of 62.5°F [16.9°C] and a surface temperature of 74.5°F [23.6°C] versus an average ambient temperature of 50.5°F [10.3°C] and a surface temperature of 53.5°F [11.9°C]). A higher temperature means softer asphalt layer with lower stiffness. The lower modulus of HMA layer is also obtained from back-calculation results.

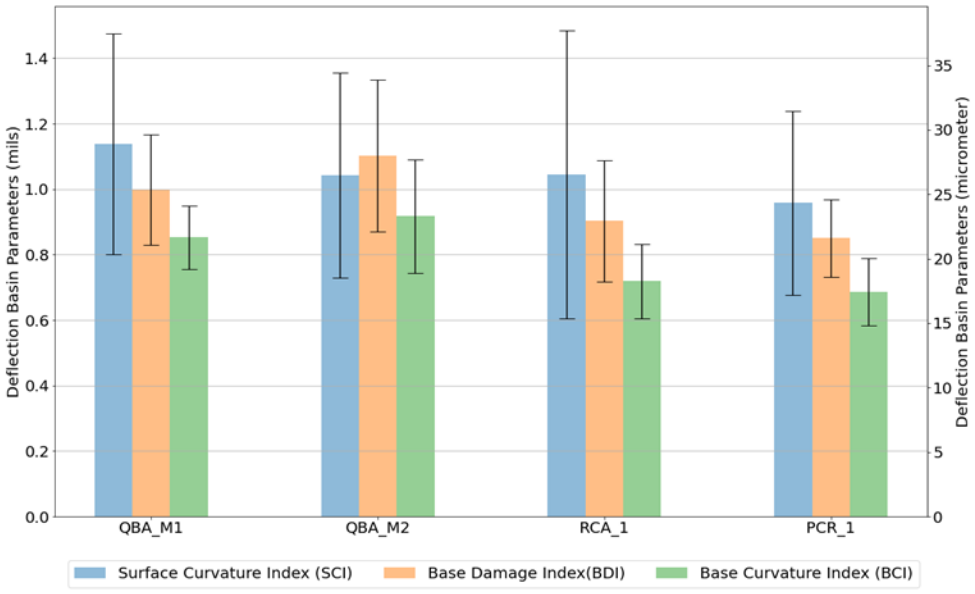

Figure 50. Chart. FWD deflection basin parameters after traffic (average values): SCI, BDI, and BCI.

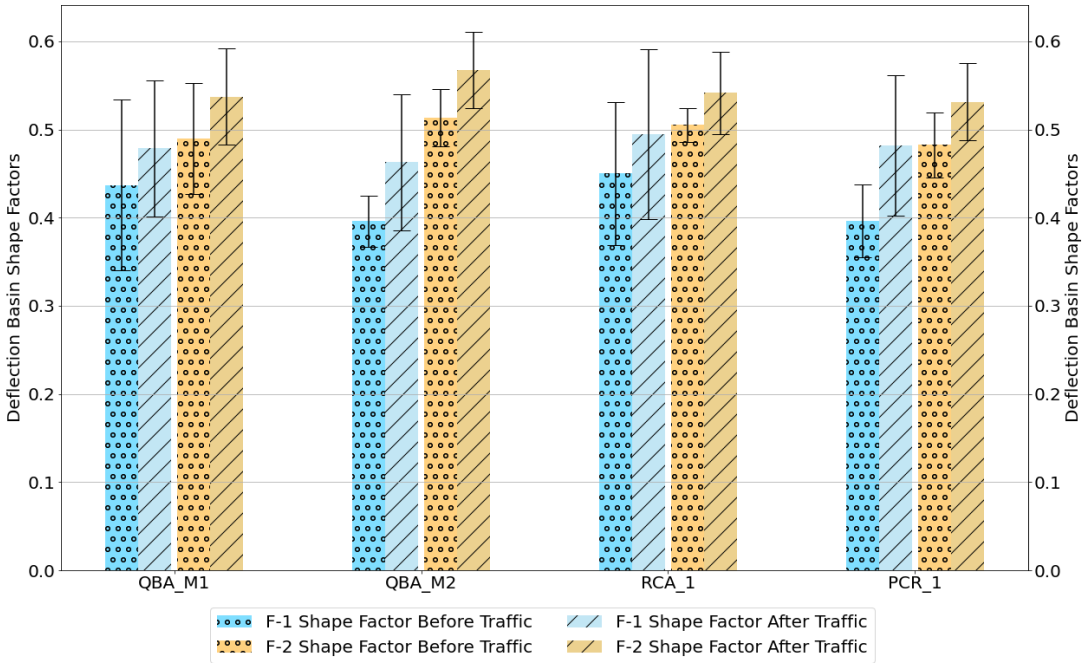

Figure 51. Chart. FWD deflection basin parameters (average values before and after traffic): shape factors F1 and F2.

Like the previous results, the shape factor F1 values are also very similar for the different sections. They are slightly lower for sections QBA_M2 and PCR_1, indicating that these sections may have slightly higher stiffness of the ASI layers, E_2, assuming the HMA layer stiffness, E_1, is the same for all sections (also verified with back-calculation). The increase of F1 factor after traffic indicates a lower E_1/E_2 ratio, which suggests that HMA stiffness decreased due to higher temperature and/or QBA mixtures, and RCA and PCR all gain stiffness after more compaction and consolidation induced by traffic loading.

Finally, the AREA parameter and the area under pavement profile (AUPP) were calculated according to the equations in Figure 45 and Figure 46, respectively. The AREA values are compared for the before and after traffic cases given the normalization involved in AREA calculation while AUPP deflection basin parameter is presented without comparison of the before and after traffic.

According to Figure 52 and Figure 53, all four sections have similar structural integrity, but conventional ASI sections are expected to be slightly stronger with higher load carrying capacity and stiffness compared to the sections with QBA mixtures. The decreased AREA values for all four sections indicate a better structural integrity after traffic (due to consolidation and shakedown of ASI layers). The increased stiffness characteristics of ASI layers contributed to the lower AREA values. Shakedown led to better compaction and void filling under repeated traffic loading, which contributed to stiffer ASI layers. The increased moduli of ASI layers are also verified by the back-calculation results presented next.

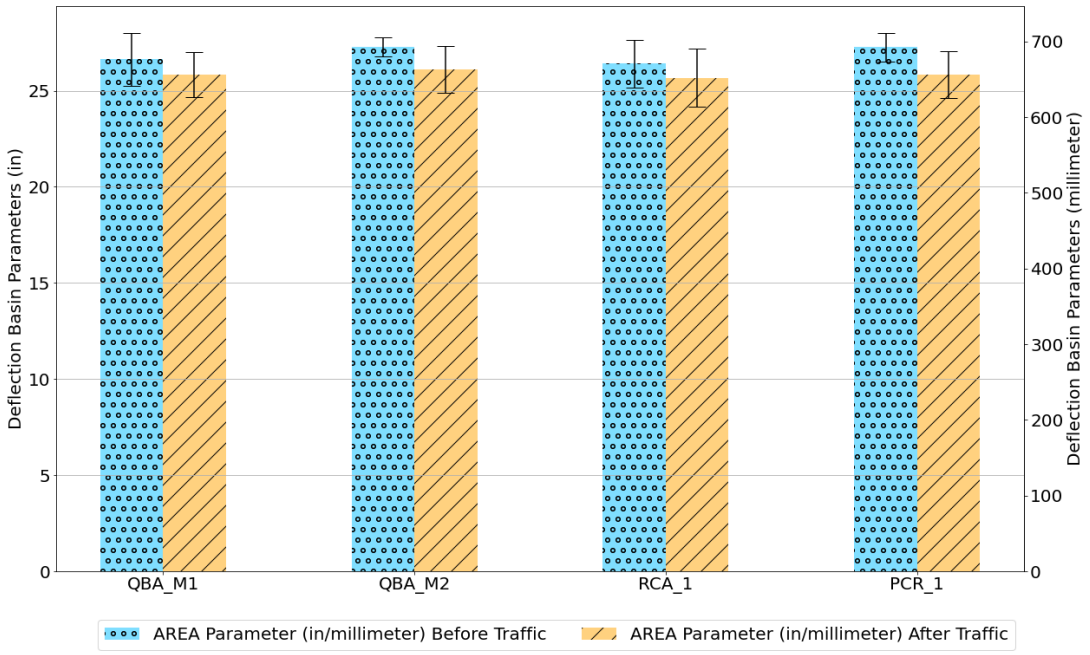

Figure 52. Chart. FWD deflection basin parameters (average values before and after traffic): AREA parameter.

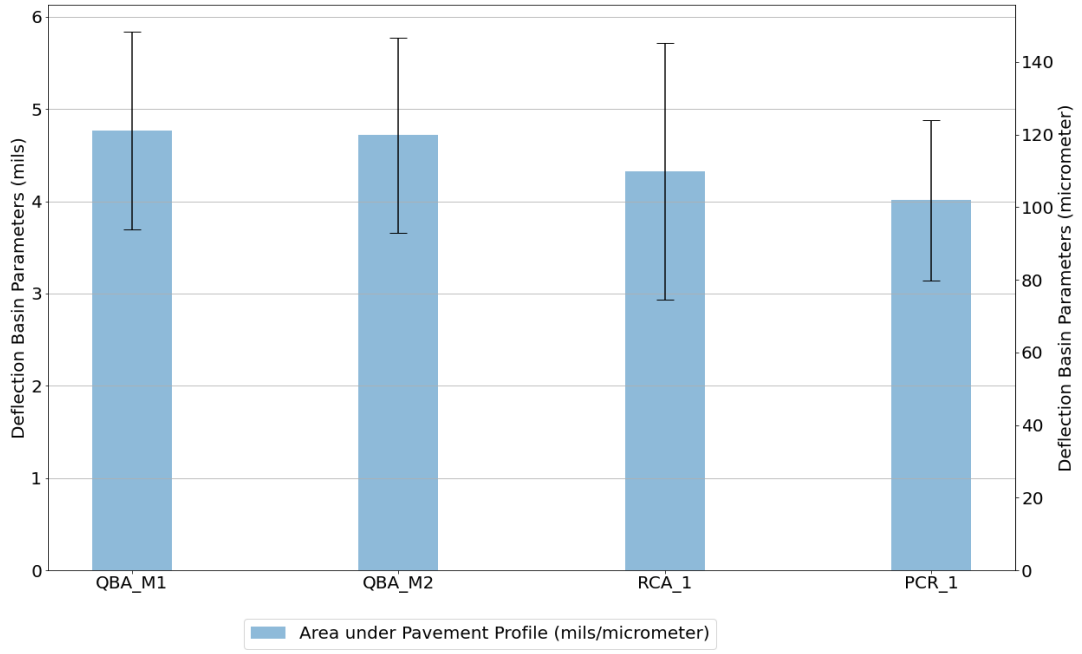

Figure 53. Chart. FWD deflection basin parameters after traffic (average values): Area under pavement profile.

Falling Weight Deflectometer Back-calculation from Deflection Data on Top of Hot-mix Asphalt

For consistency with the FWD back-calculation analyses conducted before opening the road to traffic, the moduli were estimated again using two back-calculation programs: PCASE and ELMOD. These two programs were introduced in the previous section. The same structural assumptions were made. The nominal design thickness of 10.75 in. (273 mm) for HMA was assumed at all locations, and a 12 in. (305 mm) nominal design thickness was assigned for all drop locations for QBA/CS 02 layers. The analysis process remained identical. For the HMA layer, the reference seed modulus ranged from 875,000 psi (6033 MPa) at 60°F (16°C) to a 562,375 psi (3,878 MPa) at 70°F (21°C) (Pierce et al. 2017).

Table 8 and Table 9 present the back-calculation results obtained using PCASE and ELMOD 6, respectively. Knowing the pavement structure and the expected stiffnesses of the constructed pavement layers, the results obtained by PCASE seem more reasonable and reliable, also with less variance and concentrated ranges. Nonetheless, the same trends are again obtained using the two programs for HMA, ASI, and subgrade layers. QBA_M1 and QBA_M2 sections had relatively low HMA layer moduli. Subgrade moduli are the highest for PCR_1 and the lowest for QBA_M1/QBA_M2. The ASI layer is, on average, the strongest for the RCA_1 and PCR_1 sections, followed by the QBA_M2 and QBA_M1 sections. The back-calculated layer moduli for the ASI layers follow the same trend as observed in the FWD data results before opening the road to traffic.

The lower modulus of HMA layer obtained when compared to values from the previous tests can be attributed to the higher testing temperatures. The increase in ASI layer moduli indicates the compaction and consolidation of ASI layers under repeated traffic loading and any overburden stress from upper structure. The shakedown of QBA layers with traffic resulted in a better structural integrity, and therefore, the higher moduli trend is expected. This validates that the well-designed QBA mixture (QBA_M2) can minimize loss of contacts between the large particles as the QB fines pack inside the voids and increase the structural capacity, thus benefiting the stability and leading to lower layer deformation.

Similar to the conclusions drawn from the FWD results before opening the road to traffic, the presence of 31% QB in the QBA_M2 mixture, which is higher than the maximum percentage of 25% recommended by the packing box study, slightly reduced the structural integrity of the ASI layer with the QBA compared to the conventional ASI layer behavior. Although the *average* moduli of QBA mixtures show similarity for the two QBA sections, if the moduli *ranges* are considered, the section with lower QB content of 31% (QBA_M2) is still superior in performance to the section with up to 45% QB content (QBA_M1) and even has higher modulus from FWD back-calculation at some drop locations than for the RCA_1 and PCR_1 sections.

Therefore, it can be concluded that the QBA_M2 mix is adequate as an ASI layer. The lower deflections and better structural integrity estimated from the FWD test data collected after opening the road to traffic indicate that all sections performed well under traffic loading. Also, the designs with QBA are deemed sustainable and adequate for the purpose of this project and are expected to show good performance. The results are also in accordance with previous recommendations that the use of QBA layers as a sustainable design that consumes large volumes of QB is recommended.

Table 8. PCASE Back-calculation Results (after Traffic)—Layer Moduli (Average and Range of Values)

Section / Layer	HMA Modulus (ksi)	Aggregate Subgrade Improvement Modulus (ksi)	Prepared Subgrade Modulus (ksi)
QBA_M1	1012 (488–1251)	48.3 (16.9–90.1)	20.7 (18.9–22.4)
QBA_M2	1002 (715–1306)	50.2 (24.5–106.6)	20.5 (17.1–24.7)
RCA_1	1019 (522–1244)	86.9 (65.6–100.6)	22.7 (19.6–24.9)
PCR_1	1096 (657–1454)	86.8 (27.5–106.9)	23.2 (19.4–26.7)

1 ksi = 6.895 MPa

Table 9. ELMOD 6 Back-calculation Results (after Traffic)—Layer Moduli (Average and Range of Values)

Section / Layer	HMA Modulus (ksi)	Aggregate Subgrade Improvement Modulus (ksi)	Prepared Subgrade Modulus (ksi)
QBA_M1	1073 (373–1573)	44.5 (16.1–155.4)	20.7 (14.8–26.8)
QBA_M2	1044 (456–2345)	46.0 (10.2–219.0)	21.6 (13.3–39.0)
RCA_1	1102 (331–2181)	72.9 (21.3–139.3)	24.0 (19.5–32.9)
PCR_1	1219 (411–2305)	68.9 (17.8–159.9)	24.1 (17.0–30.8)

1 ksi = 6.895 MPa

FIELD EVALUATION—IMAGE ANALYSIS

During the construction of QBA layers, images and videos of the QBA stockpiles before placement and images of the placed QBA mixes before and after compaction were captured to segment and evaluate the uniformity of QB distribution into the voids of the PCR and estimate the achieved mixing / blending ratios of QB and PCR. The collected images were processed using an innovative AI-based algorithm that can handle the segmentation task with high efficiency and requires low user dependency. The algorithm was first developed as part of a recent ICT project, R27-182 (Huang et al. 2020), to determine the grain size distribution and shape characteristics of riprap and large-sized particles. Using a larger dataset for training and utilizing more rigorous aggregate labeling criteria to label smaller particles, the AI-based algorithm was improved to have the capability of detecting and segmenting smaller particle sizes down to 3/8 in. (9.5 mm). The method operates primarily on the principle that the average volume (or mass) of a particle is proportional to its cross-sectional area. Therefore, if computer vision techniques can be used to segment the aggregate particles from the fines portion and void space, then a reliable estimate of the percent of large PCR particles and QB in each image can be estimated.

Based on the improved AI-based segmentation algorithm utilized in the I-RIPRAP software—a Windows-based software outcome of the ICT project R27-182 (Huang et al. 2020) to segment riprap particles in a stockpile—two representative images of the QBA mixes were segmented as shown in Figure 54 for the QBA_M1 mix with higher QB content and in Figure 55 for the QBA_M2 mix with lower QB content. These images revealed that 54.5% and 39.8% of the area was QB for the QBA_M1 and QBA_M2 mixes, respectively (compared to 45.5% and 30.9%, respectively, from laboratory sieve analysis). Note that the image-based technique may require further refinement and calibration to relate the percent degraded segment, i.e., percent of fines and voids, in the images to an actual gradation. Further, some of the smaller rocks are not detected, increasing the percentage of QB calculated from each image. Further refinement of the algorithm is in progress, and the images collected from this field project will be used to train and improve the accuracy of the algorithm.

Figure 54. Photo. Raw and segmented images of QBA_M1 section before compaction.

Figure 55. Photo. Raw and segmented images of QBA_M2 section before compaction.

PRELIMINARY PERFORMANCE EVALUATION—ROUGHNESS MEASUREMENT AND VISUAL SURVEYS

The constructed road was opened to traffic around October 15, 2020. On April 2, 2021, approximately 5.5 months after opening to traffic, IDOT conducted surface roughness measurement testing to determine the International Roughness Index (IRI) of road segments on both sides of the bridge, and to draw conclusions on performance of QBA sections compared to the control sections in early stages. A SSI Profiler Version 3.3.13.76 was used, with two Gocator 2342/1150/1350 sensors at the passenger's side and driver's side wheel path. Table 10 and Table 11 provide a summary of the IRI results for the westbound (control sections) and eastbound (QBA sections), respectively. Track_1 IRI values represent the driver side wheel path. Track_2 IRI values represent the passenger side wheel path. Track_1 and Track_2 IRI values are then averaged together to provide an overall IRI value for each segment. Two segments were scanned on each side of the bridge, and the IRI results were averaged. All IRI measurements were taken on the HMA pavements.

Overall, for a low-speed section of roadway built on a vertical curve, the IRI values for the eastbound and westbound sections are considered typical for IDOT. The eastbound sections with QBA layers have an average IRI of 117.53 in/mile (1855 mm/km), slightly higher and smoother than the westbound conventional ASI sections which have an average IRI of 103.81 in/mile (1638 mm/km).

Table 10. International Roughness Index results for the Westbound Conventional Sections

Segment No.	Stations (ft)	Track_1 IRI (in./mile)	Track_2 IRI (in./mile)	Average IRI (in./mile)
1	2376+50.0 2368+89.8	74.18	124.34	99.26
2	2366+14.8 2360+08.3	87.65	131.37	109.51
Average	2376+50.0 2360+08.3	80.16	127.46	103.81

1 in./mile = 15.78 mm/km

Table 11. International Roughness Index Results for the Eastbound QBA Sections

Segment No.	Stations (ft)	Track_1 IRI (in./mile)	Track_2 IRI (in./mile)	Average IRI (in./mile)
1	2360+00.0 2366+14.8	103.56	153.28	128.42
2	2368+89.8 2376+43.6	83.88	133.41	108.65
Average	2360+00.0 2376+43.6	92.72	142.34	117.53

1 in./mile = 15.78 mm/km

On April 6, 2021 (i.e., approximately 5.5 months after opening to traffic), the TRP Chair (Michael Short) walked the entire project and “did not observe any cracking, rutting, or other distresses.” He drove the project a couple of times and “did not notice any bumps or roughness in excess of what would be expected for a typical pavement.” The visual survey concluded that all sections are performing well, and the QBA sections’ performance is comparable to that of the control sections constructed on the east side of the bridge. Note that IDOT may be planning to conduct IRI measurements on a yearly basis for this section of the roadway in conjunction with the annual crack/distress visual inspections, in order to collect data for long-term performance monitoring.

CHAPTER 5: SUMMARY AND CONCLUSIONS

SUMMARY AND CONCLUSIONS

This report presented detailed procedures and results from the ICT project R27-SP43, which involved a field case study for monitoring, characterizing, and documenting the construction of aggregate subgrade improvement (ASI) layers using quarry by-product aggregates (QBA), a quarry mix of primary crushed rocks (PCR) and sand-sized quarry fines. The construction took place at Larry Power Road in Bourbonnais Township in Kankakee County, Illinois. The construction of subgrade improvements with QBA at Larry Power Road took place on July 27, 2020. The material was plant mixed using loaders at the quarry and brought to the construction site using trucks.

The research team placed two QBA mixes. The first mix (QBA_M1) consisted of 55% of railroad ballast–sized 3×1 primary crushed rocks (PCR) and 45% quarry by-products (QB) by weight. The second mix (QBA_M2) consisted of 69% and 31% of PCR and QB, respectively. The two QBA mixes as the special provision ASI were topped with a virgin capping material. Two conventional ASI sections conforming to IDOT CS 02 gradation with 6 in. (152 mm) top size were also constructed. For the conventional ASI sections, one section (RCA_1) was topped with a reclaimed asphalt pavement capping layer, while the second (PCR_1) was topped with a virgin capping material. All sections consisted of 9 in. (229 mm) of QBA/PCR topped with 3 in. (76 mm) of a dense-graded capping layer. The field project provided the opportunity to investigate proper construction methods and study effects of property variation such as the QB content on constructability and performance.

A special provision titled “Aggregate Subgrade Improvement 12 in. Special” was prepared by IDOT and added to the notice to bidders to specify the details and requirements of a QBA material. Specifically, the special provision stated the following:

> [QBA] shall consist of a mixture of surplus quarry stone sand and primary crushed stone. The surplus quarry stone sand and primary crushed stone shall be combined in the presence of the Engineer with 25% to 50% by weight surplus quarry stone sand to create the quarry by-product aggregate ... The surplus quarry stone sand shall be defined as surplus materials from the aggregate production process and shall be 100% passing the 3/8 in. (9.5 mm) sieve ... The gradation of the combined material shall be 100% passing the 6 in. (150 mm) sieve and 8% to 12% passing the No. 200 sieve ... The quarry by-product aggregate shall not be permitted to segregate during mixing, stockpiling, transporting, or placing. In the event segregation is not prevented … then all mixing shall be performed at the job site at the point of placement.

Prior to the field construction, materials were shipped to the Advanced Transportation Research and Engineering Laboratory for characterization. Primarily, materials used for the construction of QBA sections were characterized. Conducted laboratory tests included grain size distribution, specific gravity and absorption of the large PCR, packing box studies, and tests on the effect of QB content on packing of the mixture and the rock-to-rock contacts. The main conclusion from packing box studies and laboratory illustrations is that a QBA mix with 75% PCR and 25% QB (3:1 mix) is the optimized mix

to fill most of the voids without losing rock-to-rock contacts. Higher QB contents can lead to separating the larger rocks acting as the primary structure, reducing the contact points between them and potentially reducing the shear strength and load-carrying ability.

Truckloads of the aggregate mixes were end dumped on the prepared subgrade starting at the west end of the pavement construction and spread using a bulldozer over the length and width of the roadbed. Visual inspection of the aggregate in the truck loads and videos/images collected for the stockpiles and the spread material did not show evidence of severe material segregation. The segregation levels were in the typical range to what is normally seen for densely graded aggregate materials. Field sampling of the materials showed that the QBA_M1 mix had 45.5% QB-sized materials and 54.5% of 3×1 large-sized aggregates, while the QBA_M2 mix had, on average, 30.9% QB-sized materials and 69.1 large-sized 3×1 rocks. The segregation potential and mixing ratios were also closely monitored by imaging-based techniques using an AI-based segmentation algorithm to determine the uniformity of the mixes and to segment the large rocks and calculate a pixel-wise area of QB and PCR from the analyzed images.

Pavement performance data were collected from the project site by closely monitoring the field sections during and after construction of the different layers as well as in the early stages of the traffic-use phase. The quality and uniformity of the construction was monitored using destructive and nondestructive techniques such as dynamic cone penetrometer (DCP), lightweight deflectometer (LWD), and falling weight deflectometer (FWD). The following observations and conclusions were made:

- Some variability in construction quality in all ASI layers was observed from DCP data collected on top of the capping layers for the ASI layers and the underlying prepared subgrade.

- DCP data indicated that the constructed QBA layers were comparable in strength with the conventional subgrade improvement techniques. In fact, the QBA_M1 section with the higher QB content had the highest strength profile measured by DCP.

- LWD on top of the capping layers, in contrast, showed that the stiffness of the QBA layers was slightly compromised compared to conventional ASI sections. In particular, the QBA_1 section had the lowest back-calculated composite surface moduli from LWD.

- FWD data on top of the capping layers and on top of the hot-mix asphalt (HMA) layer showed a similar trend to LWD.

- Overall, using QBA layers, which had slightly lower but comparable mechanical behavior characteristics (strength and stiffness profiles) to the conventional ASI sections, did not jeopardize the structural integrity of the ASI layers.

- The presence of 31% QB in the QBA_M2 mix, which is higher than the maximum 25% recommended by the laboratory packing box study, slightly reduced the structural load taking ability of the ASI layer with QBA. The increase in the QB content to 45% in the

QBA_M1 caused a further reduction in the stiffness and layer moduli, as more QB was available to separate the large rock contact points and reduce the shear strength of the mix. Overall, however, using QBA layers did not jeopardize the structural integrity of the ASI layers. The use of QBA materials was recommended as a sustainable and durable construction practice to provide stable layers and potentially reduce deformation in the long run, particularly when QBA mixes are used with a maximum of 25%–30% QB content.

- When individual FWD drop locations were considered, for the QBA_M2 mix with the lower QB content of 31%, the back-calculated ASI layer moduli were within the same range as RCA_1 and PCR_1 mixes, and was even higher at some drop locations. The QBA_M2 mix was evidently as adequate as a traditional ASI layer.

- For the QBA_M1 with higher QB content of 45%, the ASI layer moduli are consistently lower for most locations. Given that a thick HMA layer is overlaying the ASI sections, this section is still anticipated to show good performance because the ASI layer is buried deep in the pavement and will receive relatively low stress states from moving traffic.

- The construction method used in the field with plant-mixed QBA materials was found adequate as a quick, convenient, and economic method to construct and compact QBA layers with minimal observed segregation. Visual inspection and mix characterization with imaging-based techniques after placement, and with other nondestructive methods such as DCP and LWD, are recommended to investigate and repair/eliminate any weak spots.

The designs with QBA were deemed sustainable and adequate for the purpose of this project and are expected to show good performance. In cases where the ASI may receive higher stress states, i.e., in flexible pavement sections with lower HMA thicknesses, the use of QBA layers as a sustainable design that consumes large volumes of QB is also recommended, but the QB content shall not exceed 25% in order to maintain contact between the large aggregates. Note that this percentage (25%) may vary from one mix to another depending on the PCR and QB sizes, grain size distributions, and other characteristics. When QBA layers are well designed to minimize loss of contacts between the large particles, the QBA layers can also benefit from higher stability and lower layer deformation, as the QB fines pack inside the voids and increase the structural capacity of the designed ASI layers with QBA.

RECOMMENDATIONS FOR FUTURE WORK

The field performance evaluations of quarry by-product aggregates investigated in this project highlighted such potentially successful applications of these materials as an aggregate subgrade improvement method. Certain aspects of this study may require further investigation. The following discussion outlines recommendations for further research and research needs:

- The long-term performance of the QBA layers needs to be investigated. While this project investigated the feasibility of constructing these layers and tackled any issues with field application, only the initial performance data have been so far collected from the construction activities and the early stages of opening to traffic. This initial performance assessment showed that these sections have comparable performance to conventional ASI

sections, but the long-term performance may show added advantages such as higher layer stability and reduced pavement deflection, or possibly some potential drawbacks. The presence of this demonstration project at Larry Power Road in Kankakee County, Illinois, presents a valuable opportunity to monitor the long-term performance and draw conclusions on the long-term performance trends and any added advantages/drawbacks of using QBA layers. Thus, the continued monitoring of the constructed field sections is recommended.

- The mixing proportions of QB and PCR need to be further investigated to optimize the performance and mechanical properties of pavement sections constructed with QBA. Laboratory packing studies indicated that 25% QB by weight of the total mix is ideal to keep contact between the large PCR particles acting as the primary structure. The constructed field sections at Larry Power Road utilized higher QB contents (50% and 33% of the weight of the total mix) to study such cases that utilize high volumes of quarry fines. However, this is expected to cause separation of large particles and reduction of the load bearing capacity due to formation of weak shear planes. While the initial investigations were carried out in this project, the collected field performance data did not indicate any proof of performance deficiency of QBA layer with higher than optimum QB content. Still, ongoing investigations of QBA layers with lower QB contents and the investigation of the long-term field performance are required before final conclusions can be drawn.

- The analysis of field mixing ratios and segregation potential by imaging techniques proved to be a viable technique for QBA layers characterization. The AI-based algorithm successfully segmented the large 3×1 PCR and provided a percent degraded segment value for the analyzed images, which could be correlated to the percentage of QB in each image. This field imaging technique needs to be further investigated by improving the segmentation kernel with more rigorous labelled image training. Then, more field images can be segmented to investigate the mixing ratios and segregation potential of QBA mixes more accurately. This research effort is ongoing at the time this report is being written.

- There is a need to investigate other field construction methods for mixing QB with aggregate subgrade for better uniformity. There is also a need to work with industry to determine the most cost-effective method of blending the PCA with the QB. The successful construction of quarry by-product aggregate layers when the QB was added in small increments followed by a vibratory action in R27-168 (Qamhia et al. 2018) suggests that this is a promising practice for vibrating QB into the inherent voids of constructed lifts of aggregate subgrade. However, this method is rather slow and time-consuming, which suggests that an automated technique to spread the QB uniformly and more slowly on the surface, accompanied with continuous vibration, needs to be developed. Such construction method needs to be validated and further investigated. Further, given that the cost of constructing aggregate subgrade improvement layers with this method is expected to be higher than conventional ASI layers, the additional cost needs to be justified in terms of added layer stability and reduction of layer deformation. If this construction method is applied in future demonstration projects, it should be accompanied with a life cycle analysis and a life cycle cost assessment.

REFERENCES

ASTM C117. 2017. *Standard Test Method for Materials Finer than 75-µm (No. 200) Sieve in Mineral Aggregates by Washing*. West Conshohocken, PA: ASTM International. https://www.astm.org/Standards/C117

ASTM C127. 2015. *Standard Test Method for Relative Density (Specific Gravity) and Absorption of Coarse Aggregate*. West Conshohocken, PA: ASTM International. https://www.astm.org/Standards/C127.htm

ASTM C136. 2019. *Standard Test Method for Sieve Analysis of Fine and Coarse Aggregates*. West Conshohocken, PA: ASTM International. https://www.astm.org/Standards/C136

Hoffman, M. S. 1980. Mechanistic Interpretation of Nondestructive Pavement Testing Deflections. Doctoral Dissertation, University of Illinois at Urbana Champaign.

Hoffman, M. S., and M. R. Thompson. 1981. *Nondestructive Testing of Flexible Pavements: Field Testing Program Summary*. Report No. UILU-ENG-81-2003. Springfield, IL: Illinois Department of Transportation/University of Illinois.

Horak, E. 1987. Aspects of Deflection Basin Parameters Used in a Mechanistic Rehabilitation Design Procedure for Flexible Pavements in South Africa. Doctoral dissertation, University of Pretoria. https://repository.up.ac.za/bitstream/handle/2263/23960/Complete.pdf? sequence=5

Hossain, A. S. M., and J. P. Zaniewski. 1991. "Characterization of Falling Weight Deflectometer Deflection Basin." *Transportation Research Record: Journal of the Transportation Research Board* 1293: 1–11. http://onlinepubs.trb.org/Onlinepubs/trr/1991/1293/1293-001.pdf

Hou, W., I. Qamhia, V. Mwumvaneza, E. Tutumluer, and H. Ozer. 2019. "Engineering Characteristics and Stabilization Performance of Aggregate Quarry By-Products from Different Sources and Crushing Stages." *Frontiers in Built Environment* 5: 130. https://doi.org/10.3389/fbuil.2019.00130

Huang, H., J. Luo, E. Tutumluer, J. M. Hart, and I. Qamhia. 2020. *Size and Shape Determination of Riprap and Large-sized Aggregates Using Field Imaging*. Report No. FHWA-ICT-20-002. ICT Project R27-182. Rantoul, IL: Illinois Center for Transportation/Illinois Department of Transportation. https://doi.org/10.36501/0197-9191/20-003

Illinois Department of Transportation. 2005. *Subgrade Stability Manual*. Springfield, IL: Illinois DOT Bureau of Bridges and Structures. https://idot.illinois.gov/Assets/uploads/files/Doing-Business/Manuals-Guides-&-Handbooks/Highways/Bridges/Geotechnical/Subgrade%20Stability%20Manual.pdf

Illinois Department of Transportation. 2016. *Standard Specifications for Road and Bridge Construction*. Springfield, IL: IDOT. https://idot.illinois.gov/Assets/uploads/files/Doing-Business/Manuals-Guides-&-Handbooks/Highways/Construction/Standard-Specifications/12SpecBook.pdf

Kazmee, H., and E. Tutumluer. 2015. *Evaluation of Aggregate Subgrade Materials Used as Pavement Subgrade/Granular Subbase*. Report No. FHWA-ICT-15-013. ICT Project R27-124. Rantoul, IL: Illinois Center for Transportation/Illinois Department of Transportation. https://apps.ict.illinois.edu/projects/getfile.asp?id=3517

Pierce, L. M., J. E. Bruinsma, K. D. Smith, M. J. Wade, K. Chatti, and J. Vandenbossche. 2017. *Using*

Falling Weight Deflectometer Data with Mechanistic-Empirical Design and Analysis, Volume III: Guidelines for Deflection Testing, Analysis, and Interpretation. Research Report No. FHWA-HRT-16-011. Washington, DC: Federal Highway Administration. https://www.fhwa.dot.gov/publications/research/infrastructure/pavements/16011/003.cfm

Priddy, L. P., A. Bianchini, C. R. Gonzalez, and C. S. Dossett. 2015. *Evaluation of Procedures for Backcalculation of Airfield Pavement Moduli*. Report No. ERDC/GSL-TR-15-31. Vicksburg, MS: Engineer Research and Development Center. https://usace.contentdm.oclc.org/digital/collection/p266001coll1/id/3829/

Qamhia, I., E. Tutumluer, and H. Ozer. 2018. *Field Performance Evaluation of Sustainable Aggregate By-product Applications*. Report No. FHWA-ICT-18-016. ICT Project R27-168. Rantoul, IL: Illinois Center for Transportation/Illinois Department of Transportation. https://doi.org/10.36501/0197-9191/18-019

Qamhia, I., H. Kazmee, E. Tutumluer, and H. Ozer. 2017a. "Sustainable Application of Quarry Byproducts Mixed with Large Size Unconventional Aggregates for Improved Performance." In *Materials for Sustainable Infrastructure*, edited by Leslie Struble and Gabriele Tebaldi, 262–273. Cham: Springer. https://doi.org/10.1007/978-3-319-61633-9_17

Qamhia, I., E. Tutumluer, H. Ozer, and H. Kazmee. 2017b. "Sustainable Field Applications of Quarry Byproducts Mixed with Large Size Unconventional Aggregates." In *Bearing Capacity of Roads, Railways and Airfields*, edited by Andreas Loizos, Imad L. Al-Qadi, A. (Tom) Scarpas, 1127–1134. Boca Raton, FL: CRC Press. https://doi.org/10.1201/9781315100333-151

Qamhia, I., E. Tutumluer, H. Ozer, and H. Kazmee. 2017c. "Field Performance Evaluation of Pavement Construction Platforms Utilizing Unconventional Large Size Aggregates Packed with Quarry Byproducts, and Higher Fines Aggregate Subgrade Layers." In *Airfield and Highway Pavements 2017*, edited by Hasan Ozer, Imad L. Al-Qadi, Eileen M. Velez-Vega, and Scott Murrell, 334–347. Reston, VA: ASCE. https://doi.org/10.1061/9780784480939.029

Smith, K. D., J. E. Bruinsma, M. J. Wade, K. Chatti, J. Vandenbossche, and H. T. Yu. 2017. *Using Falling Weight Deflectometer Data with Mechanistic-Empirical Design and Analysis, Volume I*. Report No. FHWA-HRT-16-009. Washington, DC: Federal Highway Administration. https://www.fhwa.dot.gov/publications/research/infrastructure/pavements/16009/

Talvik, O., and A. Aavik. 2009. "Use of FWD Deflection Basin Parameters (SCI, BDI, BCI) for Pavement Condition Assessment". *The Baltic Journal of Road and Bridge Engineering*, 4(4): 196-202. https://bjrbe-journals.rtu.lv/article/view/1822-427X.2009.4.196-202

Tutumluer, E., H. Ozer, W. Hou, and V. Mwumvaneza. 2015. *Sustainable Aggregates Production: Green Applications for Aggregate By-products*. Report No. FHWA-ICT-15-012. ICT Project R27-125. Rantoul, IL: Illinois Center for Transportation/Illinois Department of Transportation. https://apps.ict.illinois.edu/projects/getfile.asp?id=3507

APPENDIX A: AGGREGATE SUBGRADE IMPROVEMENT 12" SPECIAL

FAI Route 57 (I-57)
Project NHPP-HGM4 (021)
Section 46-2(1)HBR-2
Kankakee County
Contract No. 66961

AGGREGATE SUBGRADE IMPROVEMENT 12" SPECIAL

Description. This work shall consist of constructing an aggregate subgrade improvement using quarry by-products.

Materials. Materials shall be according to the following.

Item	Article/Section
(a) Coarse Aggregate	Note 1
(b) Reclaimed Asphalt Pavement (RAP) (Notes 2 and 3)	1031
(c) Quarry By-Product Aggregate (Note 4)	1003.01 and 1004.01

Note 1. The 3 in. (75 mm) capping aggregate shall be consist of sound durable particles reasonably free of deleterious materials and be gradation CA 6 or CA 10.

Note 2. RAP having 100 percent passing the 1 1/2 in. (37.5 mm) sieve and being well graded, may be used as capping aggregate in the top 3 in. (75 mm).

Note 3. The RAP used for aggregate subgrade improvement shall be according to the current Bureau of Materials and Physical Research Policy Memorandum, "Reclaimed Asphalt Pavement (RAP) for Aggregate Applications".

Note 4. Quarry by-product aggregate shall consist of a mixture of surplus quarry stone sand and primary crushed stone. The surplus quarry stone sand and primary crushed stone shall be combined in the presence of the Engineer with 25% to 50% by weight surplus quarry stone sand to create the quarry by-product aggregate. Mixing with loaders will be permitted provided the weights of materials being mixed can be verified and the resulting stockpile is evenly mixed and free from segregation. The surplus quarry stone sand shall be defined as surplus materials from the aggregate production process and shall be 100% passing the 3/8 in. (9.5 mm) sieve. The primary crushed stone shall be defined as the aggregate resulting after processing through one crusher and shall be 100% passing the 6 in. (150 mm) sieve. The gradation of the combined material shall be 100% passing the 6 in. (150 mm) sieve and 8% to 12% passing the No. 200 sieve. Quarry by-product aggregate shall be free of objectional deleterious material. The quarry byproduct aggregate shall not be permitted to segregate

during mixing, stockpiling, transporting, or placing. In the event segregation is not prevented during mixing, stockpiling, transporting, or placing, then all mixing shall be performed at the job site at the point of placement.

Equipment. The vibratory machine shall be according to Article 1101.01, or as approved by the Engineer.

Soil Preparation. The stability of the soil shall be according to the Department's Subgrade Stability Manual for the aggregate thickness specified.

Placing Aggregate. The maximum nominal thickness of quarry by-product aggregate placed in a single lift shall be 24 in. (600 mm).

Capping Aggregate. The top surface of the aggregate subgrade improvement using quarry by-products shall consist of a minimum 3 in. (75 mm) of capping aggregate.

Compaction. All aggregate lifts shall be compacted to the satisfaction of the Engineer. If the moisture content of the material is such that compaction cannot be obtained, sufficient water shall be added so that satisfactory compaction can be obtained.

Finishing and Maintenance of Aggregate Subgrade Improvement Using Quarry By-Products. The aggregate subgrade improvement using quarry by-products shall be finished to the lines, grades, and cross sections shown on the plans, or as directed by the Engineer. The aggregate subgrade improvement using quarry by-products shall be maintained in a smooth and compacted condition.

Method of Measurement. This work will be measured for payment according to Article 311.08.

Basis of Payment. This work will be paid for at the contract unit price per square yard for AGGREGATE SUBGRADE IMPROVEMENT 12" SPECIAL.

APPENDIX B: PHOTOS OF FIELD ACTIVITIES

Figure 56. Photo. Scooping primary crushed rocks for blending at the quarry.

Figure 57. Photo. Weighing by-product sand in loader bucket to prepare quarry by-product aggregates.

Figure 58. Photo. Blended stockpile for the QBA_M1 material.

Figure 59. Photo. Dumping quarry by-product aggregate materials at the job site.

Figure 60. Photo. Spreading quarry by-product aggregate materials using a bulldozer.

Figure 61. Photo. Final finished surface of the QBA_M1 material after compaction.

Figure 62. Photo. Conducting lightweight deflectometer testing on top of QBA_M1 layer.

Figure 63. Photo. Conducting falling weight deflectometer testing on top of the capping layer of the PCR_1 test section.

Figure 64. Photo. Final road surface—east side of bridge (April 6, 2021).

Figure 65. Photo. Final road surface—west side of bridge (April 6, 2021).

APPENDIX C: DYNAMIC CONE PENETRATION DATA ON TOP OF PREPARED NATURAL SUBGRADE (WEST SIDE OF BRIDGE)

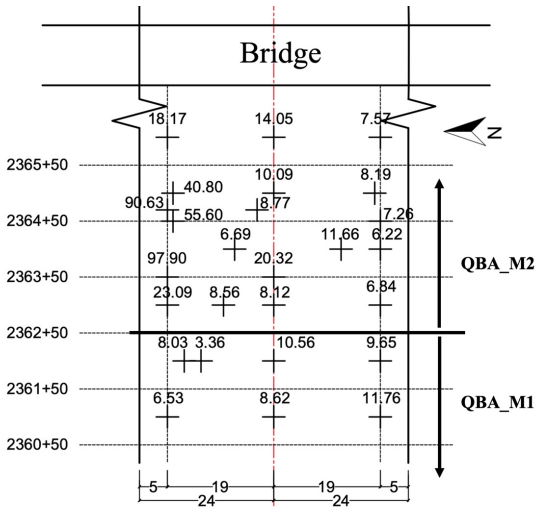

Figure 66. Plot. Achieved IBV(%) in the prepared natural subgrade (west side of bridge).

Detailed DCP profiles for the locations presented in Figure 66 are shown below in Figure 67. The numbers in Figure 66 represents average values for the top 12 in. (305 mm). For the first plot (2361+00 19' LT), 2361+00 represents the station number, the following number (19') represents the distance from the measuring location to the road centerline in feet. LT/CL/RT represents a location to the left/centerline/right side of the road, respectively (facing the direction of increasing stationing). The same nomenclature applies to all plots.

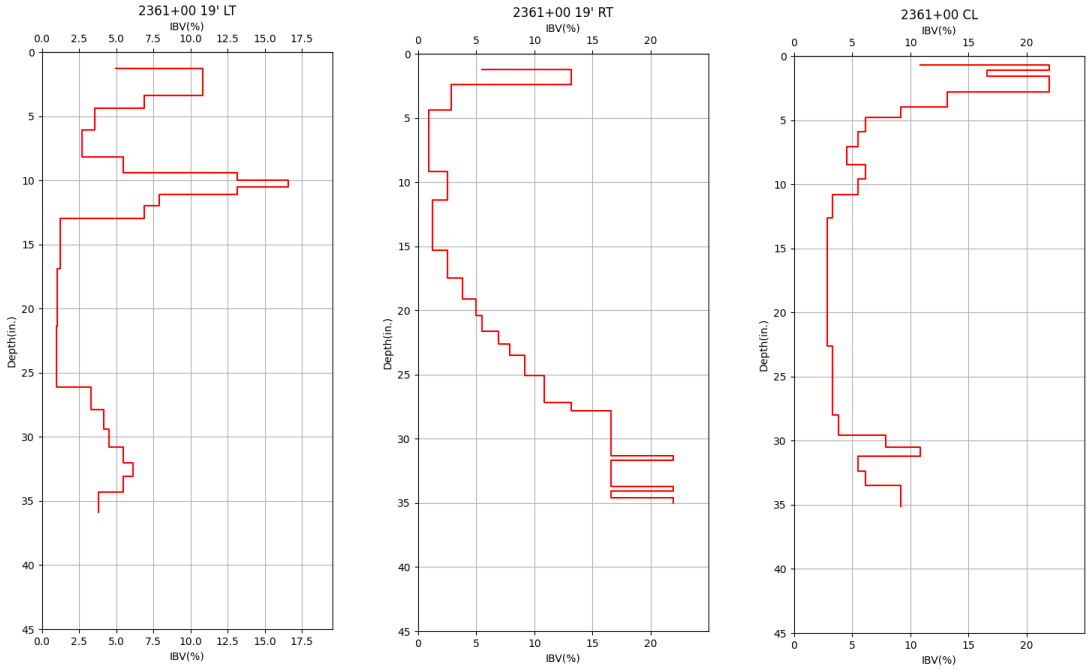

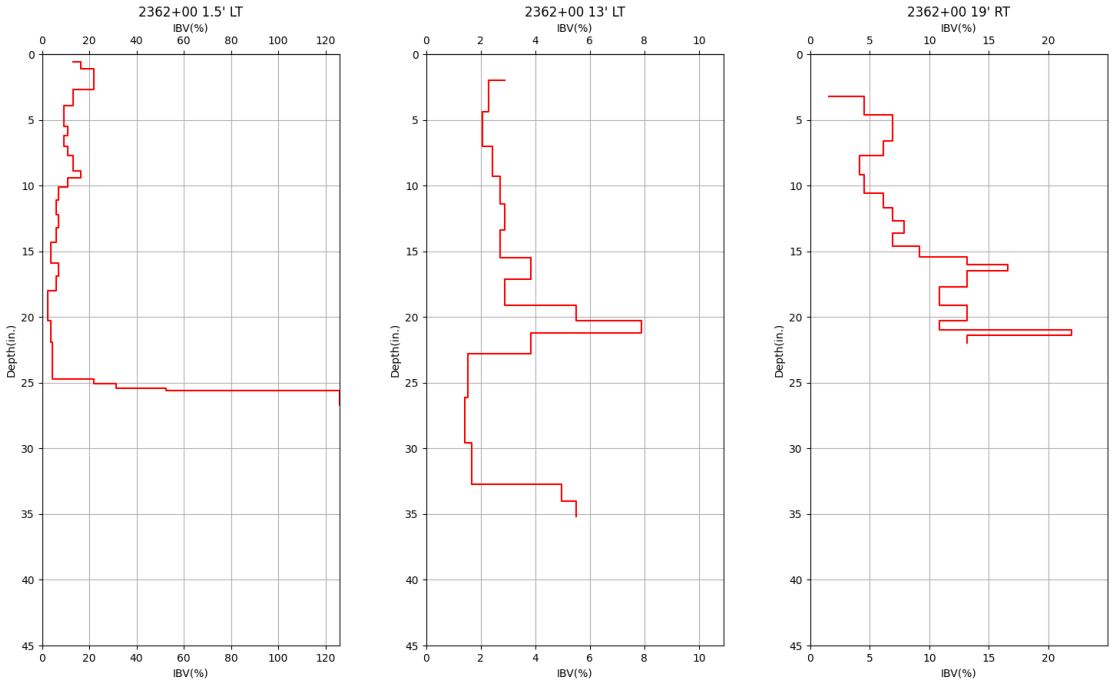
2362+00 1.5' LT
2362+00 13' LT
2362+00 19' RT
IBV(%)
Depth(in.)

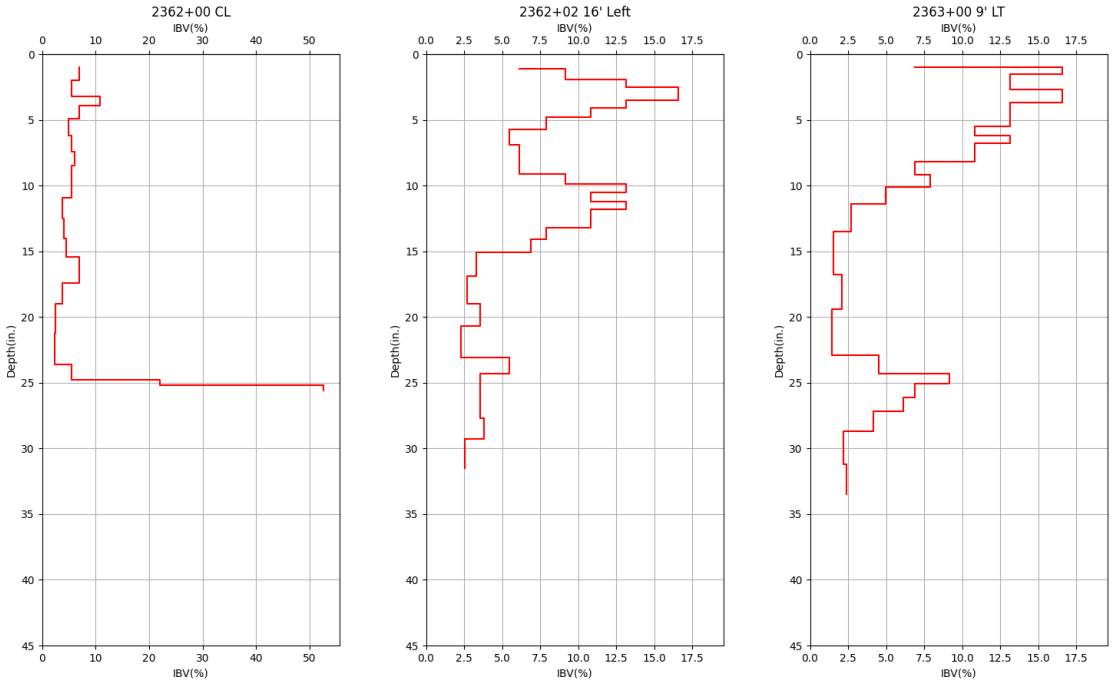
2362+00 CL
2362+02 16' Left
2363+00 9' LT
IBV(%)
Depth(in.)

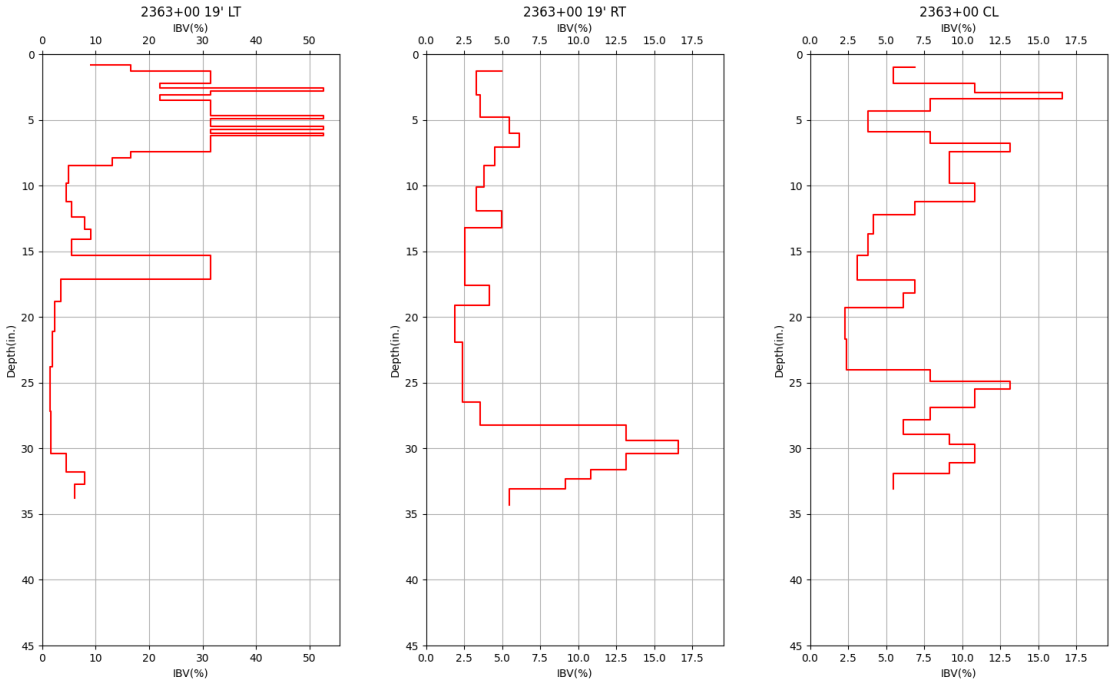
2363+00 19' LT
IBV(%)
Depth(in.)
2363+00 19' RT
IBV(%)
Depth(in.)
2363+00 CL
IBV(%)
Depth(in.)

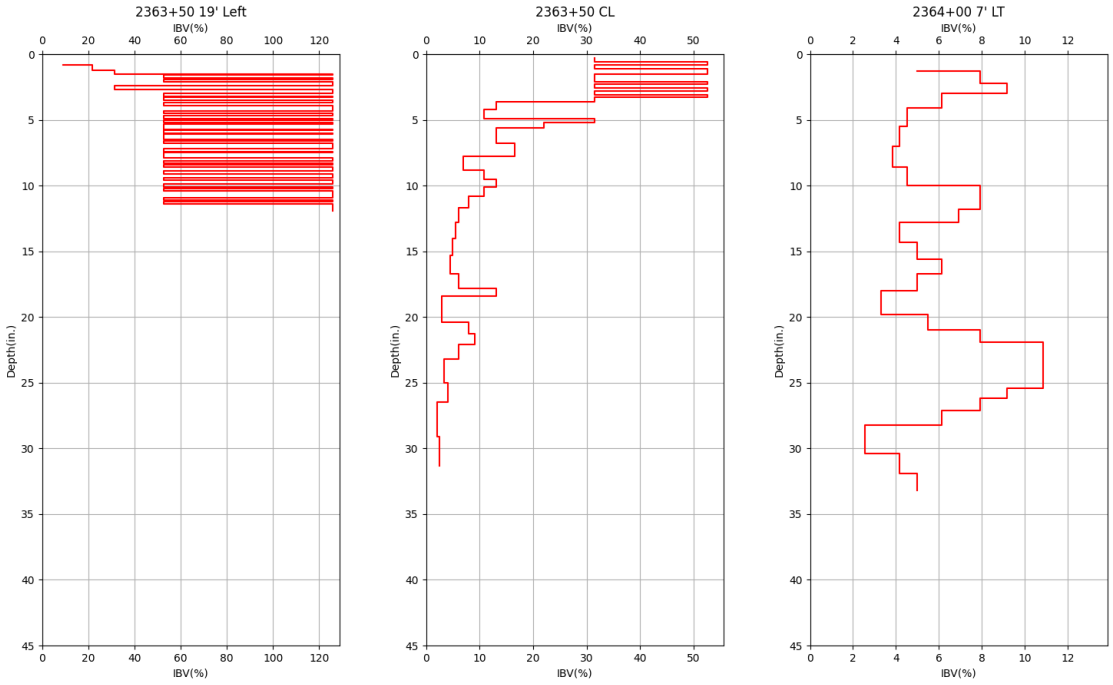
2363+50 19' Left
IBV(%)
Depth(in.)
2363+50 CL
IBV(%)
Depth(in.)
2364+00 7' LT
IBV(%)
Depth(in.)

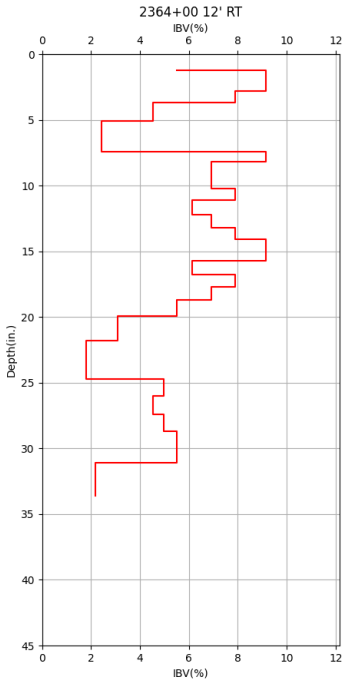
2364+00 12' RT
IBV(%)
Depth(in.)
IBV(%)

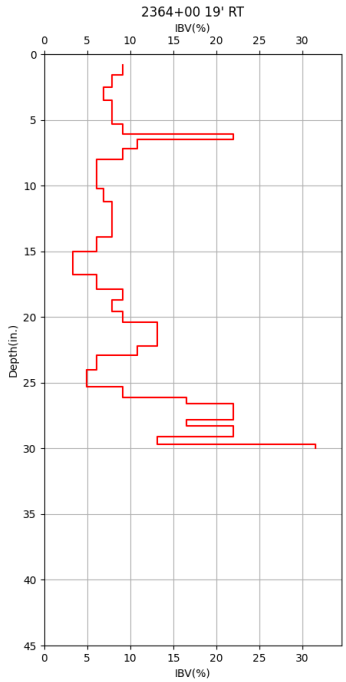
2364+00 19' RT
IBV(%)
Depth(in.)
IBV(%)

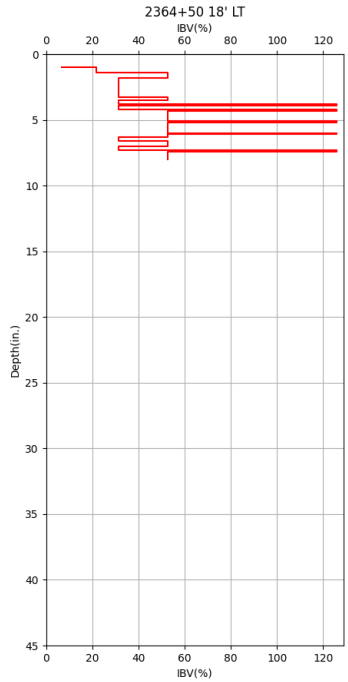
2364+50 18' LT
IBV(%)
Depth(in.)
IBV(%)

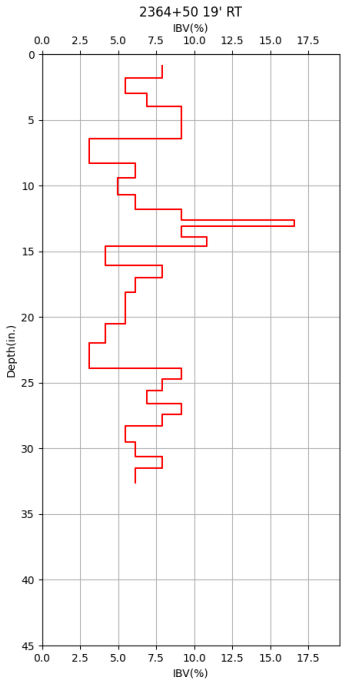
2364+50 19' RT
IBV(%)
Depth(in.)
IBV(%)

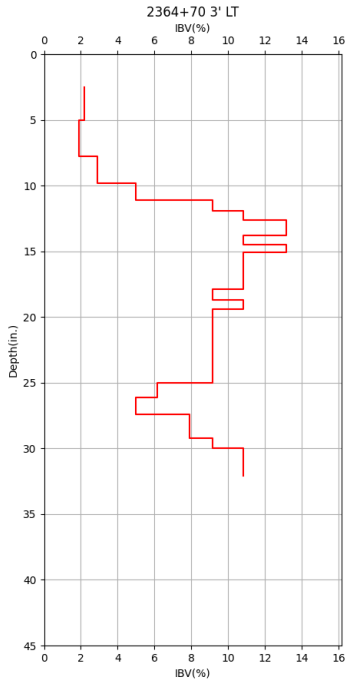
2364+70 3' LT
IBV(%)
Depth(in.)
IBV(%)

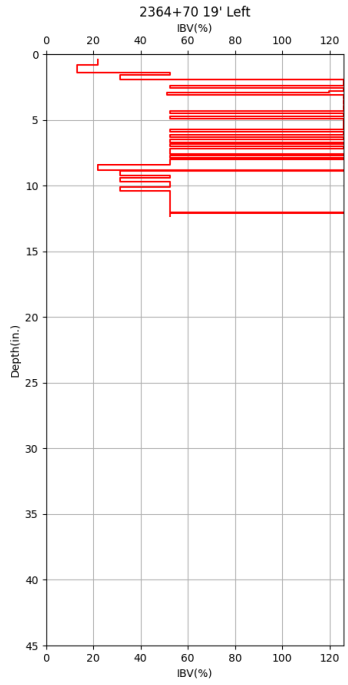
2364+70 19' Left
IBV(%)
Depth(in.)
IBV(%)

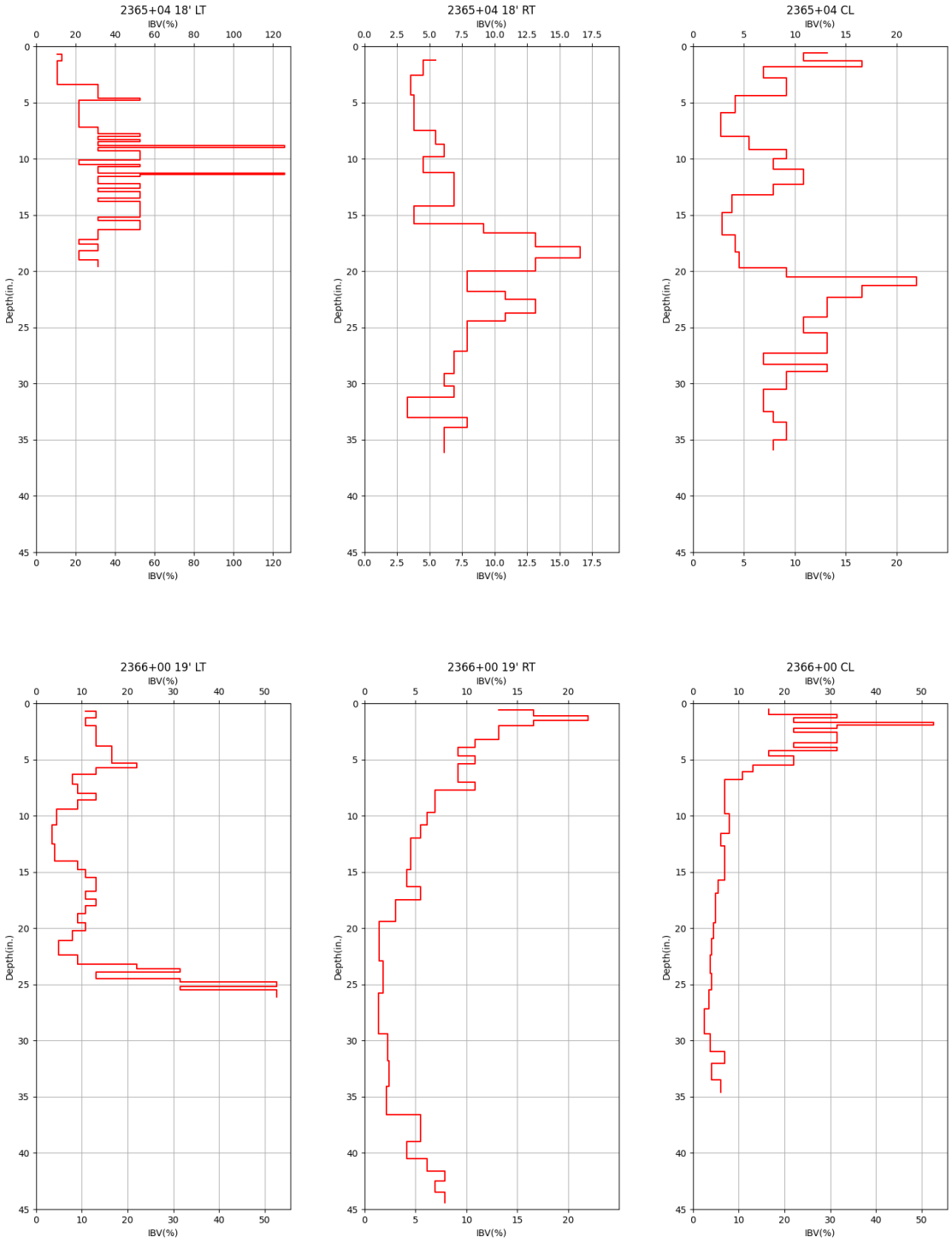

Figure 67. Graphs. DCP profiles for the prepared subgrade at different measuring points (west side of bridge).

APPENDIX D: DYNAMIC CONE PENETRATION DATA ON TOP OF PREPARED NATURAL SUBGRADE (EAST SIDE OF BRIDGE)

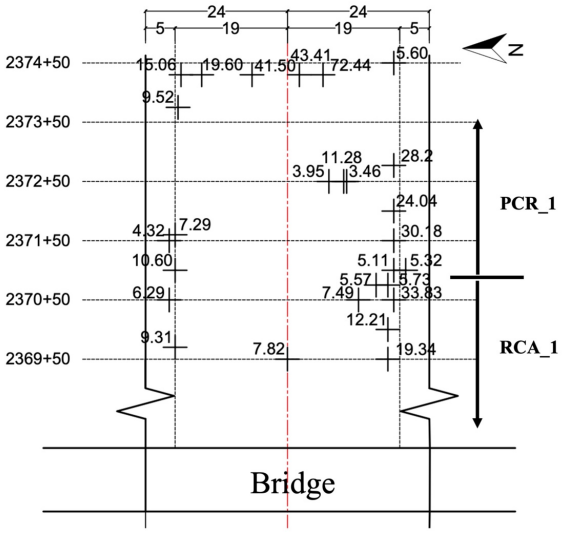

Figure 68. Plot. Achieved IBV(%) in the prepared natural subgrade (west side of bridge).

Detailed DCP profiles for the locations presented in Figure 68 are shown below in Figure 69. The numbers in Figure 68 represents average values for the top 12 in. (305 mm). For the first plot (2369+20 7.8' LT), 2369+20 represents the station number, the following number (7.8') represents the distance from the measuring location to the road centerline in feet. LT/CL/RT represents a location to the left/centerline/right side of the road, respectively (facing the direction of increasing stationing). The same nomenclature applies to all plots.

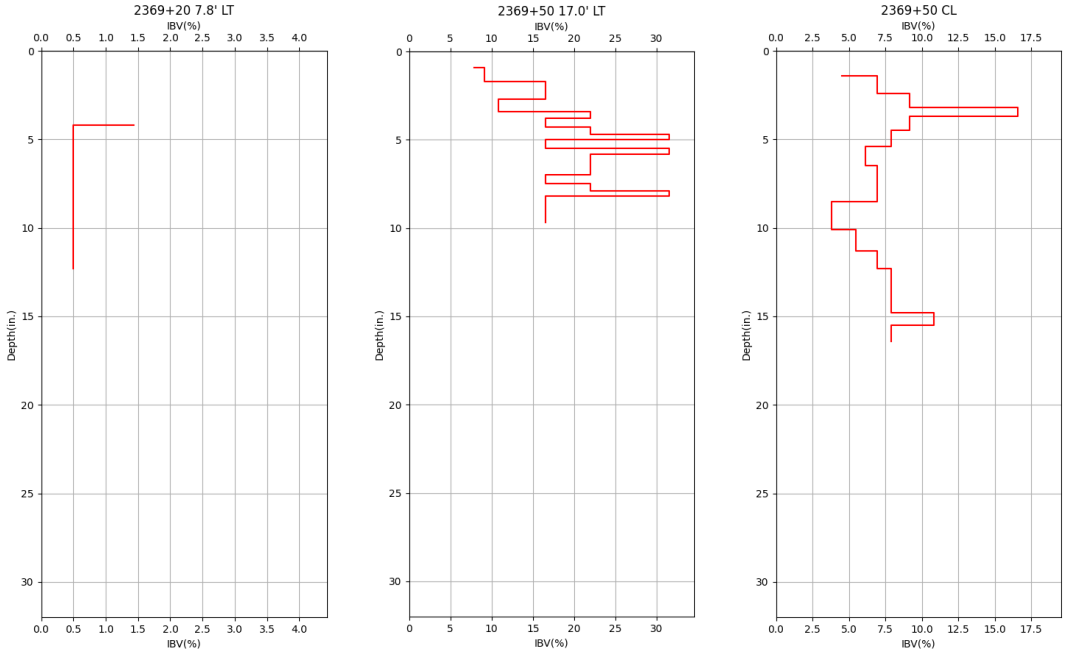

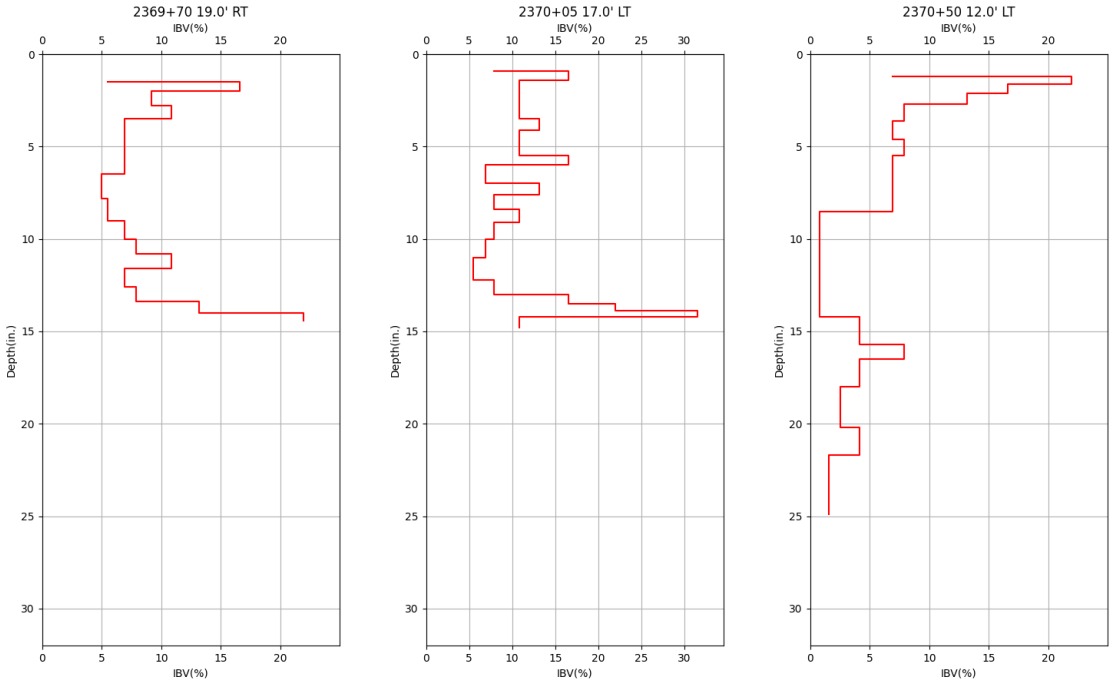
2369+70 19.0' RT
2370+05 17.0' LT
2370+50 12.0' LT
IBV(%)
Depth(in.)

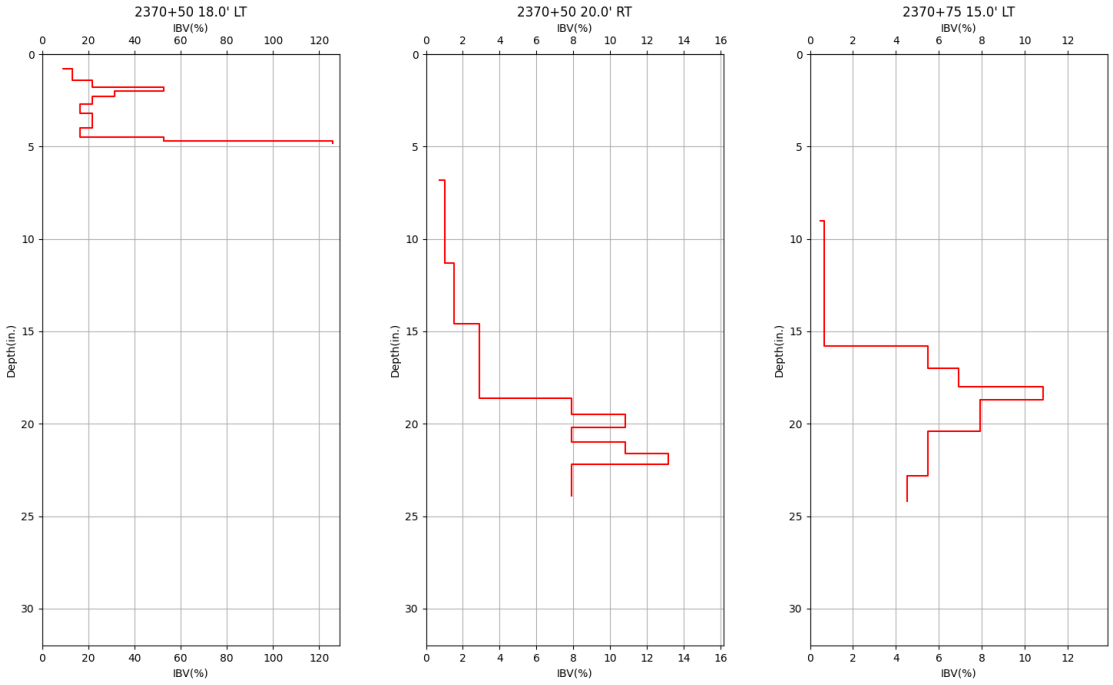
2370+50 18.0' LT
2370+50 20.0' RT
2370+75 15.0' LT
IBV(%)
Depth(in.)

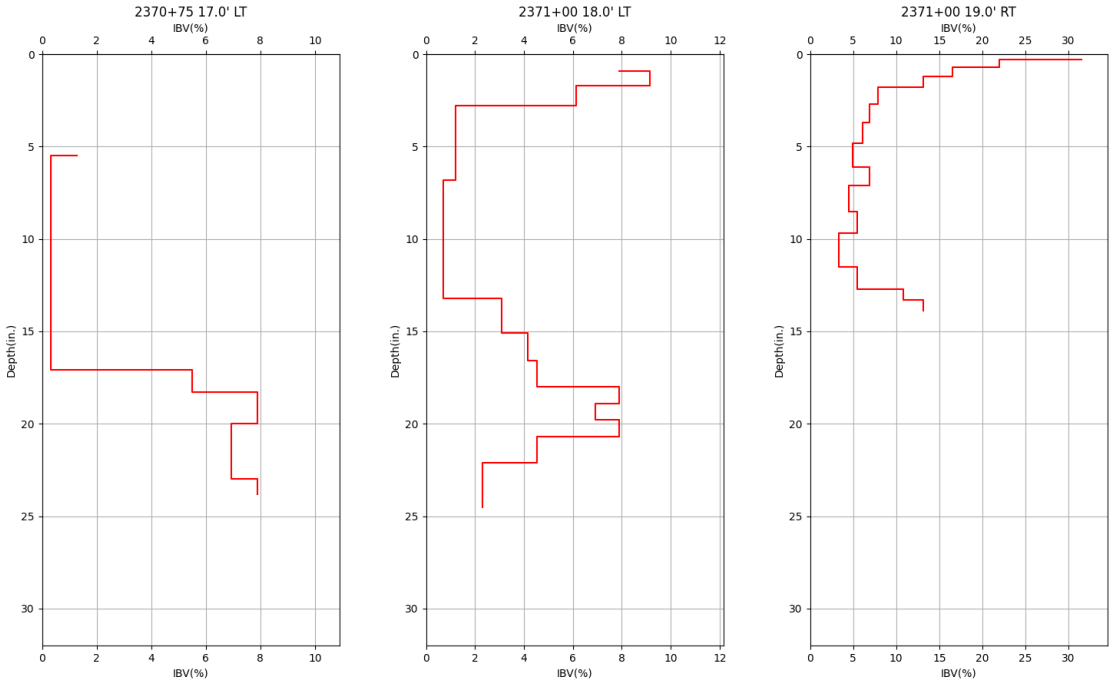
2370+75 17.0' LT
2371+00 18.0' LT
2371+00 19.0' RT
IBV(%)
Depth(in.)

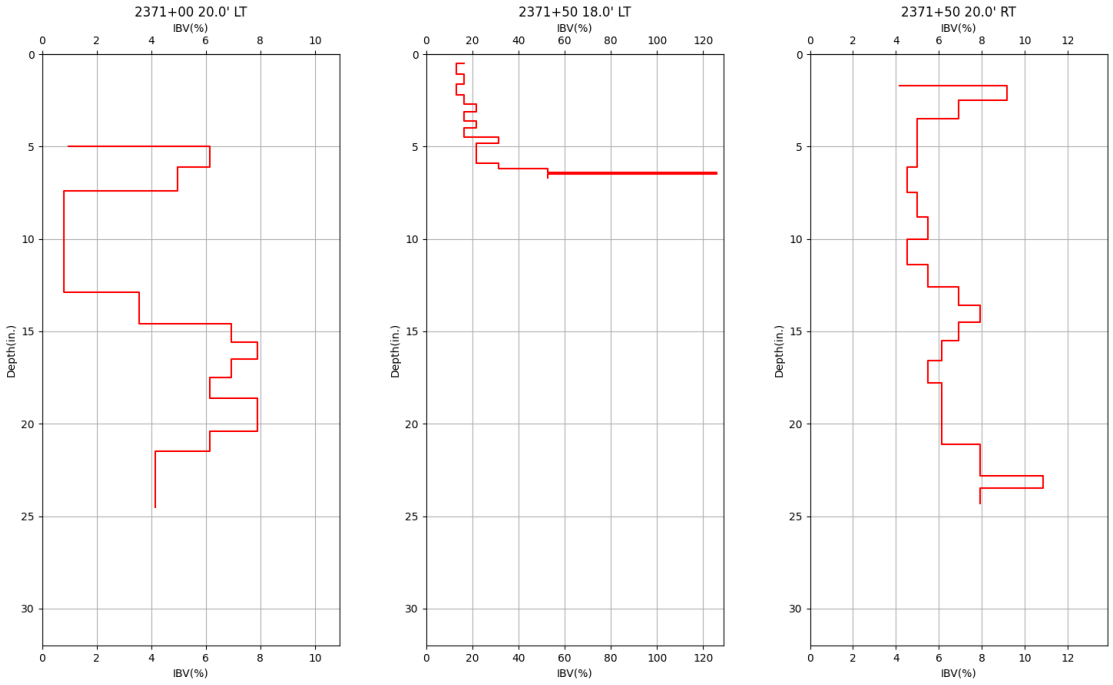
2371+00 20.0' LT
2371+50 18.0' LT
2371+50 20.0' RT
IBV(%)
Depth(in.)

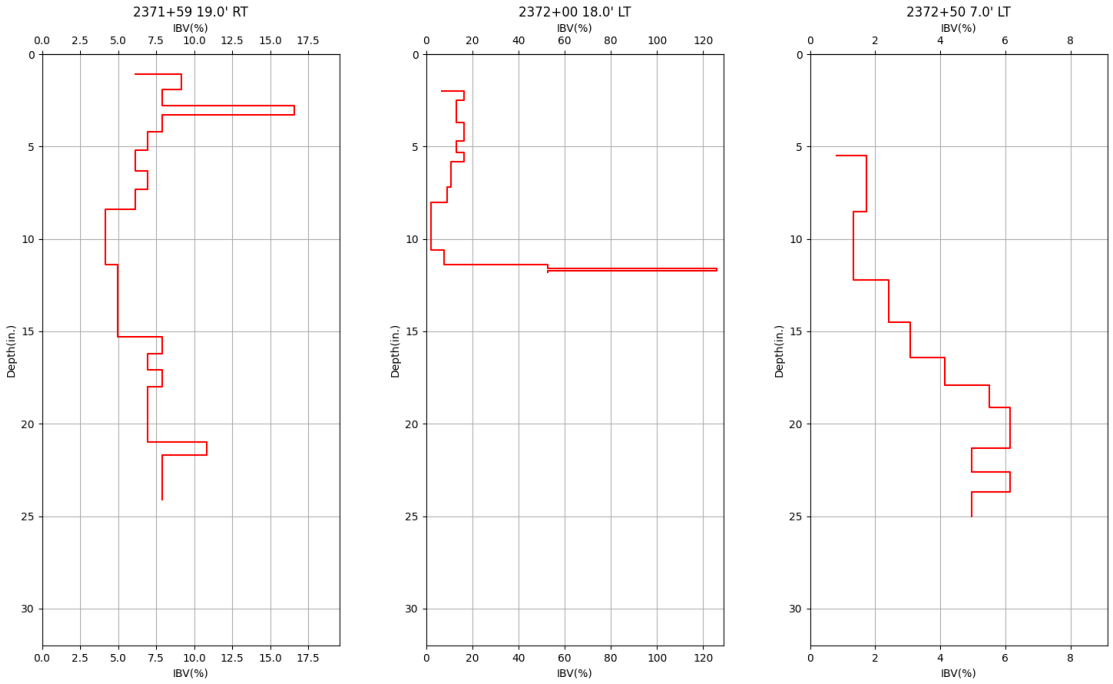
2371+59 19.0' RT
IBV(%)
Depth(in.)

2372+00 18.0' LT
IBV(%)
Depth(in.)

2372+50 7.0' LT
IBV(%)
Depth(in.)

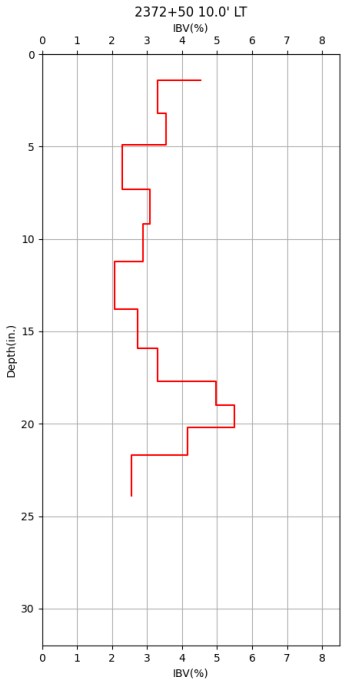
2372+50 10.0' LT
IBV(%)
Depth(in.)

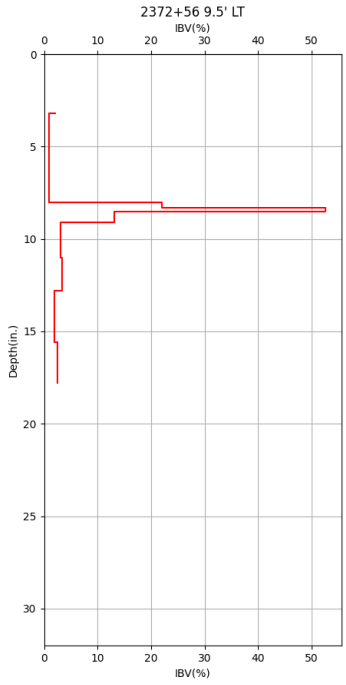
2372+56 9.5' LT
IBV(%)
Depth(in.)

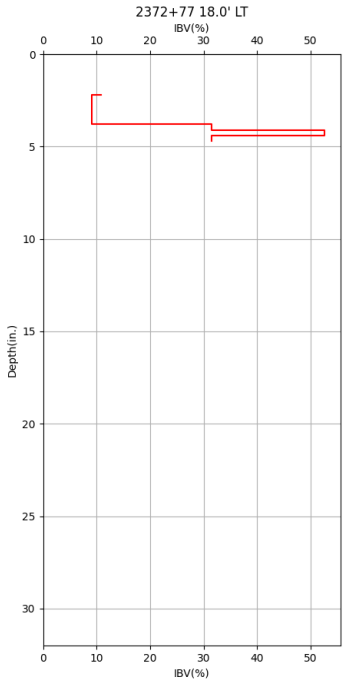
2372+77 18.0' LT
IBV(%)
Depth(in.)

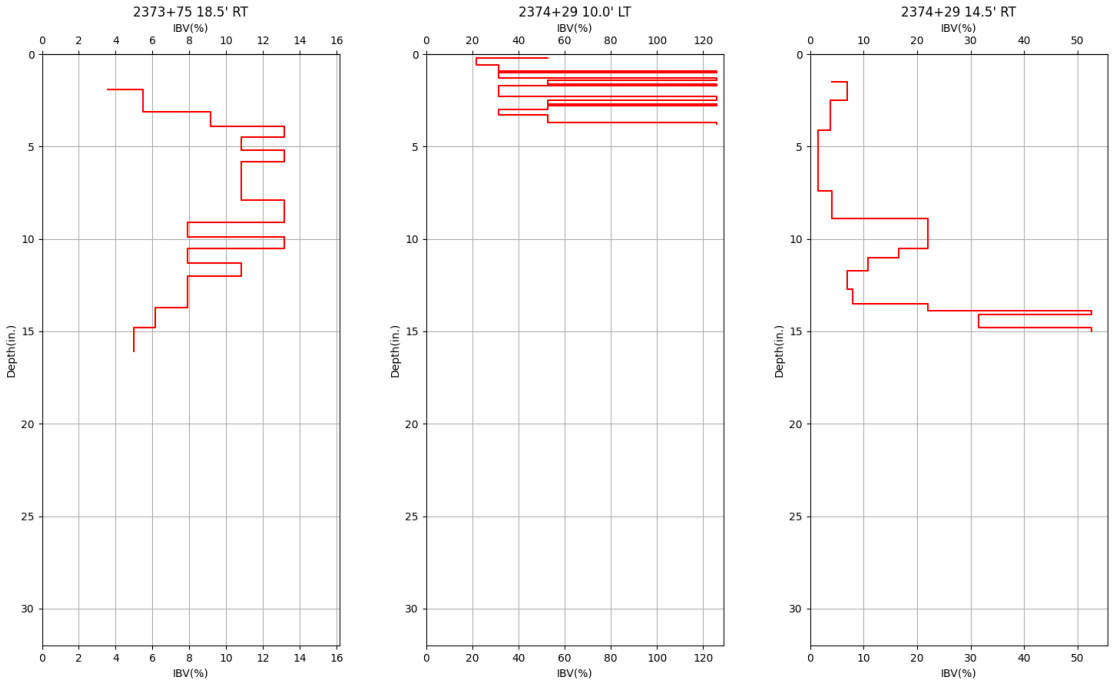
2373+75 18.5' RT
2374+29 10.0' LT
2374+29 14.5' RT
IBV(%)
Depth(in.)

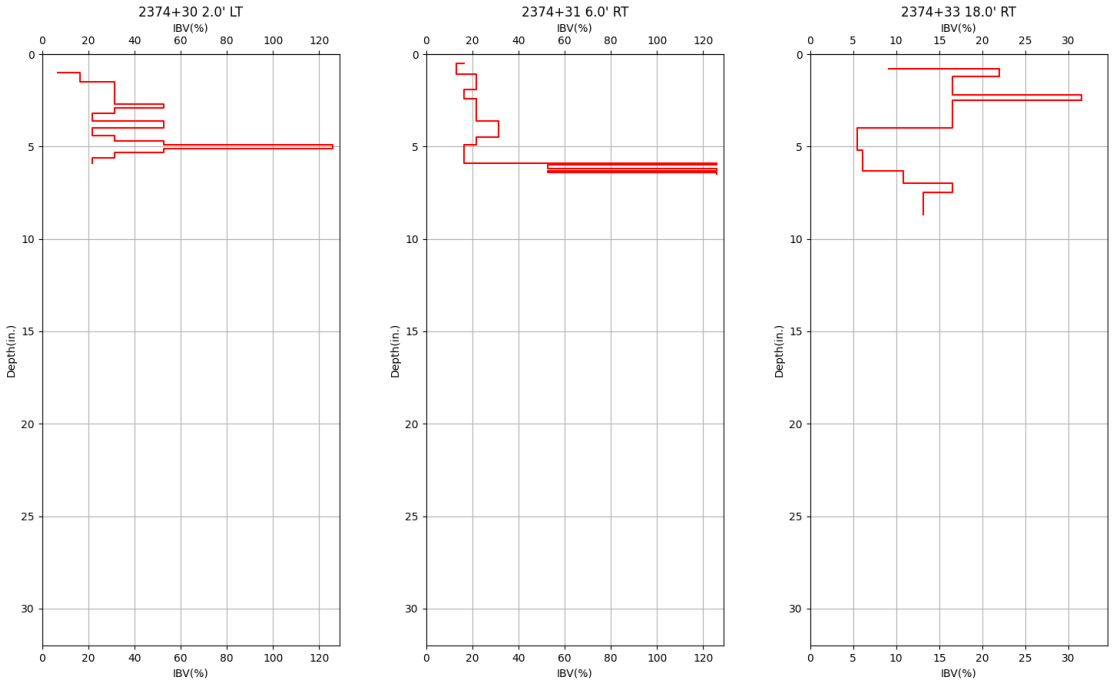
2374+30 2.0' LT
2374+31 6.0' RT
2374+33 18.0' RT
IBV(%)
Depth(in.)

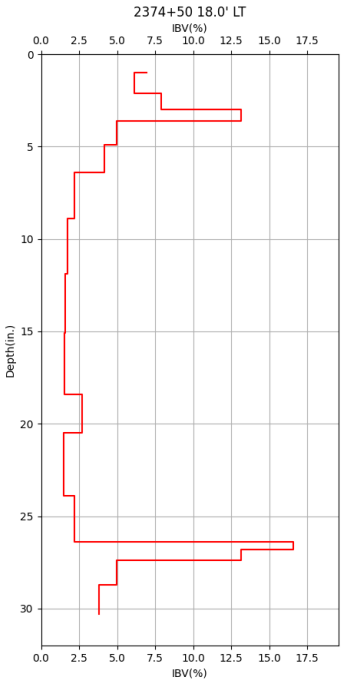

Figure 69. Graphs. DCP profiles of prepared subgrade at different measuring points (east side of bridge).

APPENDIX E: DYNAMIC CONE PENETRATION DATA ON TOP OF CAPPING MATERIALS (WEST SIDE OF BRIDGE)

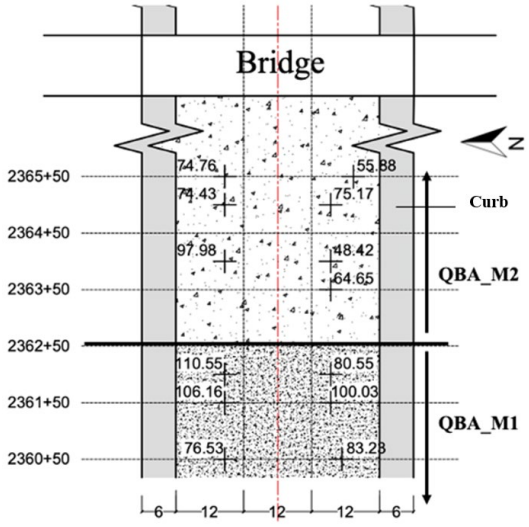

Figure 70. Plot. Achieved average IBV (%) in the ASI layers (west side of bridge).

Detailed DCP profiles for the locations presented in Figure 70 are shown below in Figure 71. The numbers in Figure 70 represents average values for the ASI layer. For the first plot (2360+50 6.64' RT), 2360+50 represents the station number, the following number (6.64') represents the distance from the measuring location to the side curb in feet. LT/CL/RT represents a location to the left/centerline/right side of the road, respectively (facing the direction of increasing stationing). The same nomenclature applies to all plots.

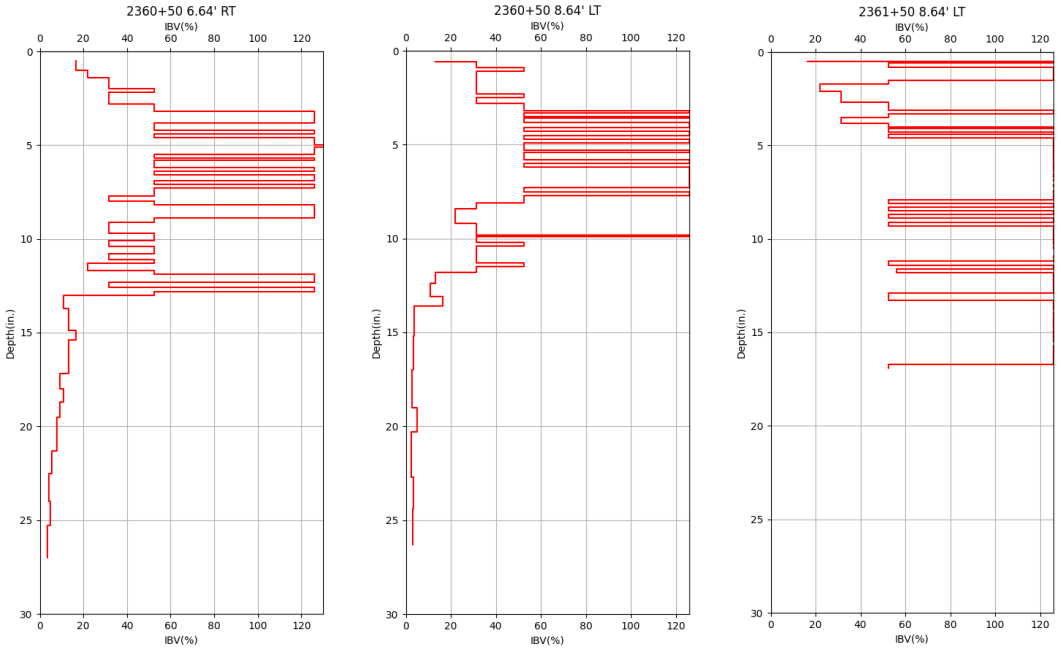

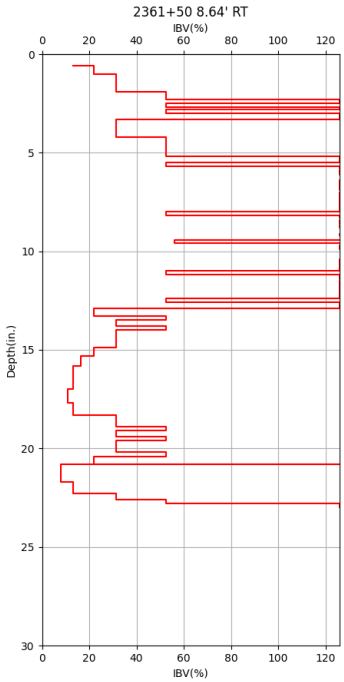
2361+50 8.64' RT
IBV(%)
Depth(in.)

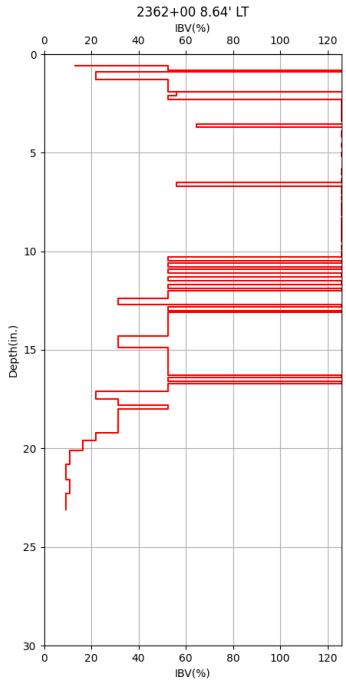
2362+00 8.64' LT
IBV(%)
Depth(in.)

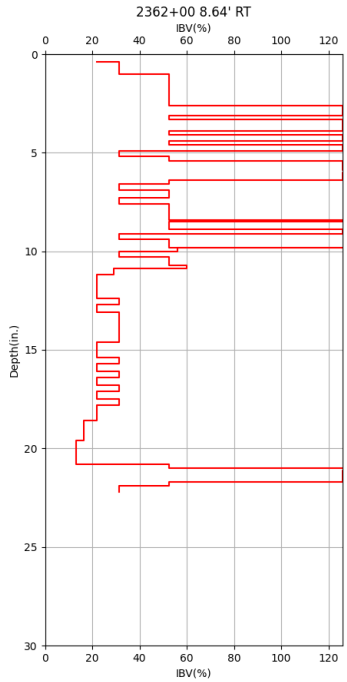
2362+00 8.64' RT
IBV(%)
Depth(in.)

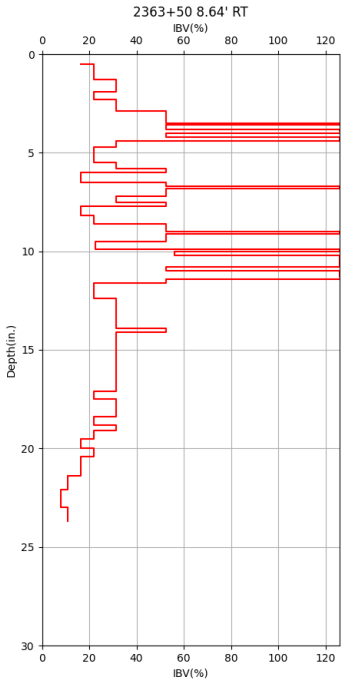
2363+50 8.64' RT
IBV(%)
Depth(in.)

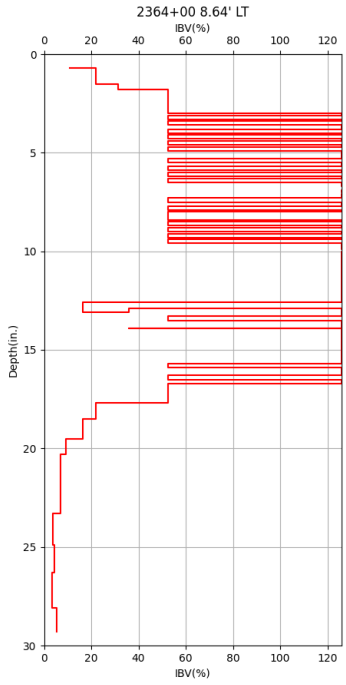
2364+00 8.64' LT
IBV(%)
Depth(in.)

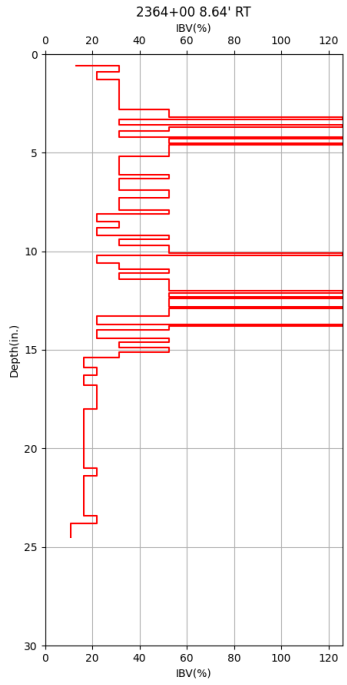
2364+00 8.64' RT
IBV(%)
Depth(in.)

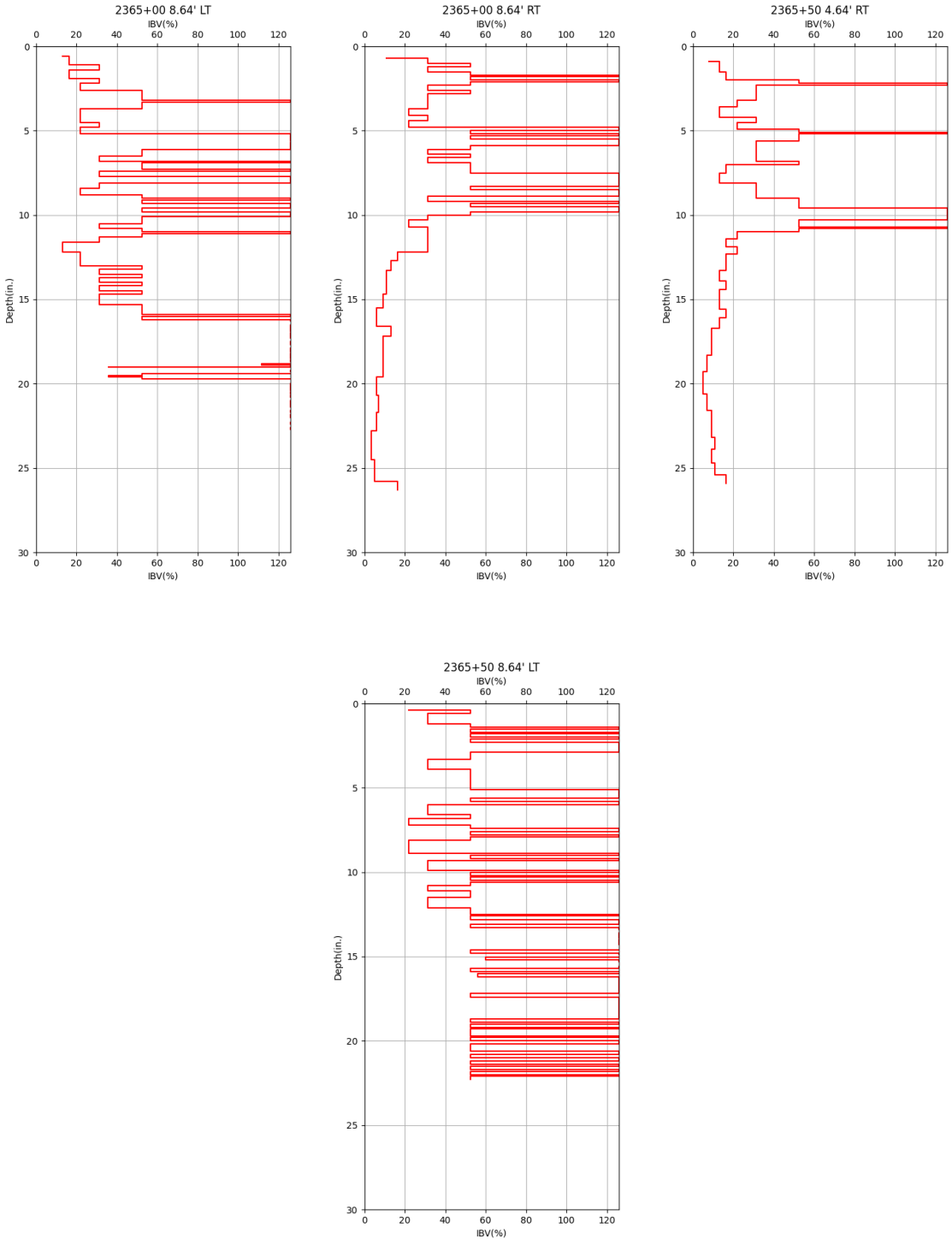

Figure 71. Graphs. IBV profiles from DCP tests on top of the capping layers (west side of bridge).

APPENDIX F: DYNAMIC CONE PENETRATION DATA ON TOP OF CAPPING MATERIALS (EAST SIDE OF BRIDGE)

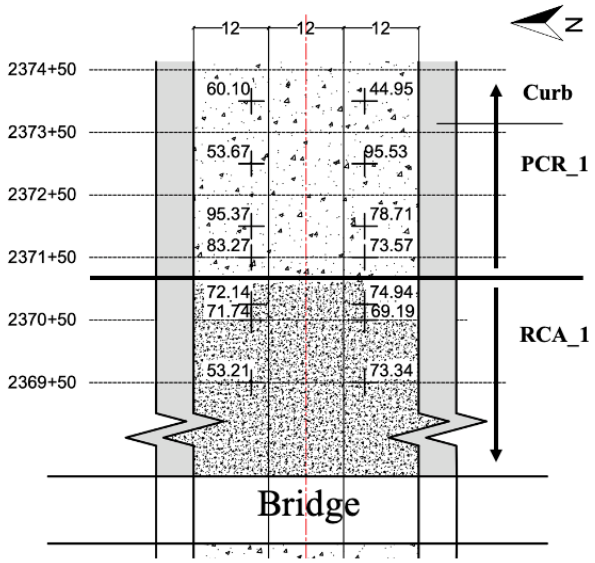

Figure 72. Plot. Achieved average IBV (%) in the ASI layers (east side of bridge).

Detailed DCP profiles for the locations presented in Figure 72 are shown below in Figure 73. The numbers in Figure 72 represents average values for the ASI layer. For the first plot (2369+50 8.64' LT), 2369+50 represents the station number, the following number (8.64') represents the distance from the measuring location to the side curb in feet. LT/CL/RT represents a location to the left/centerline/ right side of the road, respectively (facing the bridge). The same nomenclature applies to all plots.

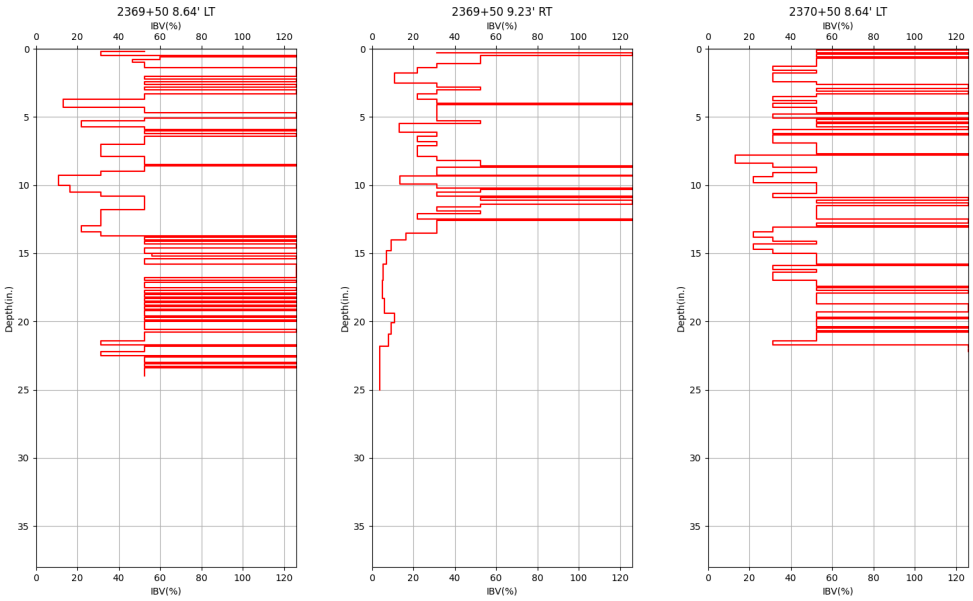

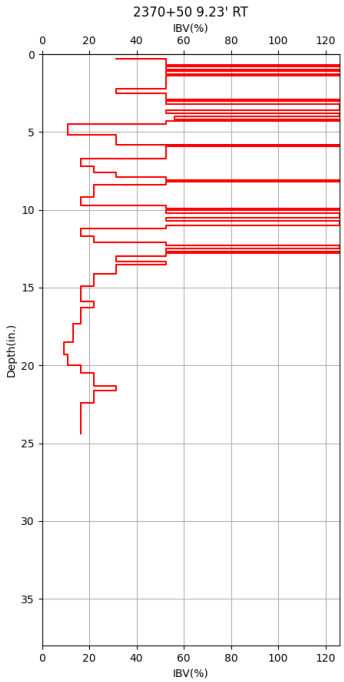
2370+50 9.23' RT
IBV(%)
Depth(in.)

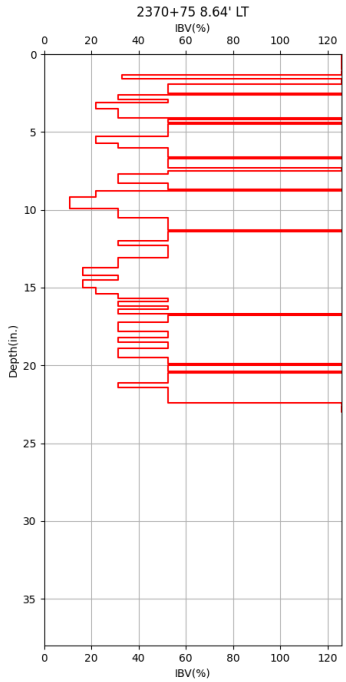
2370+75 8.64' LT
IBV(%)
Depth(in.)

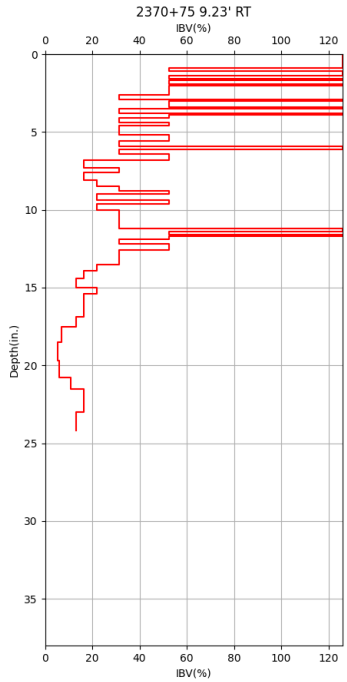
2370+75 9.23' RT
IBV(%)
Depth(in.)

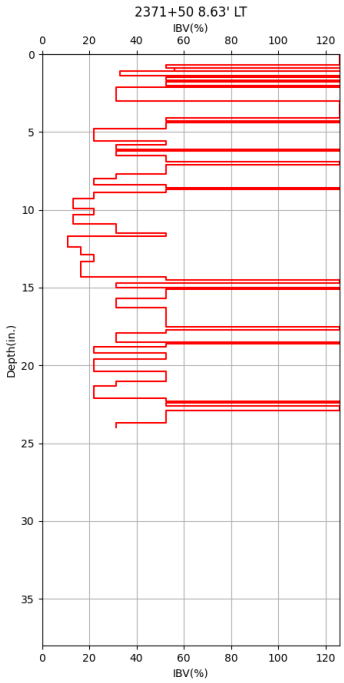
2371+50 8.63' LT
IBV(%)
Depth(in.)

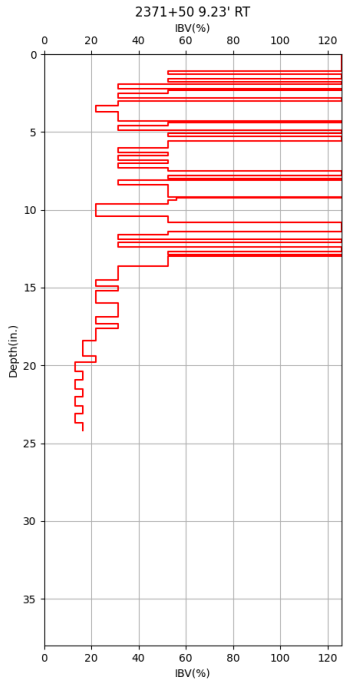
2371+50 9.23' RT
IBV(%)
Depth(in.)

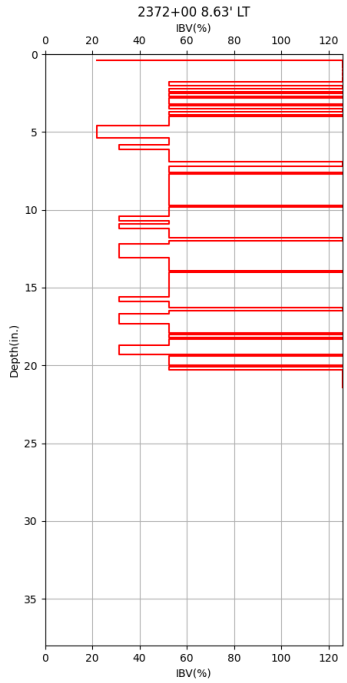
2372+00 8.63' LT
IBV(%)
Depth(in.)

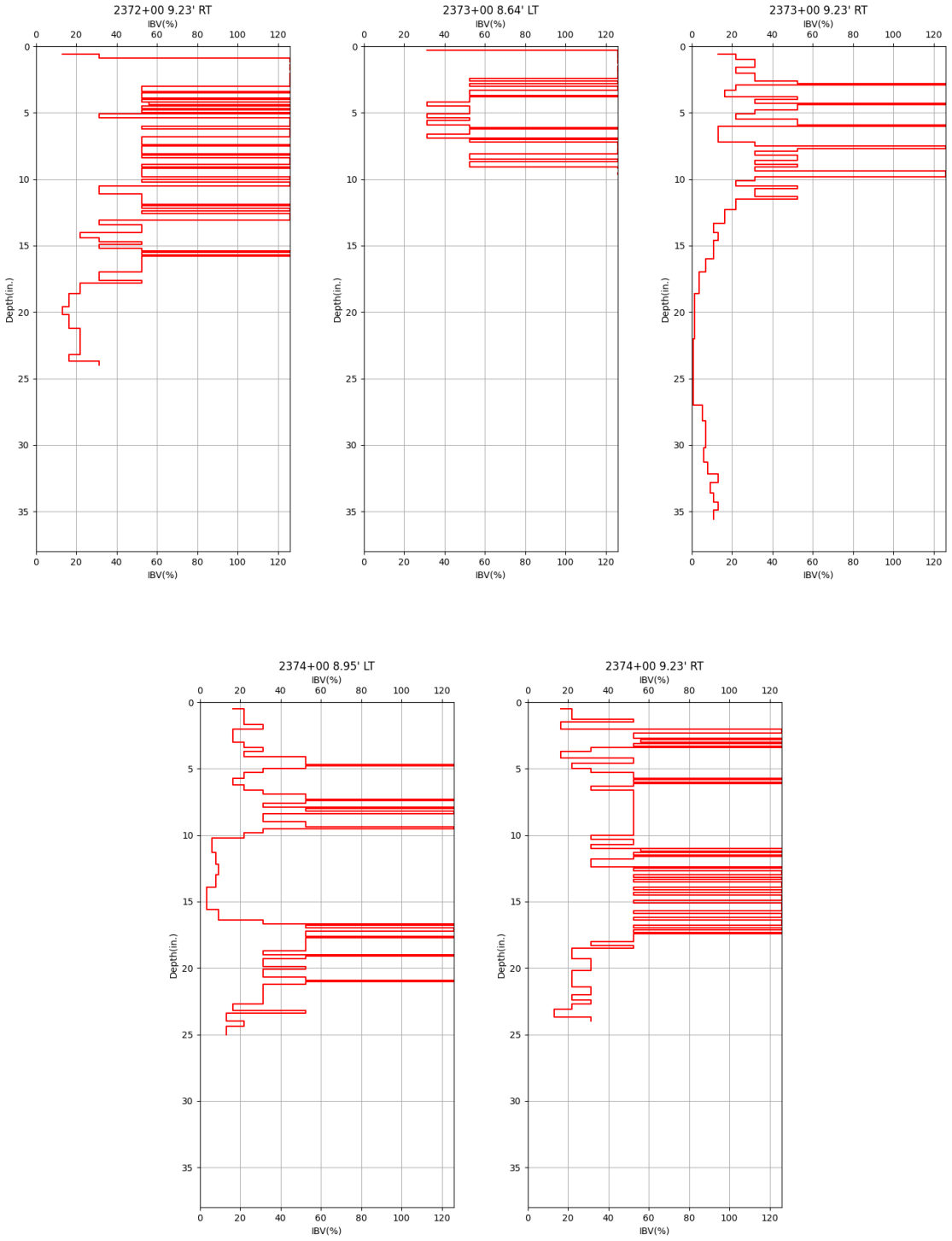

Figure 73. Graphs. IBV profiles from DCP test on top of capping layers (east side of bridge).

APPENDIX G: LIGHTWEIGHT DEFLECTOMETER DATA ON TOP OF PREPARED NATURAL SUBGRADE

Table 12. Summary of LWD Data on Top of Prepared Subgrade—West Side of Bridge

Station	Offset	s/v	Reading #1	Reading #2	Reading #3	Average	Modulus
	(ft)	(300 mm/10kg)	(mm)	(mm)	(mm)	(mm)	(MN/m^2)
2362+00	**1.5L***	9.469	2.741	2.725	2.724	2.730	**8.24**
		9.315	3.259	3.245	3.244	3.249	**6.93**
2362+00	**16L***	7.114	1.929	1.858	1.827	1.871	**12.03**
		8.290	2.722	2.667	2.567	2.652	**8.48**
2363+50	**0**	5.313	0.951	0.937	0.963	0.950	**23.68**
		5.183	0.966	0.967	0.962	0.965	**23.32**
2363+50	**19L***	2.555	0.280	0.271	0.285	0.279	**80.65**
		3.614	0.324	0.317	0.313	0.318	**70.75**
2364+00	**0**	7.513	1.754	1.775	1.763	1.764	**12.76**
		5.581	1.296	1.288	1.293	1.292	**17.41**
2364+00	**19R***	3.637	0.706	0.684	0.679	0.690	**32.61**
		5.261	1.011	0.999	1.013	1.008	**22.32**
2364+70	**0**	7.175	1.644	1.646	1.640	1.643	**13.69**
		6.946	1.536	1.478	1.482	1.499	**15.01**
2364+70	**19L***	2.800	0.488	0.486	0.469	0.481	**46.78**
		2.636	0.596	0.587	0.574	0.586	**38.64**

* Indicates the distance (in feet) and direction (left/right) from the centerline of the road—facing bridge.

APPENDIX H: LIGHTWEIGHT DEFLECTOMETER DATA ON TOP OF THE QUARRY BY-PRODUCT AGGREGATE MIXTURES

Table 13. Summary of LWD Data on Top of QBA Mixes—West Side of Bridge

Station	Offset	s/v	Reading #1	Reading #2	Reading #3	Average	Modulus
	(ft)	(300 mm/10kg)	(mm)	(mm)	(mm)	(mm)	(MN/m^2)
2363+50	**0**	4.952	0.866	0.841	0.788	0.832	**27.04**
		4.085	0.765	0.749	0.704	0.739	**30.45**
2363+50	**19L***	2.945	0.672	0.596	0.566	0.611	**36.82**
		3.604	0.593	0.552	0.543	0.563	**39.96**
2364+00	**0**	4.668	0.775	0.748	0.737	0.753	**29.88**
		4.985	0.862	0.829	0.813	0.835	**26.95**
2364+00	**19R***	5.3	0.846	0.815	0.806	0.822	**27.37**
		4.574	0.863	0.789	0.729	0.794	**28.34**
2364+70	**0**	4.188	0.717	0.706	0.697	0.707	**31.82**
		4.008	0.746	0.689	0.668	0.701	**32.10**
2364+70	**19L***	3.203	0.478	0.452	0.443	0.458	**49.13**
		3.092	0.411	0.402	0.390	0.401	**56.11**
2362+00	**1.5L***	6.097	0.858	0.837	0.830	0.842	**26.72**
		7.118	1.032	1.011	0.987	1.010	**22.28**
2362+00	**16L***	4.716	0.622	0.592	0.603	0.606	**37.13**
		5.829	0.712	0.715	0.703	0.710	**31.69**
2361+25	**0**	3.683	0.480	0.477	0.475	0.477	**47.17**
		4.387	0.784	0.737	0.679	0.733	**30.70**
2361+25	**19R***	9.165	1.302	1.294	1.292	1.296	**17.36**
		8.902	1.311	1.284	1.295	1.297	**17.35**
2360+50	**0**	9.209	1.654	1.637	1.602	1.631	**13.80**
		9.340	1.674	1.664	1.669	1.669	**13.48**
2363+52.5	**18.3L***	9.265	1.607	1.567	1.554	1.576	**14.28**
		9.460	1.521	1.524	1.514	1.520	**14.80**

* Indicates the distance (in feet) and direction (left/right) from the centerline of the road—facing bridge.

APPENDIX I: LIGHTWEIGHT DEFLECTOMETER DATA ON TOP OF THE CAPPING MATERIALS

Table 14. Summary of LWD Data on Top of Capping Material—QBA_M1 Section

Station	Offset	s/v	Reading #1	Reading #2	Reading #3	Average	Modulus
	(ft)	(300 mm/10kg)	(mm)	(mm)	(mm)	(mm)	(MN/m^2)
2362+00	**1.5L****	5.710	0.702	0.683	0.680	0.688	**32.70**
		6.121	0.653	0.663	0.650	0.655	**34.35**
2361+25	**0**	2.562	0.371	0.355	0.337	0.354	**63.56**
		2.542	0.303	0.310	0.304	0.306	**73.53**
2360+50	**0**	6.238	0.874	0.844	0.858	0.859	**26.19**
		6.667	0.827	0.787	0.805	0.806	**27.92**
2360+50	**8.64L***	7.488	1.231	1.198	1.202	1.210	**18.60**
		8.292	1.166	1.160	1.155	1.160	**19.40**
2360+50	**8.64R***	4.869	0.548	0.528	0.534	0.537	**41.90**
		5.090	0.524	0.507	0.497	0.509	**44.20**
2361+00	**8.64L***	6.194	0.709	0.697	0.680	0.695	**32.27**
		6.539	0.649	0.635	0.665	0.650	**34.62**
2361+00	**8.64R***	4.287	0.537	0.516	0.508	0.520	**43.27**
		4.517	0.475	0.469	0.472	0.472	**47.67**
2361+50	**8.64L***	3.065	0.367	0.344	0.352	0.354	**63.56**
		3.013	0.321	0.329	0.328	0.326	**69.02**
2361+50	**8.64R***	4.428	0.622	0.617	0.584	0.608	**37.01**
		4.510	0.562	0.551	0.544	0.552	**40.76**
2362+00	**8.64L***	2.955	0.405	0.368	0.375	0.383	**58.75**
		2.988	0.349	0.346	0.326	0.340	**66.18**
2362+00	**8.64R***	6.269	0.875	0.868	0.843	0.862	**26.10**
		6.152	0.806	0.806	0.791	0.801	**28.09**

* Indicates the distance (in feet) from the side curb and direction (left/right)— facing bridge.

** Indicates the distance (in feet) and direction (left/right) from the centerline of the road— facing bridge.

Table 15. Summary of LWD Data on Top of Capping Material—QBA_M2 Section

Station	Offset	s/v	Reading #1	Reading #2	Reading #3	Average	Modulus
	(ft)	(300 mm/10kg)	(mm)	(mm)	(mm)	(mm)	(MN/m^2)
2363+50	**0**	3.422	0.430	0.430	0.418	0.426	**52.82**
		3.504	0.409	0.392	0.393	0.398	**56.53**
2364+00	**0**	3.791	0.523	0.508	0.477	0.503	**44.73**
		3.858	0.458	0.454	0.455	0.456	**49.34**
2364+70	**0**	4.414	0.608	0.581	0.573	0.587	**38.33**
		4.236	0.537	0.537	0.540	0.538	**41.82**
2363+50	**8.64L***	3.426	0.489	0.474	0.439	0.467	**48.18**
		3.41	0.420	0.411	0.417	0.416	**54.09**
2363+50	**8.64R***	4.551	0.541	0.537	0.533	0.537	**41.90**
		4.783	0.543	0.516	0.530	0.530	**42.45**
2364+00	**8.64L***	4.056	0.688	0.664	0.658	0.670	**33.58**
		4.195	0.628	0.605	0.612	0.615	**36.59**
2364+00	**8.64R***	3.54	0.509	0.479	0.469	0.486	**46.30**
		3.606	0.463	0.460	0.453	0.459	**49.02**
2365+00	**8.64L***	2.736	0.410	0.407	0.382	0.400	**56.25**
		2.689	0.372	0.351	0.358	0.360	**62.50**
2365+00	**8.64R***	5.028	0.835	0.830	0.730	0.798	**28.20**
		5.374	0.739	0.759	0.745	0.748	**30.08**
2365+50	**8.64L***	2.951	0.333	0.321	0.304	0.319	**70.53**
		2.942	0.298	0.278	0.281	0.286	**78.07**
2365+50	**8.64R***	5.307	0.683	0.665	0.647	0.665	**33.83**
		5.357	0.611	0.641	0.618	0.623	**36.12**

* Indicates the distance (in feet) from the side curb and direction (left/right)— facing bridge.

Table 16. Summary of LWD Data on Top of Capping Material—RCA_1 Section

Station	Offset	s/v	Reading #1	Reading #2	Reading #3	Average	Modulus
	(ft)	(300 mm/10kg)	(mm)	(mm)	(mm)	(mm)	(MN/m^2)
2370+75	**8.96R***	3.195	0.428	0.369	0.382	0.393	**57.25**
		3.198	0.340	0.338	0.337	0.338	**66.57**
2370+75	**9.23L***	4.511	0.311	0.307	0.282	0.300	**75.00**
		4.632	0.273	0.272	0.285	0.277	**81.23**
2370+50	**8.64R***	4.042	0.345	0.355	0.344	0.348	**64.66**
		4.059	0.335	0.331	0.329	0.332	**67.77**
2370+50	**9.23L***	3.862	0.427	0.417	0.399	0.414	**54.23**
		4.052	0.409	0.383	0.386	0.393	**57.25**
2369+50	**8.64R***	2.957	0.364	0.360	0.343	0.356	**63.20**
		3.116	0.315	0.327	0.305	0.316	**71.20**
2369+50	**9.23L***	5.721	0.897	0.876	0.834	0.869	**25.89**
		6.087	0.803	0.776	0.783	0.787	**28.59**

* Indicates the distance (in feet) from the side curb and direction (left/right)—facing bridge.

Table 17. Summary of LWD Data on Top of Capping Material—PCR_1 Section

Station	Offset	s/v	Reading #1	Reading #2	Reading #3	Average	Modulus
	(ft)	(300 mm/10kg)	(mm)	(mm)	(mm)	(mm)	(MN/m^2)
2374+00	**8.95R***	5.571	0.711	0.714	0.669	0.698	**32.23**
		5.72	0.621	0.623	0.615	0.620	**36.29**
2374+00	**9.23L***	2.92	0.334	0.322	0.319	0.325	**69.23**
		2.965	0.300	0.287	0.297	0.295	**76.27**
2373+00	**8.64R***	3.357	0.197	0.180	0.186	0.188	**119.68**
		3.446	0.193	0.178	0.179	0.183	**122.95**
2373+00	**9.23L***	6.891	0.769	0.765	0.766	0.767	**29.34**
		7.282	0.790	0.787	0.801	0.793	**28.37**
2372+00	**8.63R***	2.923	0.273	0.278	0.269	0.273	**82.42**
		3.015	0.251	0.252	0.245	0.249	**90.36**
2372+00	**9.23L***	3.255	0.372	0.357	0.346	0.358	**62.85**
		3.412	0.317	0.311	0.322	0.317	**70.98**
2371+50	**8.63R***	3.833	0.296	0.302	0.285	0.294	**76.53**
		3.862	0.277	0.280	0.268	0.275	**81.82**
2371+50	**9.23L***	4.404	0.476	0.456	0.441	0.458	**49.13**
		4.534	0.419	0.426	0.423	0.423	**53.19**

* Indicates the distance (in feet) from the side curb and direction (left/right)— facing bridge.

APPENDIX J: FALLING WEIGHT DEFLECTOMETER DATA ON TOP OF CAPPING MATERIAL (WEST SIDE OF BRIDGE)

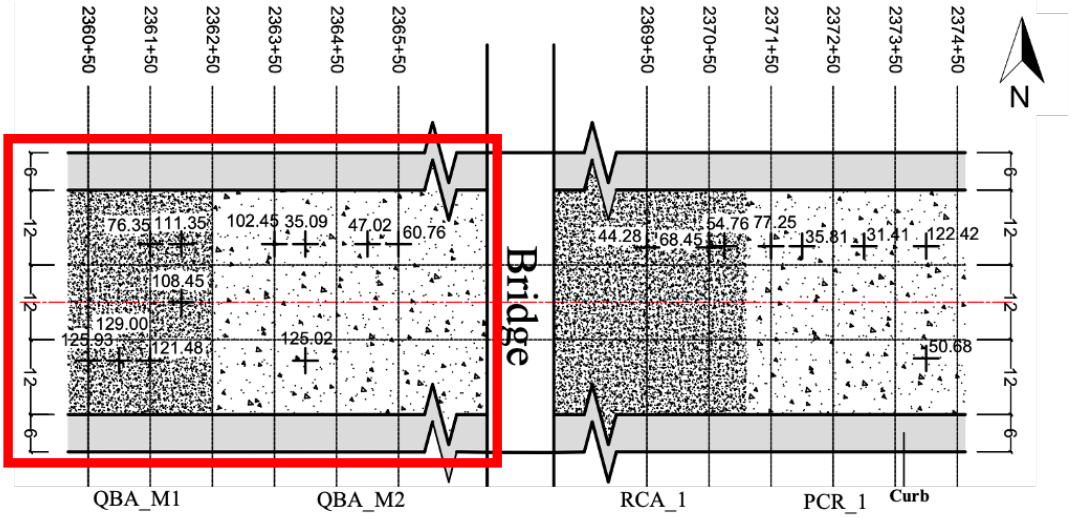

Figure 74. Plot. FWD average surface deflections (mils) of center geophone (D_0) on top of capping layer, normalized to a 12-kip (53-kN) load level.

Detailed FWD deflection basin profiles for the locations presented in Figure 74 (west side of bridge) are shown below in Figure 75. For the first plot (Location: 2360+50 EB), 2360+50 represents the station number. EB/WB indicate drop locations on the eastbound/westbound driving lanes. CL represents a test spot located at the centerline of the road. All the test locations not on the centerline have an offset of 8.64' from curb. In order to examine the deflections nonlinearity and the impact of dynamic load, three levels of loading (desirably 6-kips, 9-kips, 12-kips) are desired to be applied. The numbers presented in the legends represent the load applied by the load plate for each drop at each station. Deflections detected after each drop are plotted for each load level. The same nomenclature applies to all plots.

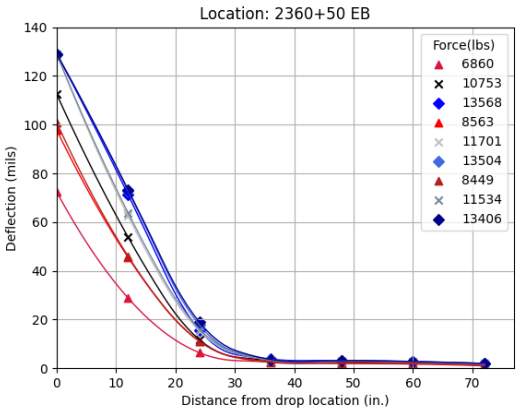

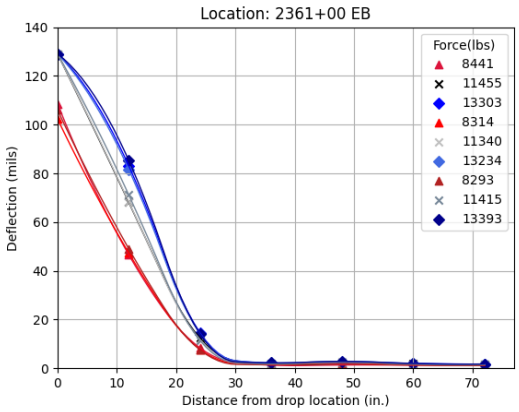

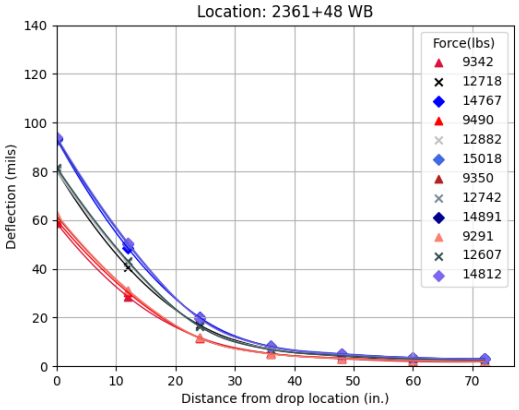
Location: 2361+48 WB
Force(lbs)
9342
12718
14767
9490
12882
15018
9350
12742
14891
9291
12607
14812
Deflection (mils)
Distance from drop location (in.)

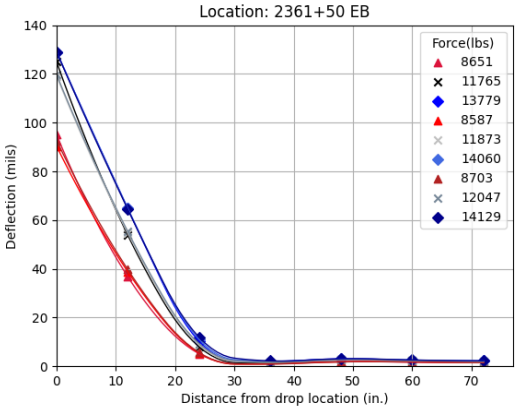
Location: 2361+50 EB
Force(lbs)
8651
11765
13779
8587
11873
14060
8703
12047
14129
Deflection (mils)
Distance from drop location (in.)

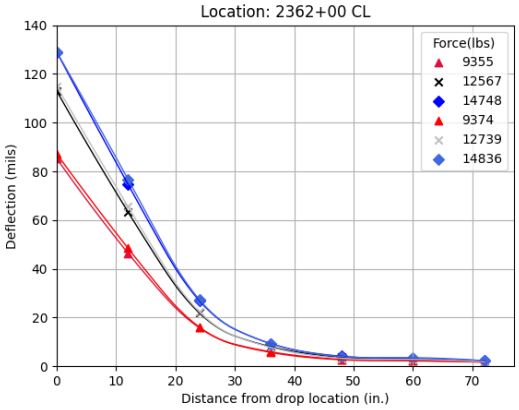
Location: 2362+00 CL
Force(lbs)
9355
12567
14748
9374
12739
14836
Deflection (mils)
Distance from drop location (in.)

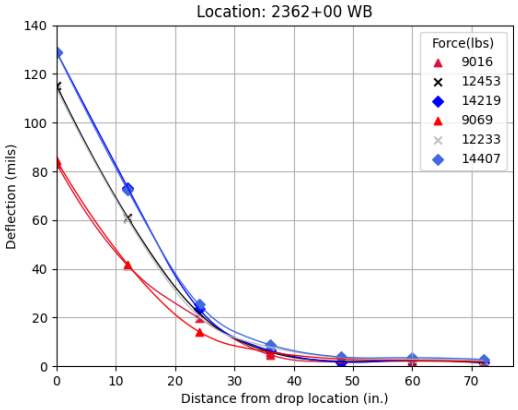
Location: 2362+00 WB
Force(lbs)
9016
12453
14219
9069
12233
14407
Deflection (mils)
Distance from drop location (in.)

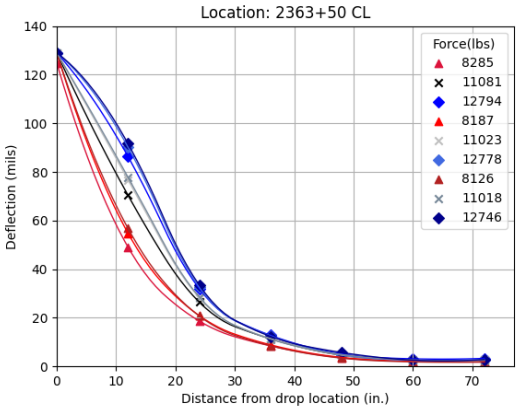
Location: 2363+50 CL
Force(lbs)
8285
11081
12794
8187
11023
12778
8126
11018
12746
Deflection (mils)
Distance from drop location (in.)

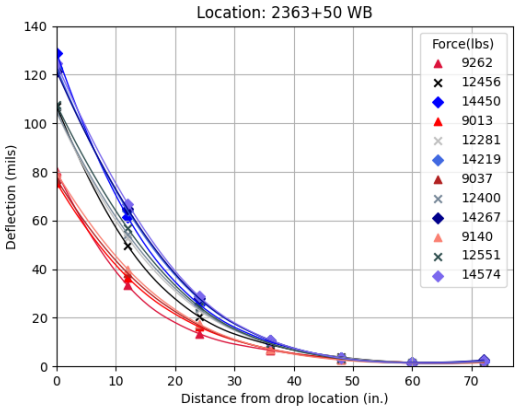
Location: 2363+50 WB
Force(lbs)
9262
12456
14450
9013
12281
14219
9037
12400
14267
9140
12551
14574
Deflection (mils)
Distance from drop location (in.)

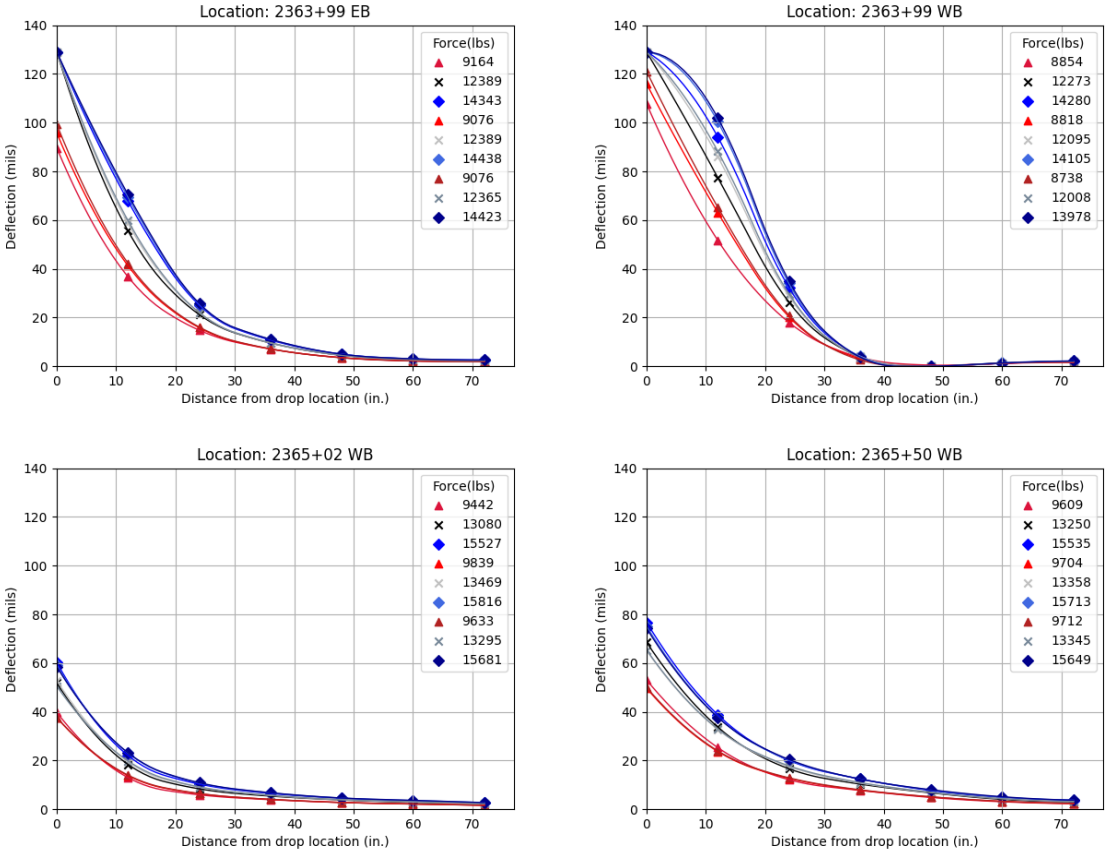

Figure 75. Graphs. FWD data on top of the capping layers at different measuring points in the QBA sections.

APPENDIX K: FALLING WEIGHT DEFLECTOMETER ON TOP OF CAPPING MATERIAL (EAST SIDE OF BRIDGE)

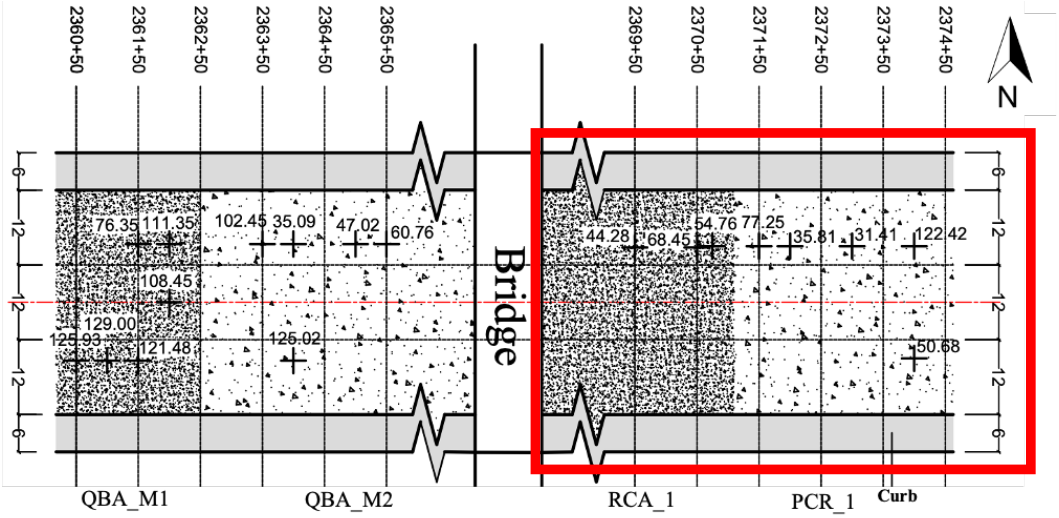

Figure 76. Plot. FWD average surface deflections (mils) of center geophone (D_0) on top of capping layer, normalized to a 12-kip (53-kN) load level.

Detailed FWD deflection profiles for the locations presented in Figure 76 (East side) are shown below in Figure 77. For the first plot (Location: 2369+50 WB), 2369+50 represents the station number. EB/WB indicate drop locations on the eastbound/westbound driving lanes. CL indicates a test spot located at the centerline of the road. In order to examine the deflections nonlinearity and the impact of dynamic load, three levels of loading (desirably 6-kips, 9-kips, 12-kips) are applied. The numbers presented in legend represent the load applied by the load plate for each drop at each station. Deflections detected after each drop are plotted for each load level. All westbound test locations have an offset of 9.23 ft. from the curb and all eastbound test locations have an offset of 8.64 ft. from the curb.

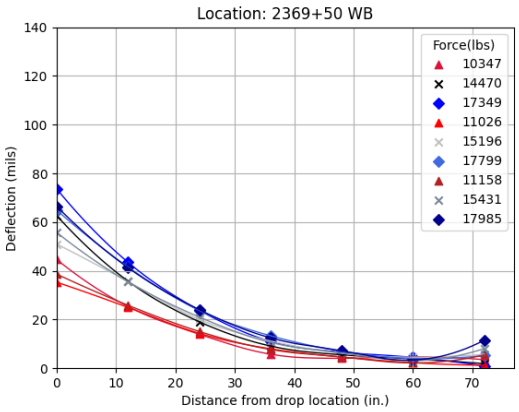

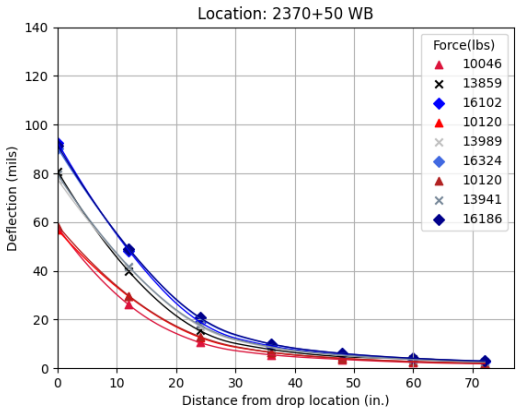

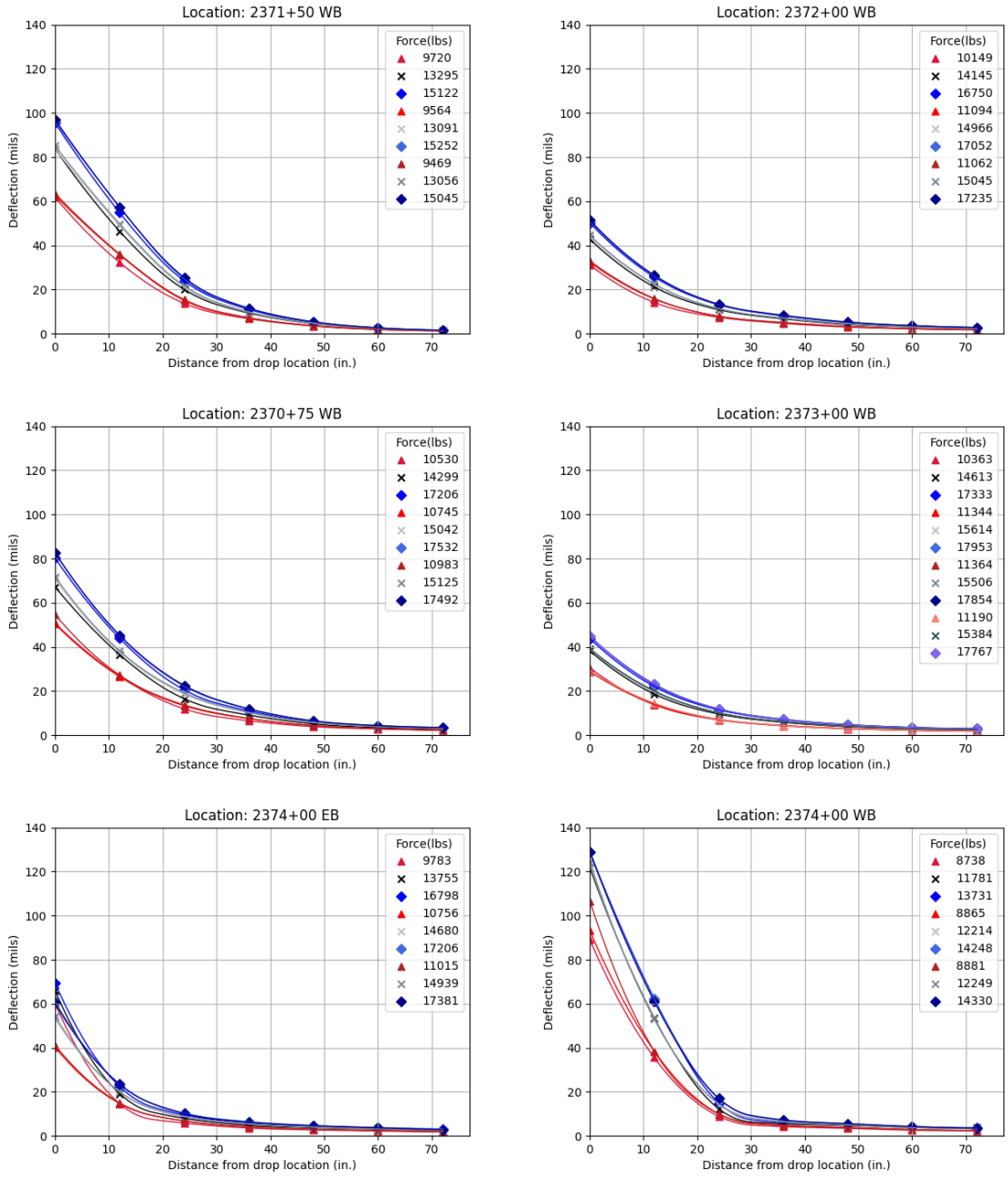

Figure 1. Graphs. FWD data on top of the capping layers at different measuring points in the conventional ASI sections.

APPENDIX L: FALLING WEIGHT DEFLECTOMETER DATA ON TOP OF HMA—AFTER CONSTRUCTION (WEST SIDE OF BRIDGE)

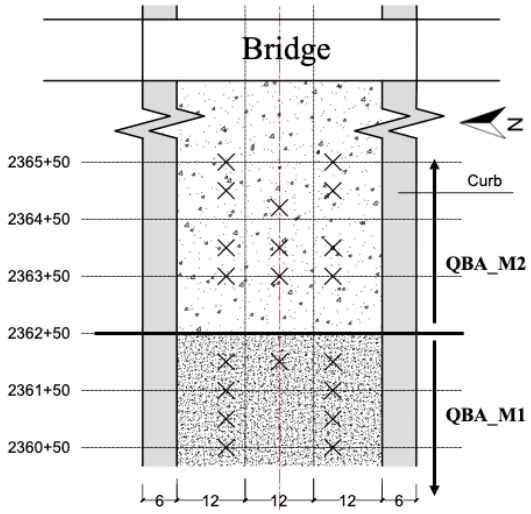

Figure 78. Plot. FWD test locations on top of HMA (west side of bridge).

Detailed FWD deflection profiles for the locations presented in Figure 78 are shown below in Figure 79. For the first plot (Location: 2360+50 EB), 2360+50 represents the station number. EB/WB indicate drop locations on the eastbound/westbound driving lanes. CL represents the test spot is located at road centerline. In order to examine the deflections nonlinearity and the impact of dynamic load, four levels of loading (6-kips, 9-kips, 12-kips and 15-kips) are applied. The numbers presented in legend represent the load applied by the load plate for each drop at each station. Deflections detected after each drop are plotted for each load level. The same nomenclature applies to all plots. All the test locations not on the centerline have an offset of 8.64' from curb.

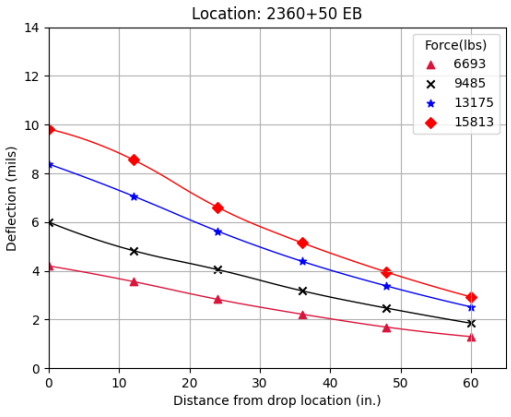

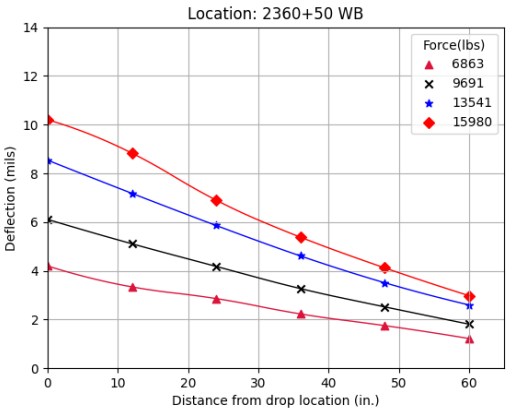

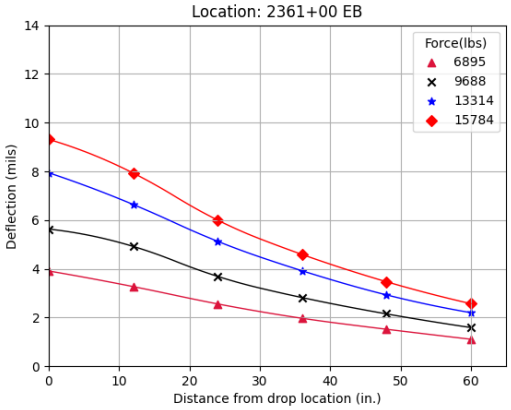
Location: 2361+00 EB
Force(lbs)
6895
9688
13314
15784
Deflection (mils)
Distance from drop location (in.)

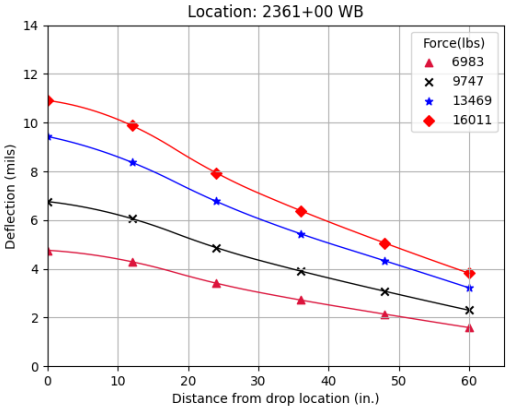
Location: 2361+00 WB
Force(lbs)
6983
9747
13469
16011
Deflection (mils)
Distance from drop location (in.)

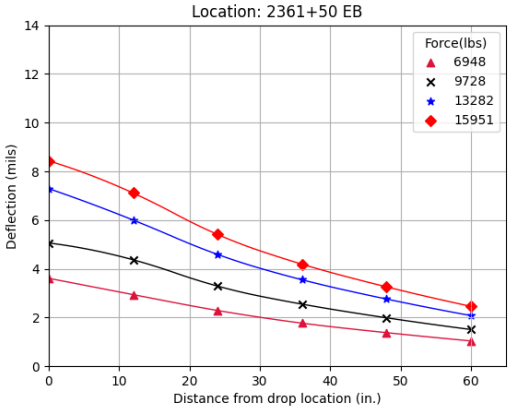
Location: 2361+50 EB
Force(lbs)
6948
9728
13282
15951
Deflection (mils)
Distance from drop location (in.)

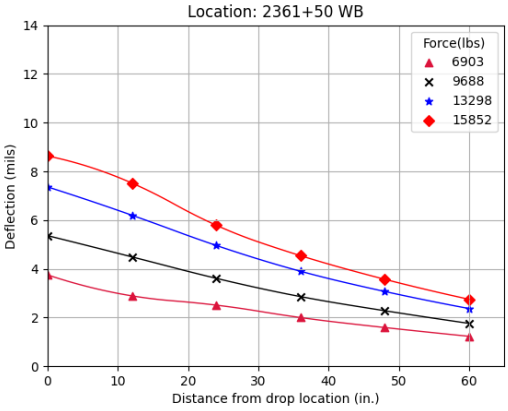
Location: 2361+50 WB
Force(lbs)
6903
9688
13298
15852
Deflection (mils)
Distance from drop location (in.)

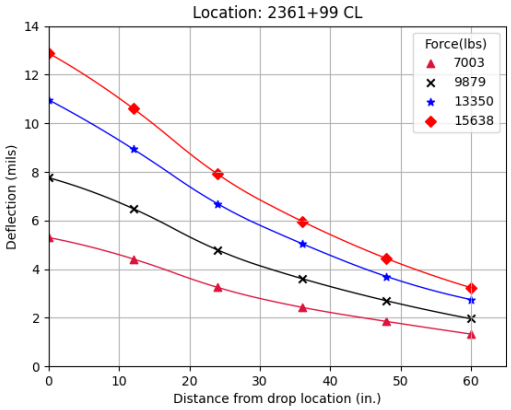
Location: 2361+99 CL
Force(lbs)
7003
9879
13350
15638
Deflection (mils)
Distance from drop location (in.)

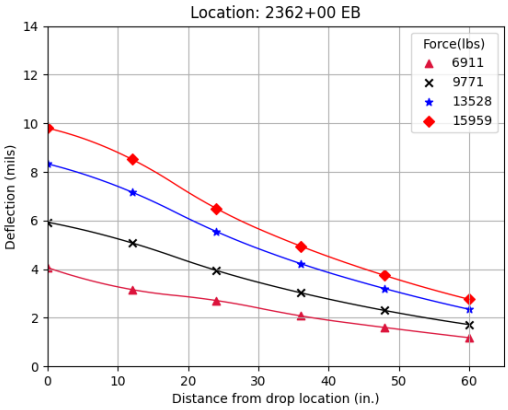
Location: 2362+00 EB
Force(lbs)
6911
9771
13528
15959
Deflection (mils)
Distance from drop location (in.)

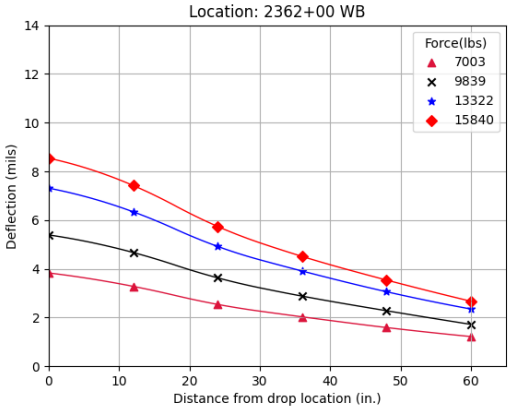
Location: 2362+00 WB
Force(lbs)
7003
9839
13322
15840
Deflection (mils)
Distance from drop location (in.)

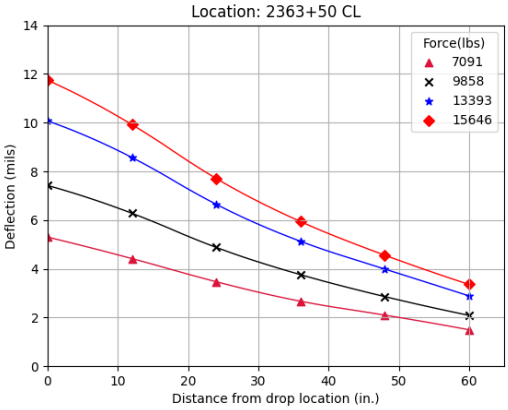
Location: 2363+50 CL
Force(lbs)
7091
9858
13393
15646
Deflection (mils)
Distance from drop location (in.)

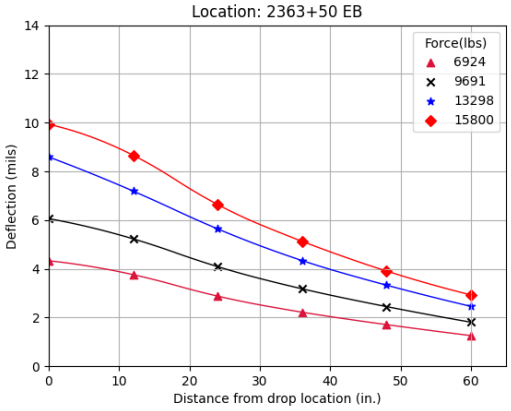
Location: 2363+50 EB
Force(lbs)
6924
9691
13298
15800
Deflection (mils)
Distance from drop location (in.)

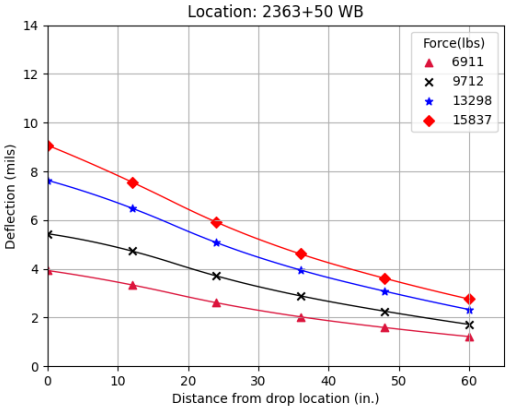
Location: 2363+50 WB
Force(lbs)
6911
9712
13298
15837
Deflection (mils)
Distance from drop location (in.)

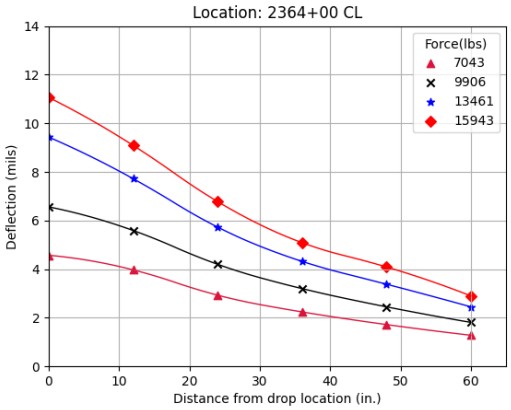
Location: 2364+00 CL
Force(lbs)
7043
9906
13461
15943
Deflection (mils)
Distance from drop location (in.)

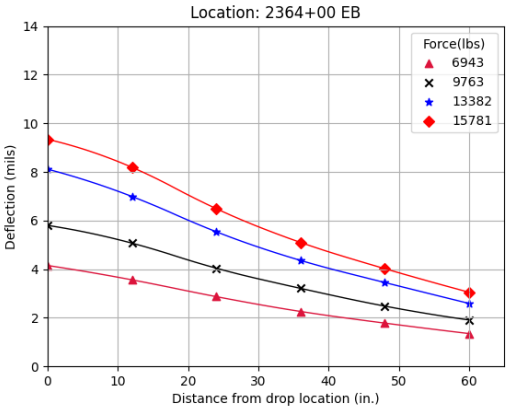
Location: 2364+00 EB
Force(lbs)
6943
9763
13382
15781
Deflection (mils)
Distance from drop location (in.)

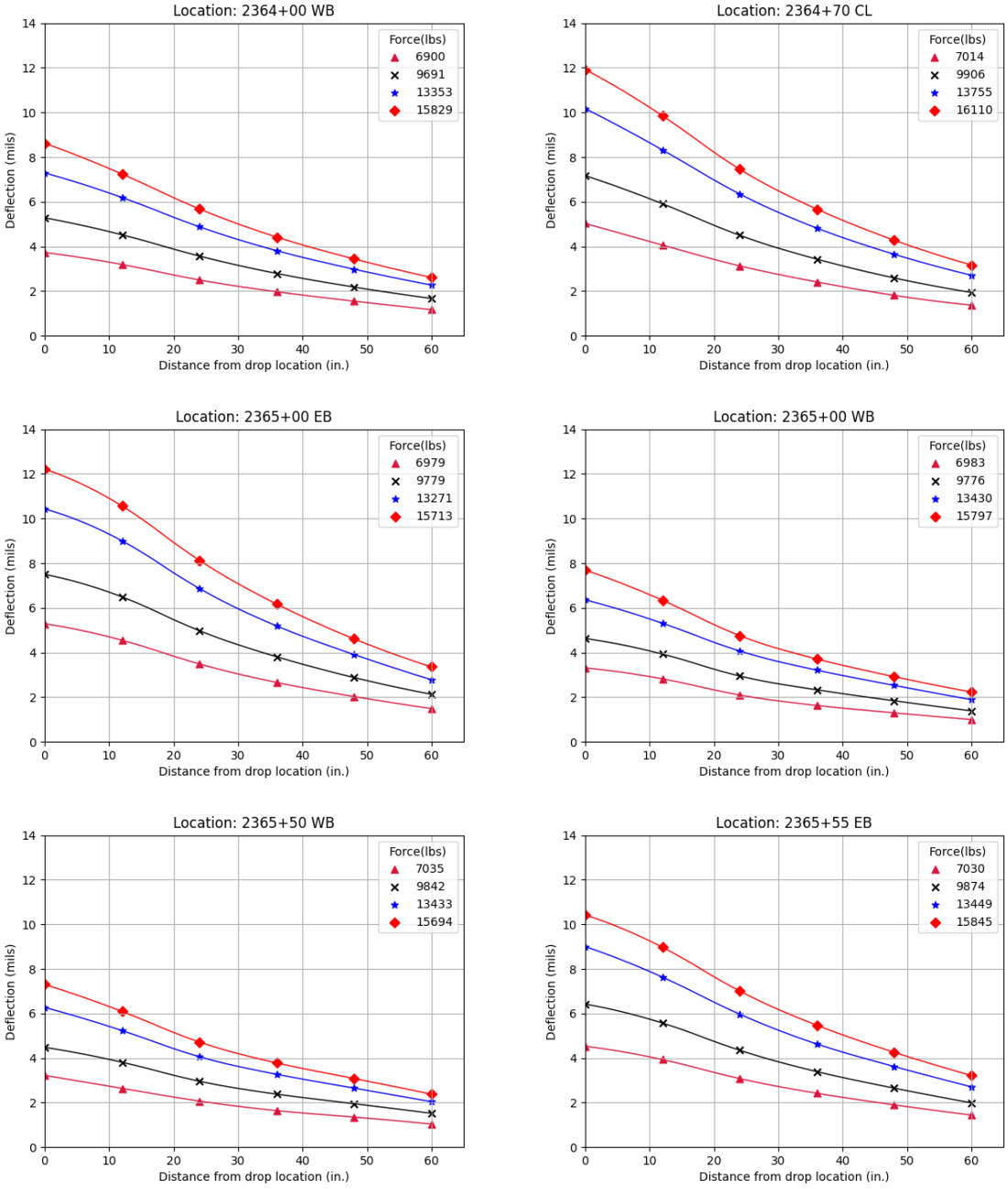

Figure 79. Graphs. FWD data on top of the HMA layer at different measuring points in the QBA sections (after construction).

APPENDIX M: FALLING WEIGHT DEFLECTOMETER DATA ON TOP OF HMA—AFTER CONSTRUCTION (EAST SIDE OF BRIDGE)

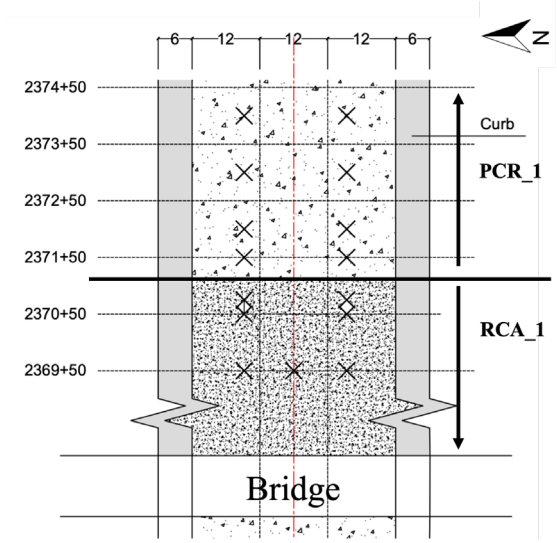

Figure 80. Plot. FWD test locations on top of HMA (east side of bridge).

Detailed FWD deflection profiles for the locations presented in Figure 80 are shown below in Figure 81. For the first plot (Location: 2369+50 CL), 2369+50 represents the station number. CL represents the test spot is located at road centerline. EB/WB indicate drop locations on the eastbound / westbound driving lanes. In order to examine the deflections nonlinearity and the impact of dynamic load, four levels of loading (6-kips, 9-kips, 12-kips and 15-kips) are desired to be applied. The numbers presented in legend represent the load applied by the load plate for each drop at each station. Deflections detected after each drop are plotted are plotted for each load level. All the westbound test locations have an offset of 9.23' from curb and the eastbound test locations have an offset of 8.64' from the curb. The same nomenclature applies to all plots.

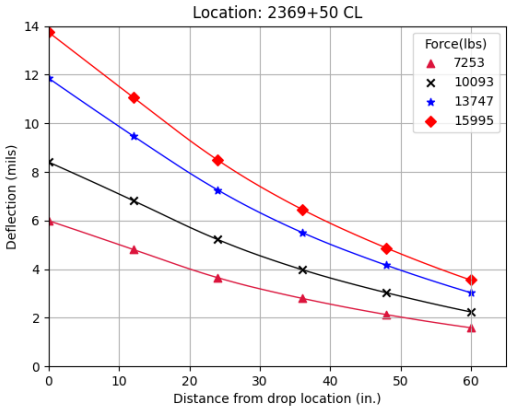

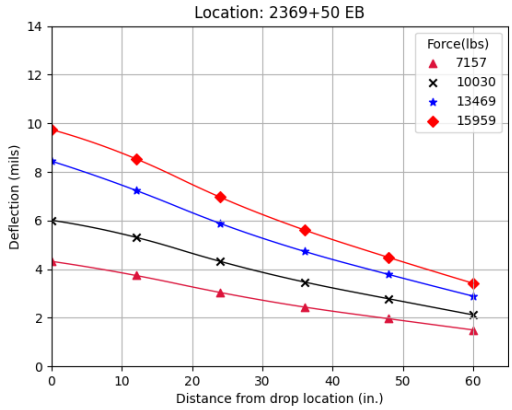

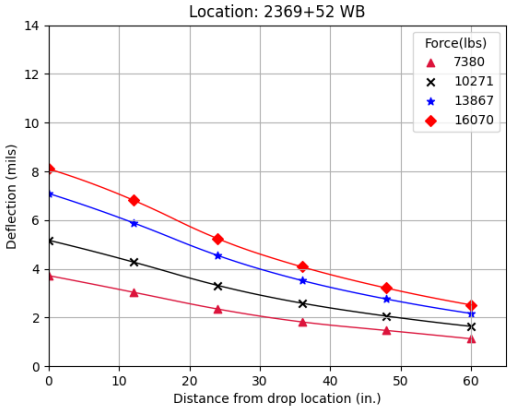
Location: 2369+52 WB
Force(lbs)
7380
10271
13867
16070
Deflection (mils)
Distance from drop location (in.)

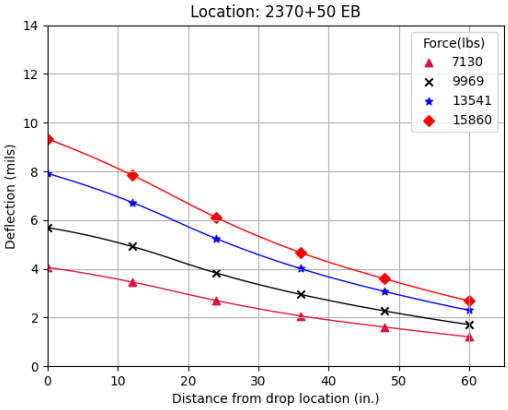
Location: 2370+50 EB
Force(lbs)
7130
9969
13541
15860
Deflection (mils)
Distance from drop location (in.)

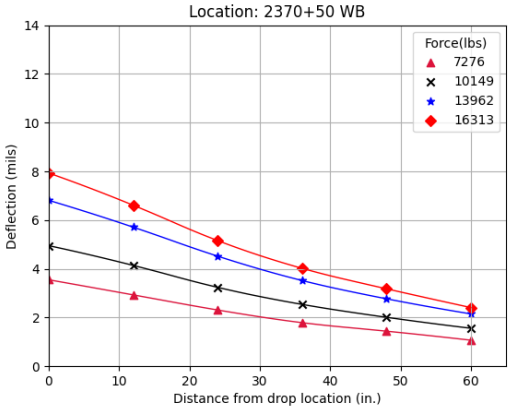
Location: 2370+50 WB
Force(lbs)
7276
10149
13962
16313
Deflection (mils)
Distance from drop location (in.)

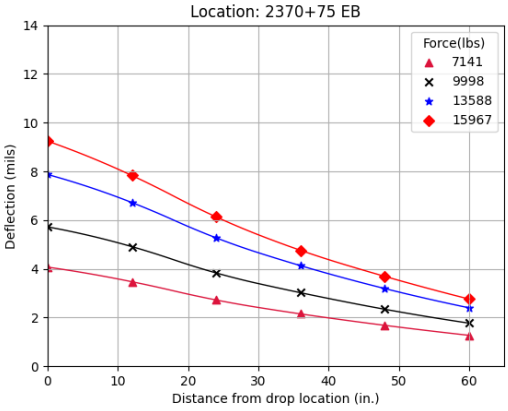
Location: 2370+75 EB
Force(lbs)
7141
9998
13588
15967
Deflection (mils)
Distance from drop location (in.)

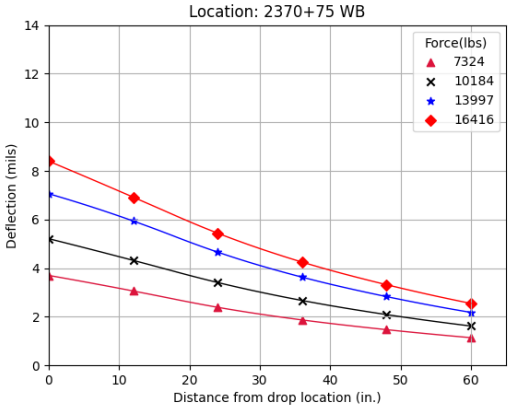
Location: 2370+75 WB
Force(lbs)
7324
10184
13997
16416
Deflection (mils)
Distance from drop location (in.)

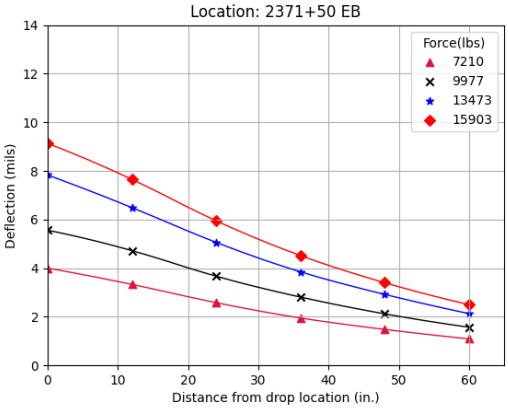
Location: 2371+50 EB
Force(lbs)
7210
9977
13473
15903
Deflection (mils)
Distance from drop location (in.)

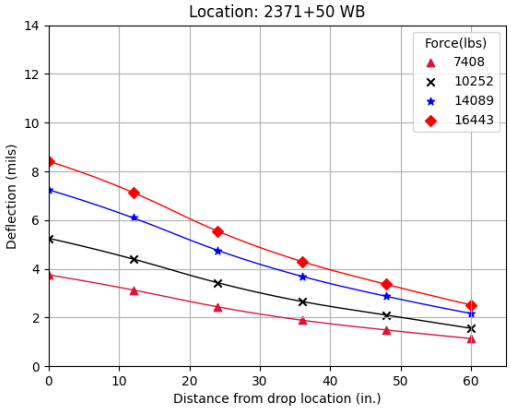
Location: 2371+50 WB
Force(lbs)
7408
10252
14089
16443
Deflection (mils)
Distance from drop location (in.)

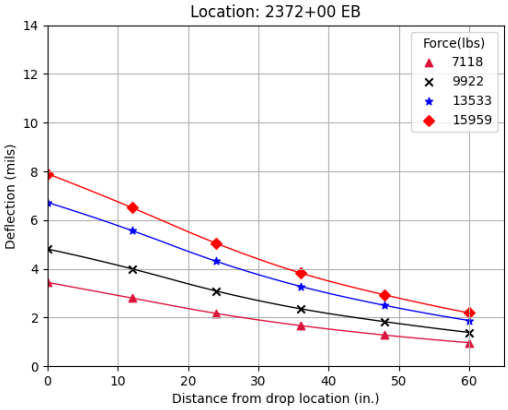
Location: 2372+00 EB
Force(lbs)
7118
9922
13533
15959
Deflection (mils)
Distance from drop location (in.)

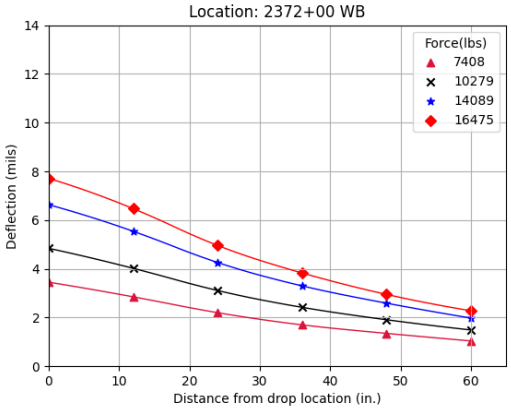
Location: 2372+00 WB
Force(lbs)
7408
10279
14089
16475
Deflection (mils)
Distance from drop location (in.)

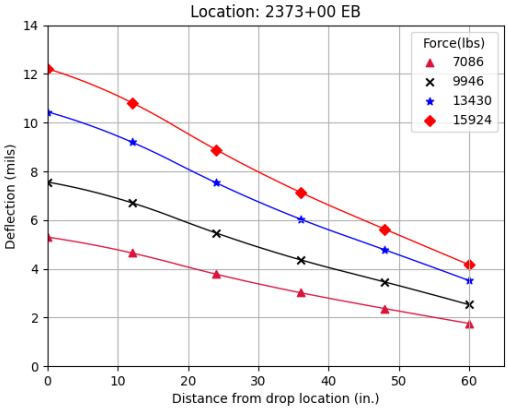
Location: 2373+00 EB
Force(lbs)
7086
9946
13430
15924
Deflection (mils)
Distance from drop location (in.)

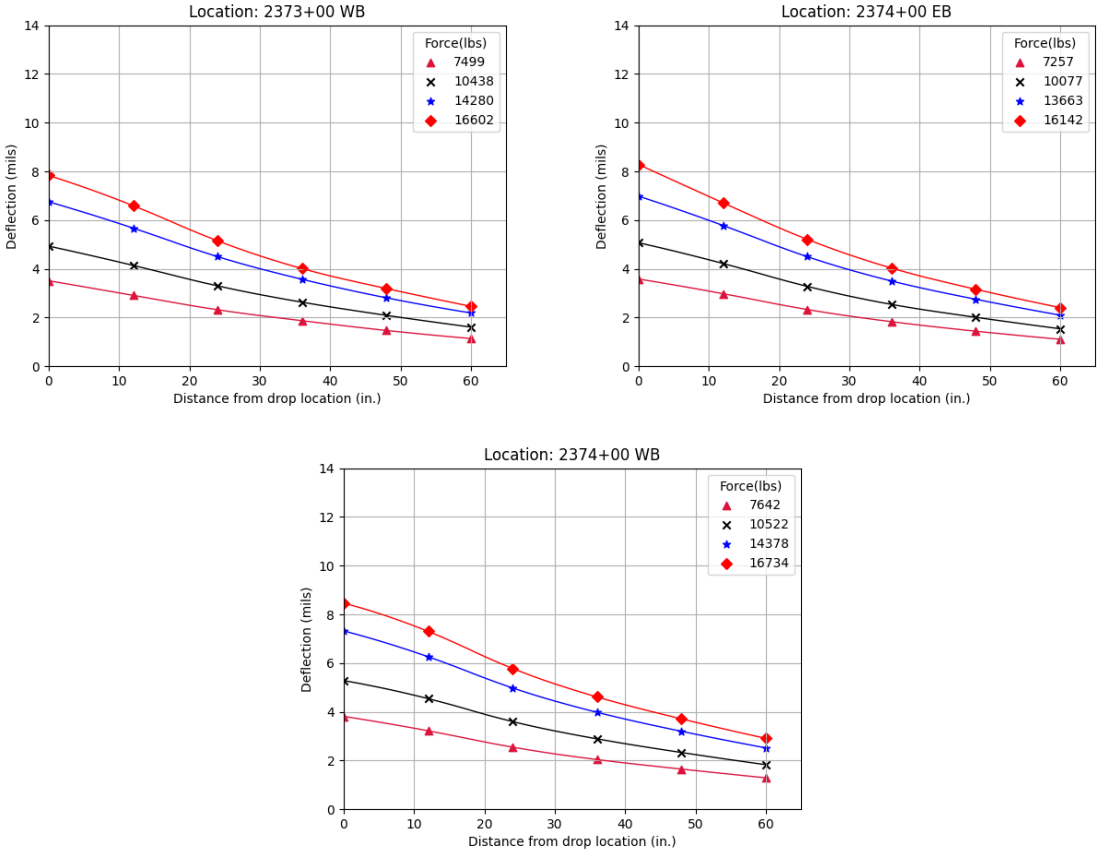

Figure 81. Graphs. FWD data on top of the HMA layer at different measuring points in the conventional ASI sections (after construction).

APPENDIX N: FALLING WEIGHT DEFLECTOMETER DATA ON TOP OF HMA—AFTER OPENING TO TRAFFIC (WEST SIDE OF BRIDGE)

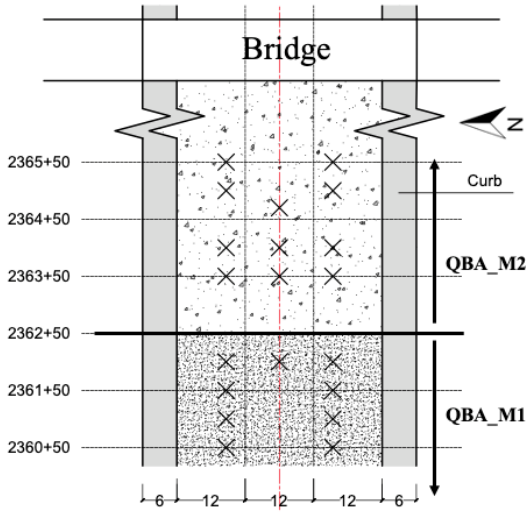

Figure 82. Plot. FWD test locations on top of HMA (west side of bridge).

Detailed FWD deflection profiles for the locations presented in Figure 82 are shown below in Figure 83. For the first plot (Location: 2360+50 EB), 2360+50 represents the station number. EB/WB indicate drop locations on the eastbound/westbound driving lanes. CL represents the test spot is located at road centerline. In order to examine the deflections for nonlinearity and the impact of dynamic load, three levels of loading (~9-kips, 12-kips and 15-kips) are applied. The numbers presented in legend represent the load applied by the load plate for each drop at each station. Deflections recorded after each drop are plotted for each load level. The same nomenclature applies to all plots. All the test locations not on the centerline have an offset of 8.64' from curb.

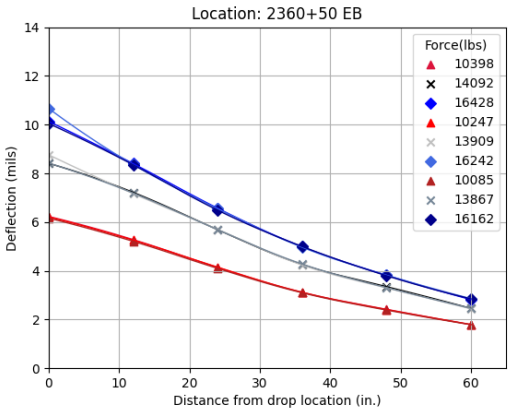

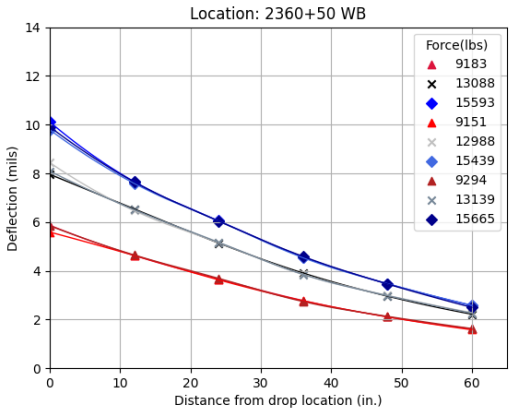

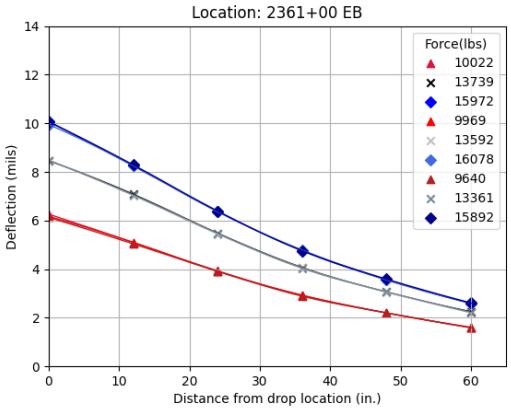
Location: 2361+00 EB
Force(lbs)
10022
13739
15972
9969
13592
16078
9640
13361
15892
Deflection (mils)
Distance from drop location (in.)

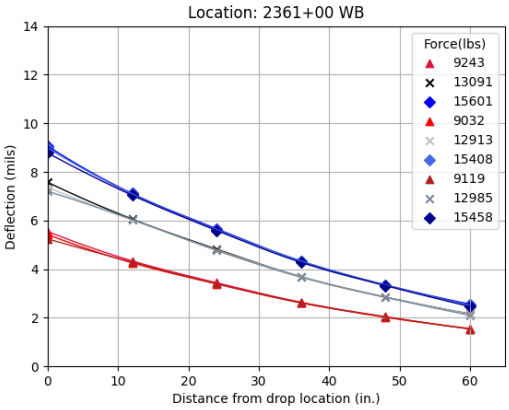
Location: 2361+00 WB
Force(lbs)
9243
13091
15601
9032
12913
15408
9119
12985
15458
Deflection (mils)
Distance from drop location (in.)

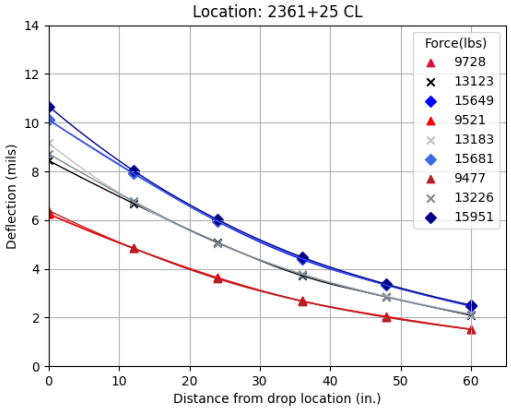
Location: 2361+25 CL
Force(lbs)
9728
13123
15649
9521
13183
15681
9477
13226
15951
Deflection (mils)
Distance from drop location (in.)

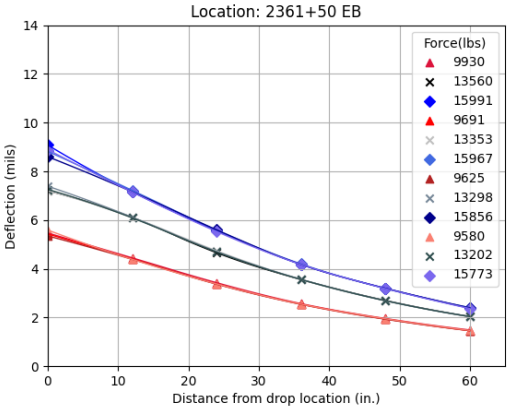
Location: 2361+50 EB
Force(lbs)
9930
13560
15991
9691
13353
15967
9625
13298
15856
9580
13202
15773
Deflection (mils)
Distance from drop location (in.)

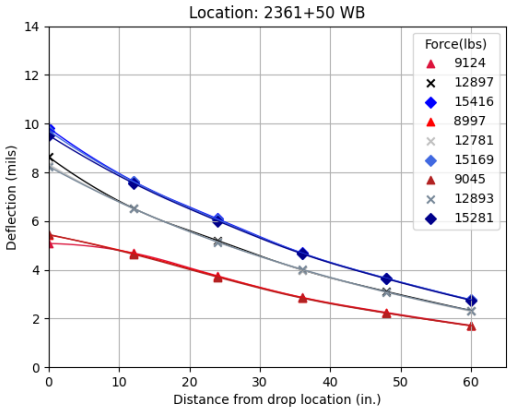
Location: 2361+50 WB
Force(lbs)
9124
12897
15416
8997
12781
15169
9045
12893
15281
Deflection (mils)
Distance from drop location (in.)

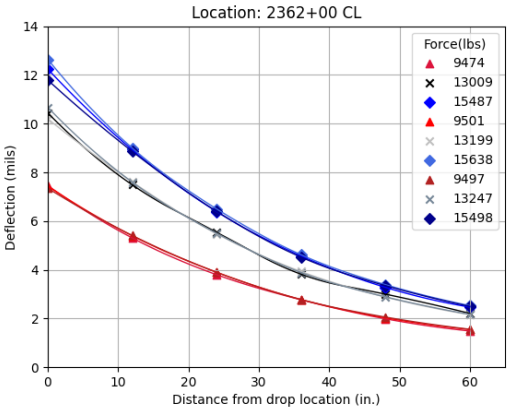
Location: 2362+00 CL
Force(lbs)
9474
13009
15487
9501
13199
15638
9497
13247
15498
Deflection (mils)
Distance from drop location (in.)

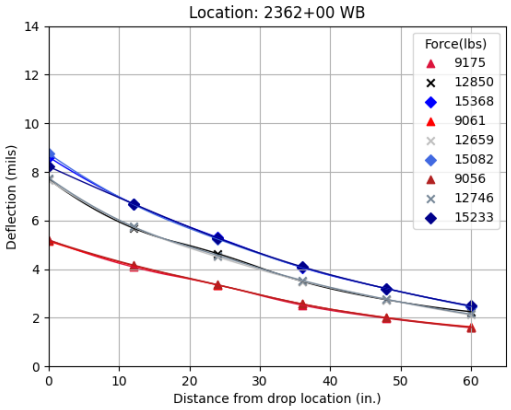
Location: 2362+00 WB
Force(lbs)
9175
12850
15368
9061
12659
15082
9056
12746
15233
Deflection (mils)
Distance from drop location (in.)

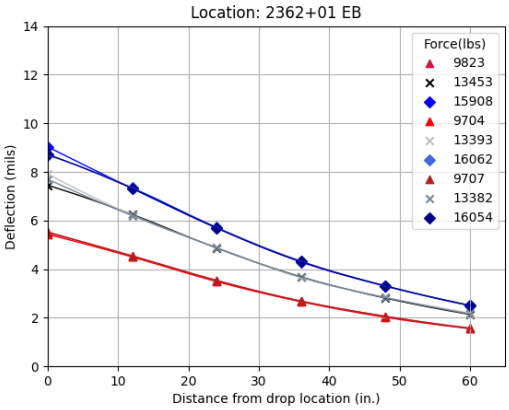
Location: 2362+01 EB
Force(lbs)
9823
13453
15908
9704
13393
16062
9707
13382
16054
Deflection (mils)
Distance from drop location (in.)

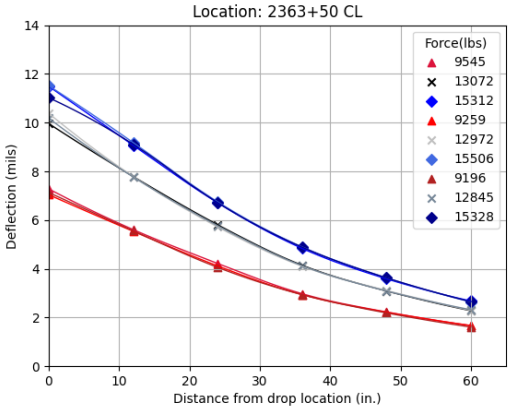
Location: 2363+50 CL
Force(lbs)
9545
13072
15312
9259
12972
15506
9196
12845
15328
Deflection (mils)
Distance from drop location (in.)

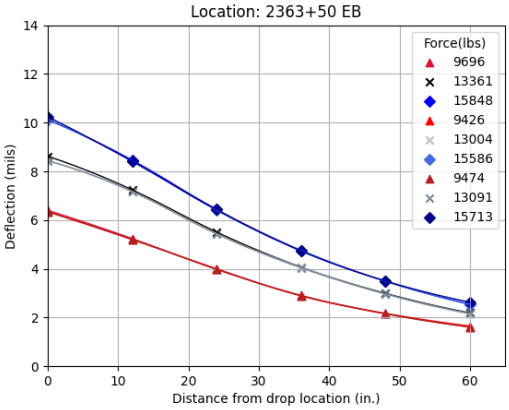
Location: 2363+50 EB
Force(lbs)
9696
13361
15848
9426
13004
15586
9474
13091
15713
Deflection (mils)
Distance from drop location (in.)

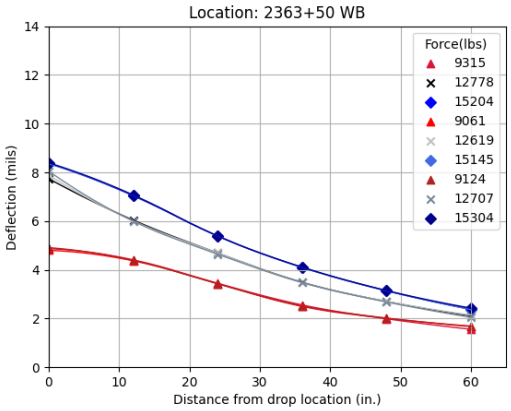
Location: 2363+50 WB
Force(lbs)
9315
12778
15204
9061
12619
15145
9124
12707
15304
Deflection (mils)
Distance from drop location (in.)

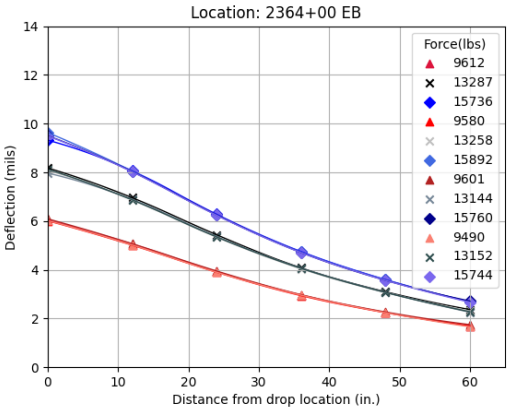
Location: 2364+00 EB
Force(lbs)
9612
13287
15736
9580
13258
15892
9601
13144
15760
9490
13152
15744
Deflection (mils)
Distance from drop location (in.)

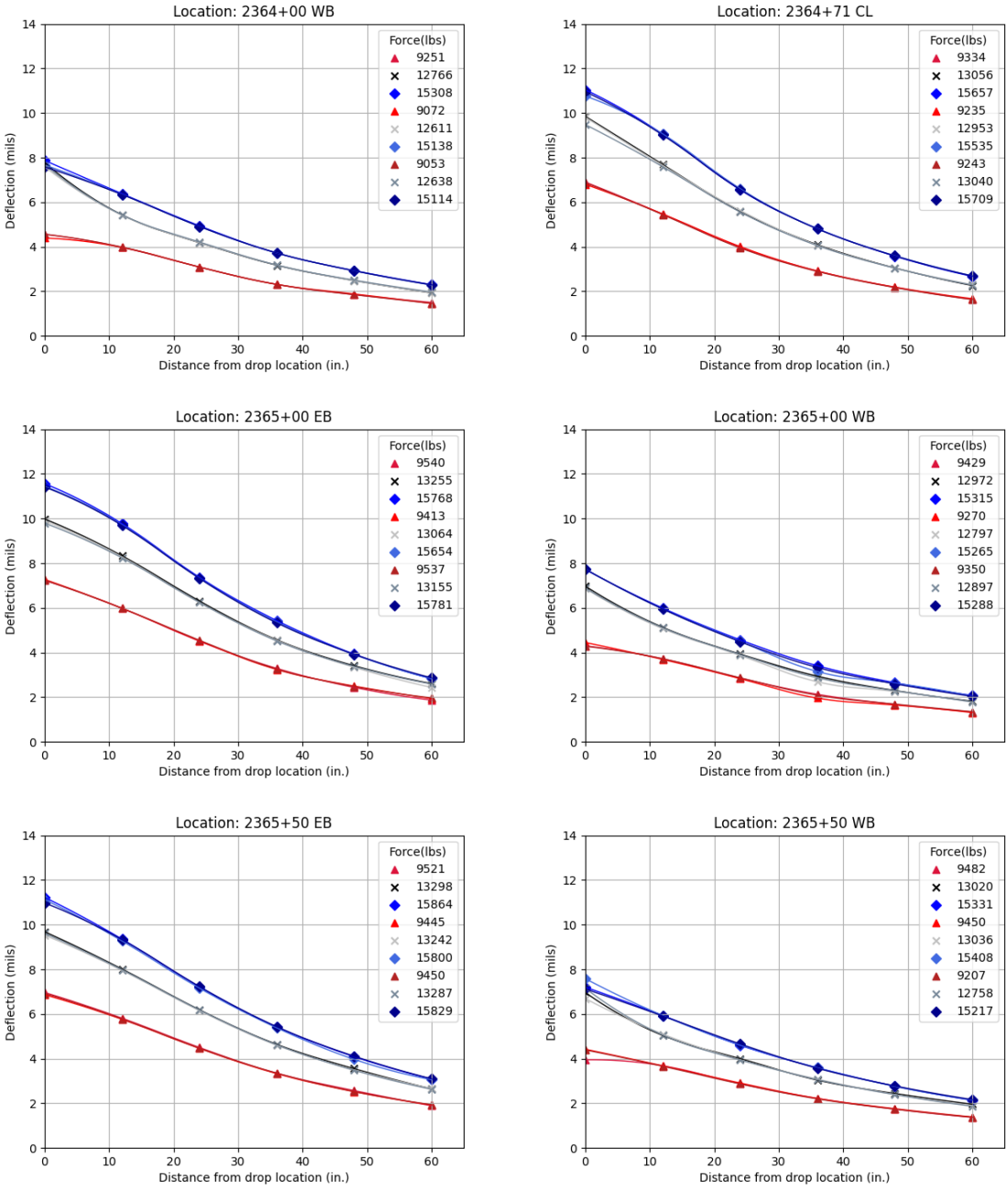

Figure 83. Graphs. FWD data on top of the HMA layer at different measuring points in the QBA sections (after opening to traffic).

APPENDIX O: FALLING WEIGHT DEFLECTOMETER DATA ON TOP OF HMA—AFTER OPENING TO TRAFFIC (EAST SIDE OF BRIDGE)

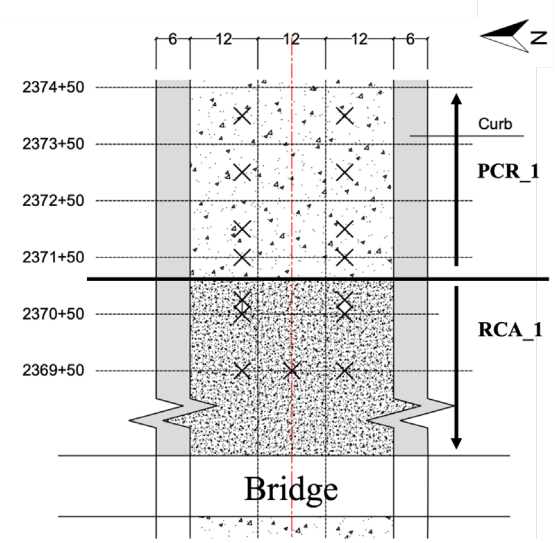

Figure 84. Plot. FWD test locations on top of HMA (east side of bridge).

Detailed FWD deflection profiles for the locations presented in Figure 84 are shown below in Figure 85. For the first plot (Location: 2369+50 CL), 2369+50 represents the station number. CL represents the test spot is located at road centerline. EB/WB indicate drop locations on the eastbound / westbound driving lanes. In order to examine the deflections for nonlinearity and the impact of dynamic load, four levels of loading (6-kips, 9-kips, 12-kips and 15-kips) are desired to be applied. The numbers presented in legend represent the load applied by the load plate for each drop at each station. Deflections recorded after each drop are plotted for each load level. All the westbound test locations have an offset of 9.23' from curb and the eastbound test locations have an offset of 8.64' from the curb. The same nomenclature applies to all plots.

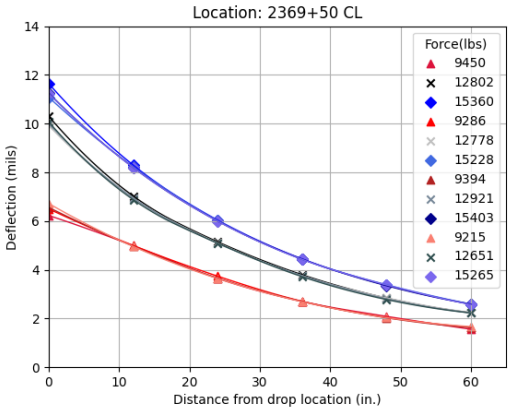

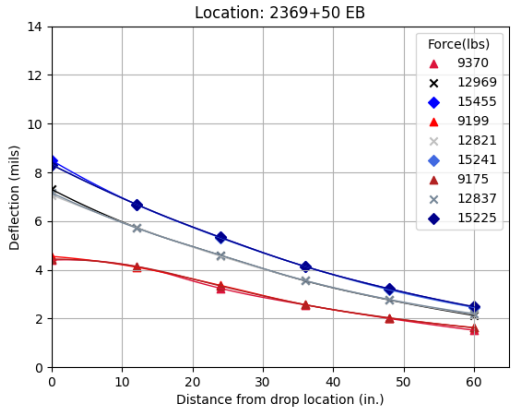

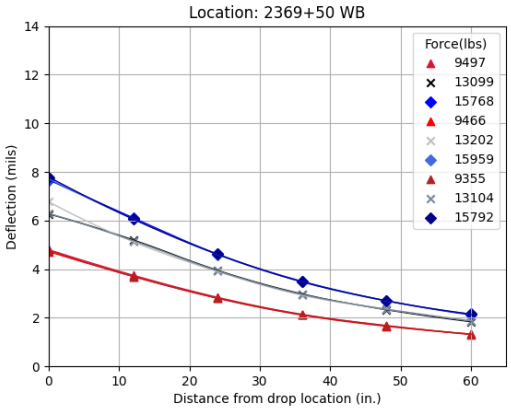
Location: 2369+50 WB
Force(lbs)
9497
13099
15768
9466
13202
15959
9355
13104
15792
Deflection (mils)
Distance from drop location (in.)

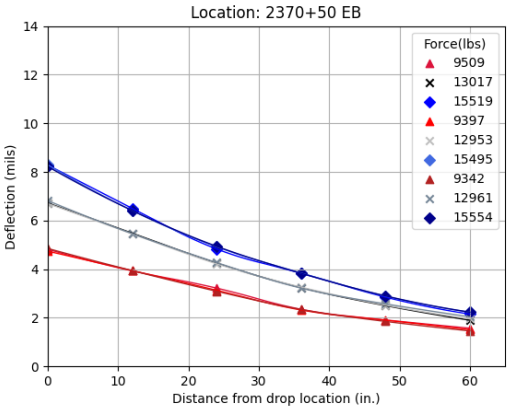
Location: 2370+50 EB
Force(lbs)
9509
13017
15519
9397
12953
15495
9342
12961
15554
Deflection (mils)
Distance from drop location (in.)

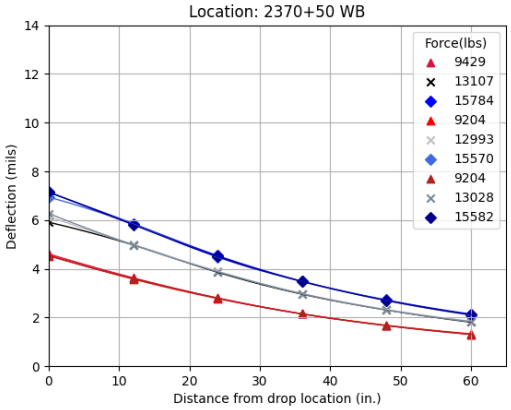
Location: 2370+50 WB
Force(lbs)
9429
13107
15784
9204
12993
15570
9204
13028
15582
Deflection (mils)
Distance from drop location (in.)

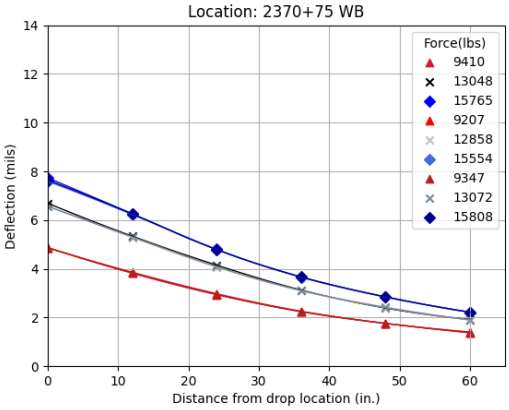
Location: 2370+75 WB
Force(lbs)
9410
13048
15765
9207
12858
15554
9347
13072
15808
Deflection (mils)
Distance from drop location (in.)

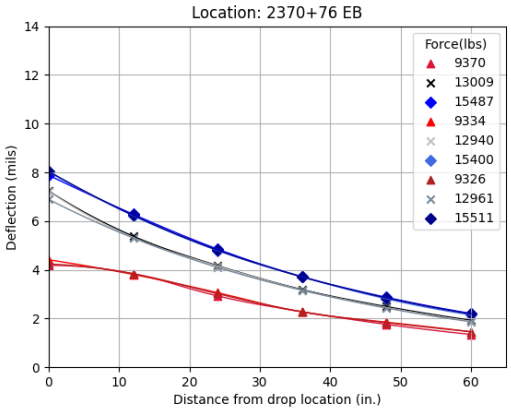
Location: 2370+76 EB
Force(lbs)
9370
13009
15487
9334
12940
15400
9326
12961
15511
Deflection (mils)
Distance from drop location (in.)

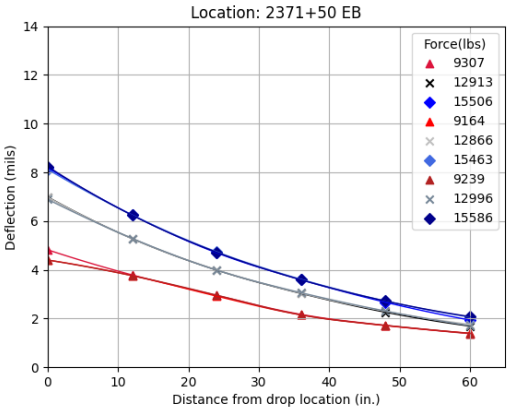
Location: 2371+50 EB
Force(lbs)
9307
12913
15506
9164
12866
15463
9239
12996
15586
Deflection (mils)
Distance from drop location (in.)

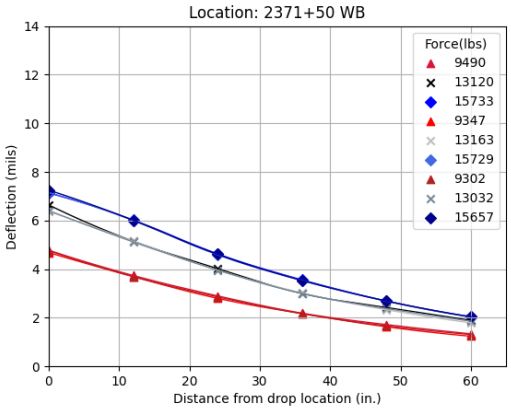
Location: 2371+50 WB
Force(lbs)
9490
13120
15733
9347
13163
15729
9302
13032
15657
Deflection (mils)
Distance from drop location (in.)

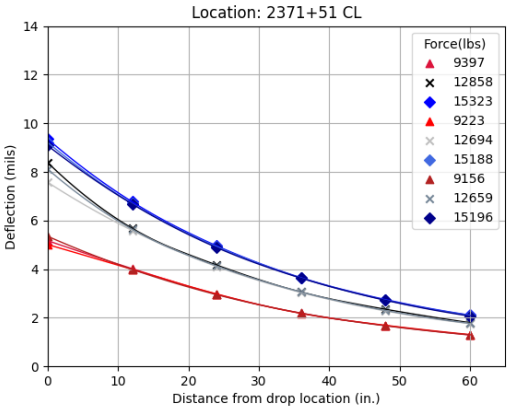
Location: 2371+51 CL
Force(lbs)
9397
12858
15323
9223
12694
15188
9156
12659
15196
Deflection (mils)
Distance from drop location (in.)

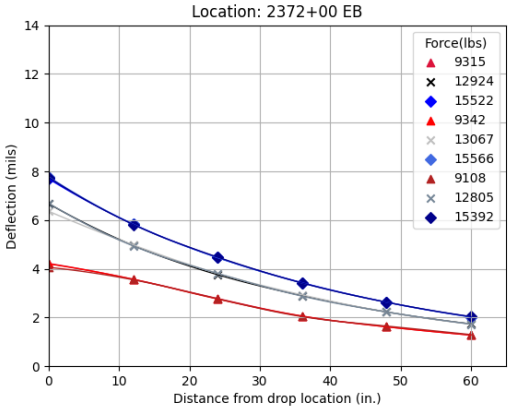
Location: 2372+00 EB
Force(lbs)
9315
12924
15522
9342
13067
15566
9108
12805
15392
Deflection (mils)
Distance from drop location (in.)

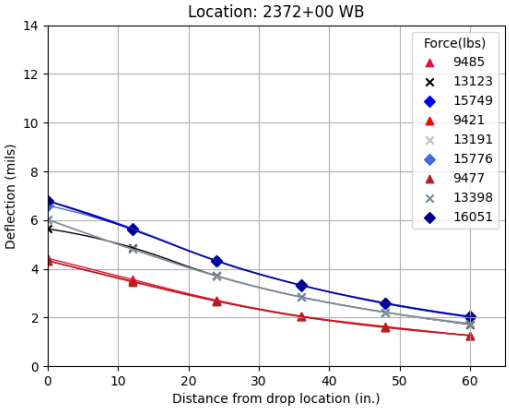
Location: 2372+00 WB
Force(lbs)
9485
13123
15749
9421
13191
15776
9477
13398
16051
Deflection (mils)
Distance from drop location (in.)

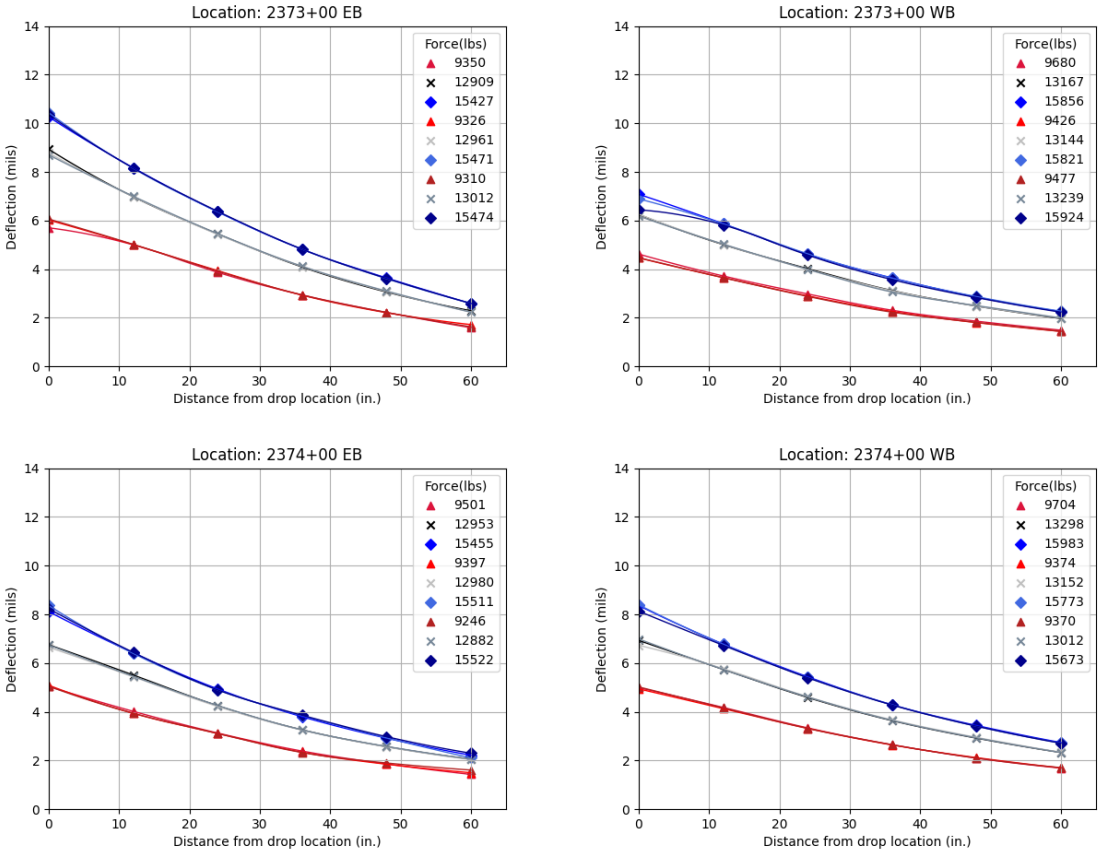

Figure 85. Graphs. FWD data on top of the HMA layer at different measuring points in the conventional ASI sections (after opening to traffic).


Illinois Department
of Transportation


ILLINOIS